

**PRECISE PREDICTIONS FOR PROCESSES OF
INTEREST AT LHC**

By
MANOJ KUMAR MANDAL
PHYS08200805003

Harish-Chandra Research Institute, Allahabad

*A thesis submitted to the
Board of Studies in Physical Sciences*

*In partial fulfillment of requirements
for the Degree of*

DOCTOR OF PHILOSOPHY

of

HOMI BHABHA NATIONAL INSTITUTE



August, 2015

Homi Bhabha National Institute¹

Recommendations of the Viva Voce Committee

As members of the Viva Voce Committee, we certify that we have read the dissertation prepared by Mr. Manoj Kumar Mandal entitled "Precise Predictions for processes of interest at LHC" and recommend that it may be accepted as fulfilling the thesis requirement for the award of Degree of Doctor of Philosophy.

Chairman – Prof. B. Mukhopadhyaya  Date: 29/2/16

Guide / Convener – Prof. V. Ravindran  Date: 29.2.16

Co-guide -  Date:

Examiner – Prof. Poulouse Poulouse  Date: 29/02/16

Member 1- Prof. Dileep Jatkar  Date: 29/2/2016

Member 2- Prof. Asesh Krishna Datta  Date: 15/03/2016

Final approval and acceptance of this thesis is contingent upon the candidate's submission of the final copies of the thesis to HBNI.

I/We hereby certify that I/we have read this thesis prepared under my/our direction and recommend that it may be accepted as fulfilling the thesis requirement.

Date: 29.2.2016

Place: Allahabad


Signature
Guide

¹ This page is to be included only for final submission after successful completion of viva voce.

STATEMENT BY AUTHOR

This dissertation has been submitted in partial fulfillment of requirements for an advanced degree at Homi Bhabha National Institute (HBNI) and is deposited in the Library to be made available to borrowers under rules of the HBNI.

Brief quotations from this dissertation are allowable without special permission, provided that accurate acknowledgement of source is made. Requests for permission for extended quotation from or reproduction of this manuscript in whole or in part may be granted by the Competent Authority of HBNI when in his or her judgment the proposed use of the material is in the interests of scholarship. In all other instances, however, permission must be obtained from the author.



Manoj Kumar Mandal

DECLARATION

I, hereby declare that the investigation presented in the thesis has been carried out by me. The work is original and has not been submitted earlier as a whole or in part for a degree / diploma at this or any other Institution / University.



Manoj Kumar Mandal

List of publications arising from the thesis

Journal

- “Three photon production in SM at NLO+PS accuracy at the LHC”, M. K. Mandal, Prakash Mathews, V. Ravindran, Satyajit Seth, *Eur.Phys.J.C*, **2014**, 74, 3044
 - “Drell-Yan, ZZ, W+ W - production in SM and ADD model to NLO+PS accuracy at the LHC”, R. Frederix, M. K. Mandal, Prakash Mathews, V. Ravindran, Satyajit Seth, *Eur.Phys.J.C*, **2014**, 74, 2745
 - “Higgs Rapidity Distribution in $b\bar{b}$ Annihilation at Threshold in N³LO QCD”, Taushif Ahmed, M. K. Mandal, Narayan Rana, V. Ravindran, *Journal of High Energy Physics*, **2015**, 1502, 131
 - “Associated production of Higgs boson with vector boson at threshold N³LO in QCD”, M. C. Kumar, M. K. Mandal, V. Ravindran, *Journal of High Energy Physics*, **2015**, 1503, 037
-

List of other publications of candidate not related to this thesis

- “Diphoton production in the ADD model to NLO+parton shower accuracy at the LHC”, R. Frederix, Manoj K. Mandal, Prakash Mathews, V. Ravindran, Satyajit Seth, P. Torrielli, M. Zaro, *Journal of High Energy Physics*, **2012**, 1212, 102
 - “A framework for Higgs characterisation”, P. Artoisenet, P. de Aquino, F. Demartin, R. Frederix, S. Frixione, F. Maltoni, M. K. Mandal, P. Mathews, K. Mawatari, V. Ravindran, S. Seth, P. Torrielli, M. Zaro, *Journal of High Energy Physics*, **2013**, 1311, 043
 - “Rapidity Distributions in Drell-Yan and Higgs Productions at Threshold to Third Order in QCD”, Taushif Ahmed, M. K. Mandal, Narayan Rana and V. Ravindran, *Phys. Rev. Lett.*, **2014**, 113, 212003
-



Manoj Kumar Mandal

Dedicated to

My Father

ACKNOWLEDGEMENTS

Here comes the time to go down the memory lane of almost 7 years at HRI to thank those whose smallest contribution has helped me to travel this long journey. Firstly, I would like to thank my supervisor Prof. V. Ravindran, with whom I have enjoyed working and without his guidance, help and endless patience this thesis would never have been seen the daylight. Working with him has been a very rewarding experience on a professional and personal level that I will always be grateful for. Then I would like to thank my collaborators Prof. Prakash Matthews, Prof. Fabio Maltoni, Dr. Rikkert Frederix for their consistent help in curbing this thesis. I also thank my other collaborators as well as friends Satyajitda, Ambresh, kumar, maguni, rana and taushif with whom I have enjoyed working a lot. I would like to take this opportunity to express my sincere gratitude to Prof. Ashoke sen and Prof. Sumathi Rao for their generous help in my life, without which I could not been able to write this line. I thank all the professors here at HRI for their contribution in my learning process. I thank all my HRI mates here for their friendship and for keeping me sane. Special thank goes to bhuru, niyogi, tarat, paromita, jonthu, ushoshi, ho-chi, rambha, animesh, bachha, sudipto, eshita, sanjoyda, dhirajda, satyada, anirbanda, atrida for making the life a wonderful one. I will take many memories with me from our time here at HRI and cherish those forever.

I would also like to acknowledge the constant funding support from RECAPP to complete all the works for this thesis. I would like to thank the people in the cluster computing facility and also to all the non-academic staff here for making the life an easy one, here.

Now it turns towards my family. The many hours, after coming from the school, spent by my father teaching me have finally paid off. The immense sacrifice made by my mother and brother for making my dream come true, aside from pushing me to a better myself, is priceless to me and really I do not have the words to express it. Simply, I love you. Finally, I would like to thank my wife Anushree for her immense support.

Contents

SYNOPSIS	1
LIST OF FIGURES	7
LIST OF TABLES	12
1 Introduction	14
1.1 Standard Model	16
1.2 Beyond Standard Model	18
1.2.1 ADD Model	19
2 Basics of QCD	22
2.1 Lagrangian of QCD	22
2.2 The running coupling	26
2.3 QCD at Collider	28
2.4 Anatomy of NLO Calculation	31
2.4.1 Virtual correction	32
2.4.2 Real emission correction	34
2.5 NLO correction matched to Parton Shower	36
2.5.1 AMC@NLO framework	42
2.6 Approximate fixed order calculation	42

3	Three photon production	46
3.1	Introduction	46
3.2	Calculational Details	47
3.2.1	Virtual contribution	48
3.2.2	Real emission contribution	50
3.3	Numerical Results	51
3.3.1	Fixed order Analysis	53
3.3.2	Discussion on NLO+PS	56
3.4	Conclusion	59
4	DY, ZZ and WW production	60
4.1	Introduction	60
4.2	NLO+PS	61
4.3	Numerical Result	62
4.4	Conclusion	71
5	VH production	72
5.1	Introduction	72
5.2	Threshold Corrections Beyond NNLO	73
5.3	Numerical Results	77
5.4	Conclusion	82
6	Rapidity distribution of the Higgs boson production	83
6.1	Introduction	83
6.2	Differential Distribution with Respect to Rapidity	84
6.2.1	Threshold Correction at NLO	85
6.2.2	Threshold Corrections Beyond NLO	94
6.2.3	Numerical Results	114

6.3	Conclusions	121
7	Summary	122
	Bibliography	125

Synopsis

Wealth of data from the Large Hadron Collider (LHC) and the Tevatron involving large number of leptons, gauge bosons and hadrons in the final state has not only provided ample opportunity to test the predictions of the Standard Model (SM), but also constrained various physics scenarios in the beyond standard model (BSM), which came into the picture to incorporate several unanswered questions like the explanation of neutrino mass, existence of dark matter, the hierarchy between the weak and Planck scale in the SM itself. Precise predictions for such SM processes are important as the quantum corrections are often comparable to the BSM effects. In addition, they are essential to reduce the theoretical uncertainties, that arise from the missing higher order quantum corrections through the renormalisation and factorisation scales. This necessitates the calculation of the higher order quantum corrections in Quantum Chromodynamics (QCD) to these SM observables at the LHC. However, the fixed order predictions, being not good enough to cover the entire phase space available, could not capture the observable effects coming from the collinear region. The parton shower (PS) technique, producing a multi-particle final state, provides reasonable estimate of these effects in those kinematical regions, thus supplying a reliable as well as realistic predictions that can serve as a testing ground of various theoretical predictions, when matched with fixed order results. In the process, specifically, the PS resums the universal leading logs utilizing the factorisation of leading order collinear singularities of the cross-section in the collinear limit, thereby missing the rich kinematics of the soft gluon emissions at higher orders. In contrast with the PS technique, the analytic resummation can primarily resum all the large logs at the threshold limit via the sudakov exponentiation and exploitation of the factorisation of QCD, capturing the soft gluon emission contributions for a specific process. So, there is always a constant pursuit of obtaining precise predictions to a varied level of precision by matching the PS with fixed order predictions, merging different multiplicity final states, including the threshold logarithms of higher orders, matching the resummed results with fixed order predictions.

Being in this decade of achieving precise results, I have worked on producing Next-to-Leading (NLO) results matched with PS for the three photon production in SM as well as a set of di-final state productions namely, l^+l^- , ZZ , WW production in SM and ADD model, thereby showing the effect of the PS on the kinematic observables and at the same time producing a set of realistic events at LHC and making them directly comparable against the experiments. I have also used the techniques of calculating the threshold corrections due to the soft QCD radiations to achieve more precise theoretical prediction for the total inclusive cross-section of the associated Higgs production with vector bosons (Z/W) and the rapidity distribution of the Higgs production from $b\bar{b}$ annihilation at LHC at third order in QCD.

At NLO in QCD, we encounter virtual as well as real emission contributions resulting from an additional parton, namely quark or anti-quark or gluon. The virtual amplitudes are often divergent when the loop momentum becomes very large and these are called Ultra-Violet (UV) divergences, which should be first regularised and then renormalised. Due to the massless quarks, anti-quarks and gluons participating in the hard processes, both virtual and real emission contributions encounter soft and collinear divergences, which are called Infra-red divergences. The divergences coming from soft gluons and from collinear partons in the final state of the real emission processes get cancelled with those coming from the virtual processes, thanks to the KLN theorem. The remaining collinear divergences from the initial states are removed by mass factorisation. We have used QGRAF to generate the symbolic description of the Feynman diagrams of the tree level born and virtual diagrams in terms of propagators and vertices, which has been translated to a suitable format by our in-house FORM codes. We have supplied Feynman rules, identities for Dirac gamma matrices, equations of motion through this code and performed various simplifications at the amplitude level in a module based approach. The divergent loop integrals are decomposed, by applying Lorentz covariance, in terms of a number of scalar coefficients, which have been evaluated numerically for every phase space point in $n = 4 + \epsilon$ dimensions, via the package PJFry. We have used AMC@NLO framework

to compute the contributions from real emission processes along with the mass factorisation terms required to remove the initial state collinear singularities. Within AMC@NLO, the stand-alone package MADGRAPH generates all the required matrix elements both at LO as well as at NLO level. As already discussed, we have prepared a set of external codes to deal with the virtual correction part and made an interface to implement it within MADFKS, which separates out the soft and collinear configurations in the real emission processes using the FKS subtraction scheme and provides IR-divergent and IR-safe contributions separately along with the mass factorisation terms. In the FKS subtraction scheme, the phase space is partitioned in such a way that each partition contains at most one soft and one collinear divergences. Now, after finding out the exact position of the divergences for a given partition, the generalized plus distribution is used to regulate them. All these steps are systematically automated in MADFKS within the MADGRAPH5 environment. The events, that are generated using AMC@NLO, also include the Monte Carlo counter terms to take care of the MC@NLO matching which prevents the occurrence of any double counting at the time of matching to PS. These events are then showered by HERWIG, PYTHIA parton shower to get the realistic events.

In case of three photon production, we have shown a number of differential distributions namely, transverse momentum, invariant mass, rapidity at LHC14 for fixed order NLO. We have reported the K-factor, defined as the ration of the prediction at NLO and LO for different set of cuts. Here, for the PS, we have employed both HERWIG and PYTHIA showers to study the differential distributions and discussed the consequences of showering the fixed order NLO results. However, we have not found much difference in the results of these two showering algorithms. Our predictions have been shown to be less sensitive to the scale uncertainties and choice of the parton distribution functions (PDF) and hence more suited for direct comparison with the data from the experiments. For the $\ell^+\ell^-$, ZZ , W^+W^- production, we have used the HERWIG shower only and the results have been available to NLO+PS accuracy for the SM and ADD model. A selection of results for LHC8 has been reported for various distributions in an attempt to identify the region of interest for extra

dimension searches. Scale and PDF uncertainties for each of these distributions have also been studied, which indicates a decrease in the uncertainties with the inclusion of the PS, as expected. In addition, the results of the search sensitivity for the extra dimensions $d = 2 - 6$, for LHC14 at 10 fb^{-1} have been presented. In the process, we have used packages, namely QGRAF, PJFry, AMC@NLO to study these processes at NLO, taking into account the PS effects and realistic experimental cuts, thereby developing a number of codes that build the interfaces among these different analytical and numerical tools, which is capable of studying other SM and BSM observables at this accuracy.

With the aim of the inclusion of the higher order threshold logarithms at higher orders in QCD for the inclusive and semi-inclusive observables for the Higgs boson production we have demonstrated one framework, which is not only able to compute the similar observables for any colorless final state produced at hadron colliders but also can provide threshold corrections to all orders in perturbation theory. The general framework that we have set up for this computation for such observables has been based on the factorization property of the QCD amplitudes. Sudakov resummation of soft gluons, renormalisation group equations and most importantly the infrared safety of the observable has played important role in achieving this task. QCD amplitudes that contribute to hard scattering cross sections exhibit rich infra-red structure through cusp and collinear anomalous dimensions due to the factorization property of the soft and collinear configurations. Massless gluons and light quarks are responsible for soft and collinear singularities in these amplitudes and also in partonic subprocesses. Singularities resulting from soft gluons cancel between virtual and real emission diagrams in infrared safe observables. While the final state collinear singularities cancel among themselves if the summation over degenerate states are appropriately carried out in such observables, the initial state collinear singular configurations remain until they are absorbed into bare PDFs.

For the Higgs boson production through bottom anti-bottom annihilation, we have shown in detail the infra-red structure of the QCD amplitudes at NLO level as well as the cancellation of the

various soft and collinear singularities through the summation of all possible degenerate states and the renormalisation of the PDFs in order to demonstrate the general framework. The predictions at different perturbative order for a number of values of the rapidity has been presented. We have examined the effects of the arbitrary variation of the renormalisation scale and the factorization scale, which has indicated a consistent improvement in the scale uncertainty with the inclusion of higher order terms. Moreover, we have seen that the dependence on the renormalisation scale for this process has been very mild. The reliability of the prediction has been also assessed by studying the rate of convergence of the perturbation series through the inspection of the ratios of different terms in the series, which clearly illustrates the considerable amount of improvement in the rate of convergence with the inclusion of higher order terms. Moreover, it exhibits, that the shape at higher orders can not be rescaled from lower orders.

We have also worked out the results of the inclusion of the threshold correction at third order in QCD for the associated production of the Higgs boson production with a vector boson (Higgs-Strahlung process), which is one of the potential channels for the Higgs boson production at the LHC. The LO amplitude is an electroweak process and hence, the higher order QCD corrections enter only in the initial state comprising of a quark and an anti-quark. This fact prompts this process to be represented in terms of the convolution of production of a virtual W or Z boson production like Drell-Yan (DY) production and decay rate of that virtual boson to a real vector boson and the Higgs boson, at every order in QCD. Therefore, the available higher order QCD corrections of DY like processes can be used to study the QCD effects in Higgs-Strahlung process. Along this direction, the results of the threshold corrections for the DY production at third order in QCD has been used in these Higgs-Strahlung processes to get an estimate of the effects from threshold Next-to-next-to-leading order (N^3LO) DY type of corrections. For the numerical implementation of the N^3LO threshold corrections, we have included the additional subroutines for the contributions coming from the threshold terms, in the code `vh@nn1o` in a similar fashion as at the 2-loop level. This easily has enabled us to compute the N^3LO threshold corrections using the PDFs supplied by

LHAPDF and the strong coupling constant as in the public code `vh@nnlo`. We have presented the numerical results for associated production of the Higgs boson with vector boson at the LHC for the proton-proton center of mass energies of 7, 8, 13 and 14 TeV. The threshold contributions has been observed to make up to 75% of the exact QCD correction at NLO level while they are about 60% at Next-to-next-to leading order (NNLO) level, showing the significant contribution of the large logarithms that arise in the threshold limit. We have also estimated the theory uncertainties from the factorization and renormalisation scales and from the choice of the PDFs. While the hard part at the $N^3\text{LO}$ level is yet to be computed, we believe that these results, providing the first predictions in this direction towards the computation of the full $N^3\text{LO}$ for Higgs-Strahlung processes, will be useful for the phenomenological studies related to Higgs Physics at LHC.

List of Figures

2.1	the strong coupling constants as measured at different scales Q	27
3.1	Transverse momentum distribution of the hardest photon $P_T^{\gamma_1}$ (left panel) and invariant mass distribution $M_{\gamma\gamma\gamma}$ of the three photon (right panel) for the fixed order NLO and LO.	51
3.2	Rapidity distribution of the hardest photon Y^{γ_1} (left panel) and the three photon system $Y^{\gamma\gamma\gamma}$ (right panel) for the fixed order NLO and LO.	52
3.3	Separation of the softer photons (γ_2, γ_3) in comparison with the hardest one (γ_1) at LO and NLO.	53
3.4	Transverse momentum distribution of the hardest photon ($P_T^{\gamma_1}$) with R_γ variation for a fixed value of $n=1$ and $\varepsilon_\gamma=1$ (left panel) and for another fixed value of $n=1$ and $\varepsilon_\gamma=0.1$ (right panel).	54
3.5	Three photon transverse momentum distribution $P_T^{\gamma\gamma\gamma}$ for the fixed order NLO and NLO+PS.	55
3.6	Transverse momentum distribution $P_T^{\gamma_1}$ of the hardest photon (left panel) and invariant mass distribution $M_{\gamma\gamma\gamma}$ of the three photon system (right panel) for the fixed order NLO and NLO+PS.	58
3.7	Three photon rapidity distribution for the fixed order NLO and NLO+PS.	59

4.1	Fixed order NLO results (dashed brown) along with the NLO+PS results (solid blue) for the $\log_{10}(P_T)$ distribution of the e^+e^- (left), ZZ (middle) and W^+W^- (right) pair.	63
4.2	Invariant mass ($M_{e^+e^-}$) distribution (left) and transverse momentum distribution (right) of the e^+e^- pair for ADD ($d = 2$) and SM in Drell-Yan process. The right one is in $M_{e^+e^-} > 600$ GeV region.	64
4.3	Rapidity distribution (left) of e^+e^- pair and the angular distribution (right) are given for $d = 2$ in ADD and also for SM in Drell-Yan process for $M_{e^+e^-} > 600$ GeV.	65
4.4	Transverse momentum (left) and rapidity (right) distribution of final state positron in ADD ($d = 3$) and SM for Drell-Yan process for $M_{e^+e^-} > 600$ GeV.	66
4.5	Transverse momentum (left) and rapidity (right) distribution of final state electron in ADD ($d = 4$) and SM for Drell-Yan process for $M_{e^+e^-} > 600$ GeV.	66
4.6	Four-lepton invariant mass (M_{4l}) distribution for ADD ($d = 2$) and SM for decay products coming from the ZZ process.	68
4.7	Transverse momentum (left) and rapidity (right) distribution of the e^+e^- pair coming from ZZ decay for ADD ($d = 3$) and SM, when $M_{4l} > 600$ GeV.	68
4.8	Transverse momentum (left) and rapidity (right) distribution of the $\mu^+\mu^-$ pair coming from ZZ decay for ADD ($d = 4$) and SM, when $M_{4l} > 600$ GeV.	69
4.9	Invariant mass ($M_{e^+\mu^-E_{\cancel{T}}}$) distribution (left) of all the final state decay products of WW and the total missing transverse energy distribution (right) for $d = 5$ and SM. The right one is restricted within $2000 < M_{e^+\mu^-E_{\cancel{T}}} < M_S$ GeV.	69
4.10	Transverse momentum distribution (left) and rapidity distribution (right) of the final state positron which comes from W^+ decay for WW production process in both ADD ($d = 6$) and SM when, $2000 < M_{e^+\mu^-E_{\cancel{T}}} < M_S$ GeV.	70

5.1	Scale uncertainties of DY like contributions to ZH production cross sections for LHC13 by varying the factorization and renormalization scales in the range $0.1 < \mu/Q < 10.0$, where $\mu = \mu_F = \mu_R$	78
5.2	Scale uncertainties of DY like contributions to ZH production cross sections for LHC13. In the left panel, we show the renormalization scale uncertainty for $0.1 < \mu_R/Q < 10.0$ keeping $\mu_F = Q$ fixed. In the right panel, we show the factorization scale uncertainty for the similar range variation as μ_R	79
6.1	The comparison between NLO and NLO _{SV} with the renormalization scale $\mu_R = m_H$ and factorization scale $\mu_F = m_H/4$ at 8 TeV(left panel) and 13 TeV (right panel) LHC.	115
6.2	The rapidity distribution of the Higgs boson at NLO, NNLO(SV) and N ³ LO(SV) at 8 TeV(left panel) and 13 TeV (right panel) LHC. The band indicates the uncertainty due to renormalization scale.	118
6.3	The rapidity distribution of the Higgs boson at NLO, NNLO(SV) and N ³ LO(SV) at 8 TeV(left panel) and 13 TeV (right panel) LHC. The band indicates the uncertainty due to factorization scale.	118
6.4	The distribution of $K_1^{(SV)}$, K_1 , $K_2^{(SV)}$ and $K_3^{(SV)}$ at different perturbative order at 8 TeV(left panel) and 13 TeV (right panel) LHC.	119
6.5	The distribution of K_{NLO} , $K_{\text{NNLO}}^{(SV)}$ and $K_{\text{N3LO}}^{(SV)}$ at different perturbative order at 8 TeV(left panel) and 13 TeV (right panel) LHC.	120

List of Tables

3.1	Total cross sections for the 3-photon production at the LHC. The results are shown for two different cuts at LO, NLO, and the associated K-factor. Relative statistical errors of the Monte Carlo are below 10^{-5}	53
3.2	Total cross sections for the 3-photon production at the LHC for various Frixione isolation parameters. We have taken $p_T^\gamma > 20$ GeV at NLO.	55
4.1	Lower bounds on M_S for various extra dimensions d at the 14 TeV LHC with integrated luminosity of 10 fb^{-1} at 3-sigma and 5-sigma signal significance.	71
5.1	DY like contributions (in pb) to ZH production cross sections at the LHC for different center of mass energies (TeV) with MSTW2008 PDFs. The factorization and renormalization scales are set to $\mu_F = \mu_R = Q$	77
5.2	Total cross sections (in pb) for ZH production at the LHC for different center of mass energies (in TeV).	80
5.3	Total cross sections (in pb) for ZH production at LHC13 for different PDFs.	80
5.4	Total cross sections (in pb) for WH production at the LHC for different center of mass energies (in TeV).	80
6.1	Contributions at LO, NLO, NNLO(SV) and N ³ LO(SV) with the renormalization scale $\mu_R = m_H$ and factorization scale $\mu_F = m_H/4$ at 8 TeV LHC.	116
6.2	Contributions at LO, NLO, NNLO(SV) and N ³ LO(SV) with the renormalization scale $\mu_R = m_H$ and factorization scale $\mu_F = m_H/4$ at 13 TeV LHC.	117

Chapter 1

Introduction

At the moment, we, the particle physicists, are going through an exciting phase in the history of particle physics. The ATLAS and CMS group at the Large Hadron Collider (LHC) has discovered the most sought after particle, the missing piece in the Standard Model (SM), namely the Higgs boson [1, 2]. The SM is the holy grail of the particle physics in the sense that it describes all the interactions between the elementary particles. The three fundamental forces, namely weak, electromagnetic and the strong force are completely described by the SM. The Higgs boson completes the SM itself in the sense that it explains the mystery of the origin of the mass of the fundamental particles in the SM. However, in spite of its tremendous success, the fourth fundamental force, namely the gravitational force can not be described by the SM. The gravitational effects, being important on astrophysical scales, are supposed to be tiny enough to safely neglect them in most calculations dealing with interactions of elementary particles. But, still a complete theory describing all type of interactions between the elementary particles should contain the gravitational force. Moreover, the SM particle content can only describe 5% of this universe where as almost 95% energy content described by the dark matter and dark energy can not be explained within the SM framework. There are also certain experimental evidences like the neutrino oscillation, which requires the neutrino to be massive, can not be explained in the SM, where the neutrinos are treated as massless particle. All these shortcomings of the SM indicates towards new physics, thus paving the way of a plethora

of beyond standard models (BSM) trying to accommodate these questions.

On the other hand, the properties of SM particles has been measured to an unprecedented accuracy and so far no deviations has been found. Therefore, it suggests that no matter how the underlying theory describing nature might look like, in the limit of low energies, it has to imitate the SM at least in some way. These facts, namely that after countless experiments no deviation has been found for SM predictions till now as well as we know that the theory can not describe every interactions between the elementary particles puts us on alert with the upcoming run of the LHC at more higher energy, than ever. In this scenario, all the properties of the particles and the couplings should be measured with highest possible accuracy to look for certain deviations and at the same time all the beyond standard models (BSM) should be tested with a greater accuracy. To measure any deviation or to test the BSM models, the experimental observations should be compared with the theoretical predictions. With the accumulation of more data from the upcoming runs at LHC, the experimental uncertainties are surely going to decrease. So, to have any hope of penetrating the so far unexplored territory of the SM, the theoretical uncertainties should also decrease at the level of experiments. This, in turn needs an accurate description of the scattering processes at the LHC, thus demanding the inclusion of higher order terms in the QCD, as it will reduce the theoretical uncertainties arising from the missing higher order quantum corrections through the renormalisation and factorisation scales. The requirement of the inclusion of the higher order radiative corrections become vivid with the discovery of the Higgs boson, where the next-to-leading order prediction was almost twice the prediction at the leading order. Without, the precise prediction from the Higgs boson cross-section after the inclusion of higher order radiative corrections, it could not have been possible to pin-point this as a SM Higgs boson. In the same pathway, this thesis deals with the calculation of higher order radiative corrections for the processes of interest at LHC. We briefly discuss the particle content of the SM and then the shortcoming of the it, thus motivating the appearance of the BSM models. We specifically discuss the Large extra dimension models in this chapter. In the chapter 2, we start with the basic ingredients of the Quantum chromo-dynamics (QCD). We discuss the Lagrangian of the QCD, quantization and the renormalisation of it. Then

we show the different parts of a next-to-leading order calculation and describe the matching of the parton shower with a introduction to parton shower algorithms. After that, we also discuss the threshold corrections to approximate the higher orders. In chapter 3 we show the application of matching the parton shower with next-to leading order results and report various observations. The chapter 4 deals with the di-lepton, ZZ , WW production in SM and ADD model and present the results at next-to leading order after matching with parton shower. We apply the techniques of obtaining the threshold corrections at third order in QCD to obtain the inclusive cross-section of the production of the Higgs boson associated with a vector boson in chapter 5. We also present the framework for obtaining the threshold corrections in QCD in chapter 6, thereby producing the results for the rapidity distribution of the Higgs boson production from bottom quark annihilation. Here we start with a brief introduction of the SM in the next section.

1.1 Standard Model

The SM is an outstandingly successful and well tested theory for the description of the elementary particles and their interactions. The SM describes three of the four fundamental forces, namely weak, electromagnetic and strong force with an unrivaled precision. However, the gravity is not included as the Einstein field equations describing it can not be quantised in a consistent way. The spectrum of the particles in the SM consists of fermions and bosons. The fermions have half-integer spin while the bosons have integer spin. The fermions are further divided into left and right handed quarks

$$\begin{aligned}
 & \begin{pmatrix} u \\ d \end{pmatrix}_L, \quad \begin{pmatrix} c \\ s \end{pmatrix}_L, \quad \begin{pmatrix} t \\ b \end{pmatrix}_L \\
 & u_R, \quad d_R, \quad c_R, \quad s_R, \quad t_R, \quad b_R
 \end{aligned} \tag{1.1}$$

and left and right handed leptons.

$$\begin{pmatrix} e \\ \nu_e \end{pmatrix}_L, \quad \begin{pmatrix} \mu \\ \nu_\mu \end{pmatrix}_L, \quad \begin{pmatrix} \tau \\ \nu_\tau \end{pmatrix}_L$$

$$e_R, \quad \mu_R, \quad \tau_R \tag{1.2}$$

There is no right handed neutrino as they have not been observed in any of the experiments and as a result they do not exist in SM, thus keeping the neutrino massless. The bosons in the SM with spin 1 are the force carriers of the strong and electroweak force. The gluons act as the force carrier of the strong force. The photons act as the force courier of the electromagnetic force whereas the W and Z bosons are the carrier of the weak force. In addition, there exists a boson of spin 0, the only fundamental scalar particle in the model, that is the Higgs boson, which has been recently discovered at LHC by both the experiments ATLAS [1] and CMS [2]. This whole particle spectrum can be described via a quantum field theory based on the principle of the local gauge invariance with the underlying gauge group $SU(3)_C \times SU(2)_L \times U(1)_Y$, namely the SM. It comprises of Quantum Chromo dynamics (QCD) [3,4], which describes the strong interactions between quarks and gluons in terms of the $SU(3)_C$ gauge group, and the electroweak interactions [5, 6], which are described via the $SU(2)_L \times U(1)_Y$ group. The group $SU(2)_L \times U(1)_Y$ is spontaneously broken to $U(1)_{em}$, the group of Quantum Electrodynamics (QED), through the introduction of a scalar field which acquires a non-vanishing vacuum expectation value. This phenomenon is called the electroweak symmetry breaking (EWSB) and the scalar field is the Higgs field. The fermions and the heavy gauge bosons $W^{+/-}$ and Z acquire mass through this symmetry breaking in a gauge invariant way, which is also known as the Higgs mechanism [7–10].

1.2 Beyond Standard Model

Over the last decades the SM has been tested to an unprecedented accuracy in countless experiments. However, so far no significant deviations have been found and with the recent discovery of the Higgs boson it has become the most successful theory to explain the phenomenons in the particle physics. However, there are certain questions still unanswered in the SM. An obvious shortcoming of the SM is the lack of an explanation for the gravitational interaction between massive particles. So far no convincing embedding of this fundamental force in the SM has been achieved. Furthermore, a unification of the strong and electroweak interactions has not been achieved yet. The renormalisation group equation of the couplings in the SM suggest that the couplings should unify after extrapolation of the corresponding coupling to a high energy scale. However, it has not been realized completely in the SM framework. In addition to this experimental observations hinting at physics beyond standard model (BSM) is the existence of dark matter. There is no viable candidate for this dark matter, which constitutes almost 25% of the energy content of our universe. Even the so-called dark energy, accounting roughly 70% of the total energy content of the universe, whose existence is postulated in order to explain the expansion of the universe has not been explained in the SM. There are also certain experimental observations indicating towards BSM. The observation of neutrino oscillation implies that neutrino should have mass, however the SM forbids any mass term for the neutrinos, thus clearly indicating to the pathway of BSM. There exists also the so-called hierarchy problem which tries to understand the large difference between the electroweak scale (1 TeV) and the Planck scale (10^{19} GeV). All of these arguments clearly point towards new physics not explained in the SM and as a result many beyond standard models were postulated to explain these shortcomings of the SM. In this context, to address the hierarchy problem mainly, along with other inefficiencies of the SM, a large number of extra dimensional models came into the picture. In this thesis, we will discuss only the Large extra dimension (LED) models prescribed by Arkani-Hamed, Dimopolous and Dvali, which is also abbreviated as ADD model [11–13].

1.2.1 ADD Model

Arkani-Hamed, Dimopolous and Dvali proposed a very interesting idea of allowing extra spatial dimensions to our usual 4 space-time dimension pioneered by Arkani-Hamed, Dimopolous and Dvali. So, the number of space-time dimension is assumed to be $4 + d$, where d is the number of extra spatial dimensions. As, in the real life we do not observe any of these extra dimensions, so these are compactified on a d -dimensional torus of radius $R/2\pi$. The introduction of these extra spatial dimensions modify both electromagnetic and gravitational inverse square laws. However, the inverse square law of the electromagnetic forces has been tested to a very high precision $\sim M_{EW}^{-1}$ and no indication of deviation has been found. On the other hand the gravitational forces has not been probed to a accuracy of $\sim M_{Pl}^{-1}$. Moreover, it has only been probed to $\sim 1\mu m$ [14], till date. So, the SM fields are kept constrained, where they are localized in the 3-dimensional brane and the gravity is allowed to propagate in all the dimensions taking the advantage of the possibility of the modification of it, depending on the present accuracy. As a result of it, the fundamental scale M_S of the full theory can be related to the effective Planck scale (M_{Pl}) in 4-dimension through the volume of the compactified d extra spatial dimensions.

$$M_{Pl}^2 \sim M_S^{d+2} R^d. \quad (1.3)$$

Now, if we put the $M_S \approx M_{EW}$ then the full theory has only one fundamental scale, thereby solving the hierarchy problem present between the two fundamental scales in the usual 4 space-time dimension. With this the value of R can be estimated from Eq. 1.3 keeping the usual value of M_{Pl}

$$R \sim 10^{\frac{30}{d}-17} \text{cm} \times \left(\frac{1\text{TeV}}{M_{EW}} \right)^{1+\frac{2}{d}}. \quad (1.4)$$

From the Eq. 1.4, we can observe that $d = 1$ is excluded empirically as it implies deviation from the Newtonian gravity over a range of solar system distances ($R \sim 10^{13}$ cm), which is not the case. For all $d \geq 2$, however, the modification of gravity only becomes noticeable at distances smaller than those currently probed by experiment.

The spectrum of this model consists of the SM fields and a tower of Kaluza-Klein (KK) modes of the graviton fields, resulting from the compactification of the extra dimensions. In the effective theory valid below the scale M_S , these gravitons couple to the SM fields irrespective of their charge, colour and flavour, as given by the following Lagrangian [15, 16]

$$\mathcal{L} = -\frac{\kappa}{2} \sum_{\vec{n}=0}^{\infty} T^{\mu\nu}(x) h_{\mu\nu}^{(\vec{n})}(x), \quad (1.5)$$

where $\kappa = \sqrt{16\pi}/M_{Pl}$ and $T^{\mu\nu}$ is the energy-momentum tensor of the SM fields on the 3-brane. The $h_{\mu\nu}^{(\vec{n})}$ contains one spin-2 state, $(n-1)$ spin-1 states and $n(n-1)/2$ spin-0 states for any given KK level \vec{n} . All these states are mass-degenerate and mass of the n^{th} level is given by,

$$m_{\vec{n}}^2 = \frac{4\pi^2 \vec{n}^2}{R^2}. \quad (1.6)$$

This mass spectrum is cutoff at the scale M_S . The zero mode of the KK tower corresponds to the 4-dimensional massless graviton.

The Feynman rules for the above interaction Lagrangian are given in [15, 16]. With this Lagrangian, the graviton fields can interact with the SM fields virtually in the intermediate state or can be produced really in the final state. In the context of collider phenomenology, this indicates interesting signals that can be explored at the present LHC. The virtual exchange of the gravitons can lead to the deviation from the SM predictions whereas the real emission of the gravitons can lead to the missing energy signal. Although the coupling of the graviton field to the SM fields is suppressed by M_{Pl} order, the large multiplicity of the available KK graviton modes lead to observable effects. In a process involving a virtual exchange of KK modes from SM particles, the sum of KK propagators

$\mathcal{D}(Q^2)$ is given by

$$\begin{aligned}\kappa^2 \mathcal{D}(Q^2) &= \kappa^2 \sum_n \frac{1}{Q^2 - m_n^2 + i\epsilon}, \\ &= \frac{8\pi}{M_S^4} \left(\frac{Q}{M_S}\right)^{(d-2)} \left[-i\pi + 2I(\Lambda/Q)\right],\end{aligned}\tag{1.7}$$

where, Q is the invariant mass of the final state particles. The integral $I(\Lambda/Q)$ is a result of the summation over the non-resonant KK modes and the term proportional to π is due to the resonant production of a single KK mode [15]. Λ is the explicit cut-off on the KK sum which is identified with the scale of the extra dimension theory M_S [15, 16]. The κ^2 suppression in a virtual exchange is compensated for by the high multiplicity, after the KK modes are summed over. This collective contribution of the KK modes result in their non-negligible interaction with the SM fields and offer the best possibility of probing the low scale quantum gravity effects at the LHC. In this thesis, we follow the approach of [15] retaining the details of the number of extra dimensions.

Chapter 2

Basics of QCD

Wealth of data from the Large Hadron Collider (LHC) and the Tevatron involving large number of leptons, gauge bosons and hadrons in the final state not only provides ample opportunity to test the predictions of the SM, but also constrains various physics scenarios in the BSM. Signatures of BSM are often plagued by the large SM background and hence careful study of wide variety of SM processes has been underway [17–19] as emphasized in the chapter 1. To facilitate this purpose we discuss the basics of QCD in the following sections. We start with a brief overview of the Lagrangian of QCD and then discuss the issues of renormalisation of QCD Lagrangian. Then we discuss the most striking feature of the QCD, namely the asymptotic freedom. After that we discuss the procedure of obtaining the predictions at colliders using the perturbative QCD as the guiding principle.

2.1 Lagrangian of QCD

QCD is the renormalisable quantum theory of the strong interaction in the SM. As already mentioned previously, it is based on the gauge group $SU(3)$ which describes the interactions of the quarks and the gluons. There are six flavours of quarks of spin- $\frac{1}{2}$ and each of these flavours come in three colors which furnish the fundamental representation of the $SU(3)$ gauge group. The gluons

which are the carriers of this strong force transform under the adjoint representation of this gauge group. The Lagrangian of the QCD can be divided mainly in three parts.

$$\mathcal{L} = \mathcal{L}_{classical} + \mathcal{L}_{gauge-fixing} + \mathcal{L}_{ghost} \quad (2.1)$$

The classical part consists the interaction between the quarks and the gluons.

$$\mathcal{L}_{classical} = \sum_{i=1}^{n_f} \bar{\psi}_i (i\gamma^\mu D_\mu - m_i) \psi_i - \frac{1}{4} Tr[F_{\mu\nu}^a F^{a\mu\nu}], \quad (2.2)$$

where the summation on i runs over all the quark flavours and

$$F_{\mu\nu}^a = \partial_\mu A_\nu^a - \partial_\nu A_\mu^a - g_s f_{abc} A_\mu^b A_\nu^c, \quad (2.3)$$

$$D_\mu = \partial^\mu - ig_s T^a A_\mu^a \quad (2.4)$$

The $F_{\mu\nu}^a$ represents the field strength tensor of the gluonic field and D_μ is the covariant derivative. The mass of the i^{th} flavour is denoted by m_i and g_s is the strong coupling constant while T^a and f^{abc} are the generators and the structure constants of the gauge group SU(3), respectively. They obey the following relation.

$$[T^a, T^b] = if_{abc} T^c, \quad (2.5)$$

The classical Lagrangian part suffers from the fact that it is impossible to define the propagator of the gluonic field at the time of quantization to obtain a consistent quantum theory of the quarks and gluons. It stems from the point that the gluon fields have the freedom of gauge transformations, which can be removed by putting constraint on these gauge fields, denoted by gauge-fixing. Here we choose the covariant-gauge with parameter ξ , which is manifestly Lorentz-invariant.

$$\mathcal{L}_{gauge-fixing} = -\frac{1}{2\xi} (\partial^\mu A_\mu^a)^2, \quad (2.6)$$

Still, we have to include the \mathcal{L}_{ghost} , consisting of the ghost fields, which cancel the effects of the unphysical time like and longitudinal polarization states of the gauge fields to obtain a consistent quantized theory. This is defined as the following:

$$\mathcal{L}_{ghost} = \partial^\mu \bar{\chi}^a (\partial_\mu \chi^a - g_s f^{abc} \chi^b A_\mu^c), \quad (2.7)$$

Here the ghost fields $\chi, \bar{\chi}$ are the complex scalar field obeying the Fermi statistics.

With the construction of these three pieces now the Lagrangian in Eq. 2.1 describes a consistent quantum theory of the quarks and the gluons. The Feynman rules can be derived following the standard procedures to compute gauge invariant products of the quantum field operators. Using these rules, physical observables like scattering cross-section, decay rates can be calculated by using the techniques of perturbation theory and treating the strong coupling constant as an expansion parameter. Now the physical amplitude for a scattering process can be written as the sum of all the topologically distinct Feynman diagrams, which is true in every perturbative order. The higher order amplitudes contain loop diagrams where the loop momentum should be integrated fully. These integrals often face divergence, known as ultra-violet (UV) divergence, in the usual 4 space-time dimension. These divergent integrals are made tentatively finite by introducing suitable techniques known as regularization procedure. One of the systematic way of doing it is to analytically continue the theory to $n = 4 + \varepsilon$ space-time dimension, known as dimensional regularisation (DR) which preserves both Lorentz as well as gauge invariance. As a result of it these divergences show up as poles in the usual 4 space-time dimension. Now we can redefine the perturbation series by readjusting the definition of the bare fields and the bare parameters (couplings, masses, ...) to absorb the singularities, thereby rendering finite physical amplitudes. This is called renormalisation which we will describe below. The renormalisation procedure starts with defining the bare fields

and the parameters in terms of the renormalised ones.

$$\begin{aligned}
A_\mu^a &= Z_3^{1/2} A_{\mu,R}^a, & \psi &= Z_2^{1/2} \psi_R, \\
\chi^a &= \tilde{Z}_3^{1/2} \chi_R^a, & g_s &= Z_g^{1/2} g_{s,R}, \\
\xi &= Z_3^{1/2} \xi_R, & m_i &= Z_m m_{i,R}
\end{aligned} \tag{2.8}$$

where, the constants Z_3, \tilde{Z}_3 and Z_2 are called the gluon, ghost and quark field renormalisation constants, respectively while the constants Z_g and Z_m are called coupling constant and mass renormalisation constants. Now putting back these redefinitions in 2.1 we get

$$\begin{aligned}
\mathcal{L}(\psi, A_\mu^a, \chi^a, g_s, m_i, \xi) &= \mathcal{L}_R(\psi_R, A_{\mu,R}^a, \chi_R^a, g_{s,R}, m_{i,R}, \xi_R) \\
&+ \mathcal{L}_c(\psi_R, A_{\mu,R}^a, \chi_R^a, g_{s,R}, m_{i,R}, \xi_R, Z_i)
\end{aligned} \tag{2.9}$$

where, \mathcal{L}_R has the same precise functional form like \mathcal{L} , only all the parameters and the fields replaced by their renormalised counterparts with the subscript denoted by R . The counter term Lagrangian \mathcal{L}_c is chosen in such a way that it preserves all the symmetry of the theory. After this, the Ultra-Violet (UV) divergences coming from the loop momentum being infinite, which appear as poles due to the dimensional regularisation, are absorbed by adjusting the constants Z_i suitably to make the amplitudes finite. These Z_i s are only unambiguously defined up to the divergent pieces. During the adjustment, finite pieces can also be redistributed in terms of bare and renormalised quantities, in principle. This freedom is removed via the choice of a specific renormalisation scheme. In this thesis, we have used the modified minimal subtraction scheme ($\overline{\text{MS}}$) where we include the γ_E and $\log 4\pi$ finite pieces with the pole term in the combination

$$\frac{1}{\epsilon} - \gamma_E + \log 4\pi \tag{2.10}$$

The details of these has been discussed extensively in the reference [20].

2.2 The running coupling

Till now, we have used dimensional regularization to handle the UV divergences appearing in the loop diagrams. In the process of going from 4 to $4 + \varepsilon$ dimensions, we have introduced an arbitrary ‘renormalisation’ scale μ_R , in order to keep consistent dimensions (units) for all quantities. In $n = 4 + \varepsilon$ dimension, the bare and renormalized strong coupling constant looks like this

$$\hat{g}_s = \hat{g}_s \left(\frac{1}{\mu} \right)^{\frac{\varepsilon}{2}}, \quad g_{s,R} = g_s \left(\frac{1}{\mu_R} \right)^{\frac{\varepsilon}{2}} \quad (2.11)$$

Now we define $\hat{\alpha}_s(\mu^2)$ and $\alpha_s(\mu_R^2)$ by,

$$\hat{\alpha}_s(\mu^2) = \frac{g_s^2(\mu^2)}{4\pi}, \quad \alpha_s(\mu_R^2) = \frac{g_{s,R}^2(\mu_R^2)}{4\pi} \quad (2.12)$$

Then the g_s equation in Eq. 2.8 looks like

$$\hat{\alpha}_s(\mu^2) \mu^{-\frac{\varepsilon}{2}} = Z_g \left(\alpha_s(\mu_R^2), \frac{1}{\varepsilon} \right) \alpha_s(\mu_R^2) \mu_R^{-\frac{\varepsilon}{2}} \quad (2.13)$$

The observation that the left hand side of the above equation is independent of the renormalisation scale μ_R , implies that the variation of it with respect to μ_R will be zero. This is called renormalisation group (RG) equation.

$$\begin{aligned} \mu_R^2 \frac{d}{d\mu_R^2} \ln \alpha_s(\mu_R^2) &= \frac{\varepsilon}{2} - \mu_R^2 \frac{d}{d\mu_R^2} \ln Z_g(\mu_R^2) = \frac{\varepsilon}{2} + \frac{1}{\alpha_s(\mu_R^2)} \beta(\alpha_s(\mu_R^2)) \\ &= \frac{\varepsilon}{2} - \sum_{i=0}^{\infty} \alpha_s^{i+1}(\mu_R^2) \beta_i \end{aligned} \quad (2.14)$$

where, we define the beta function as

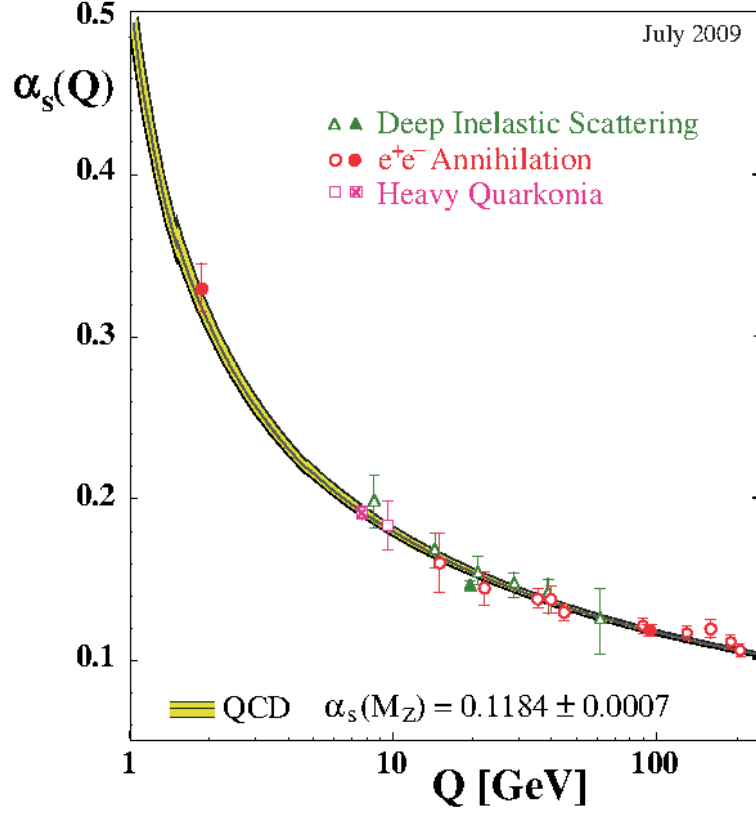


Figure 2.1: the strong coupling constants as measured at different scales Q .

$$\beta(\alpha_s(\mu_R^2)) = -\alpha_s(\mu_R^2)\mu_R^2 \frac{d}{d\mu_R^2} \ln Z_g(\mu_R^2) \quad (2.15)$$

Using the one loop and two loop results of Z_g we get

$$\begin{aligned} \beta_0 &= \frac{11}{3}C_A - \frac{2}{3}n_f T_f, \\ \beta_1 &= \frac{34}{3}C_A^2 - 4T_F n_f C_F - \frac{20}{3}T_F n_f C_A, \end{aligned} \quad (2.16)$$

The negative sign in the beta function is the origin of the asymptotic freedom, which implies that the coupling becomes weaker at high energy scales, i.e., the quarks and gluons almost become free particles. Consequently, it implies that for large momentum transfer, we can study the interaction between the quarks and gluons by means of a perturbative expansion, evaluating the Feynman diagrams. Conversely, at low energy scales the coupling grows strong, causing quarks and gluons

to be tightly bound into the hadrons. The negative sign in the beta function comes as a result of the interaction between the gluons.

By solving the Eq. 2.14 we get the following expression for the strong coupling constant to one loop accuracy:

$$\alpha_s(Q^2) = \frac{\alpha_s(\mu_0^2)}{1 + \beta_0 \alpha_s(\mu_0^2) \ln(Q^2/\mu_0^2)} + \mathcal{O}(\alpha_s^2(\mu_0^2)) \quad (2.17)$$

Only for scales $Q \gg \mu_0$, the value of the strong coupling constant corresponds to $\alpha_s(Q^2) \ll 1$, thus making the perturbation theory valid in terms of expansion of the small parameter $\alpha_s(Q^2)$. The reference scale at which the perturbation theory fails is called the Λ_{QCD} , which is taken as 200 MeV, the value being closely connected with the scale of hadron masses.

In the figure 2.1 we show the summary of measurements of the strong coupling at various energy scales, which exhibits a tremendous agreement with the theoretical prediction for the running of α_s , shown as a band. the band represents the uncertainty associated with fixing the initial condition from the measurement at the time of solving the renormalisation group equation.

Using this property, namely the asymptotic freedom of QCD, we can predict the observables at the colliders involving high momentum transfers. In the high energy range the strong coupling constant becomes small and we can expand the observables in a perturbative series using the strong coupling constant as the expansion parameter. In the next section we show in details the procedure of predicting the observables at collider.

2.3 QCD at Collider

Usually, at colliders, the phenomenons with high momentum transfer are investigated. Here the colliding particles may be leptons, hadrons or lepton and hadron. In this thesis, we discuss the hadron-hadron cross-section in the context of LHC. In the parton model, the hadronic cross-section ($\sigma^{H_1 H_2}$) can be expressed in terms of the bare partonic cross-sections $\hat{\sigma}_{ab}$, $a, b = q, \bar{q}, g$ and bare

parton distribution functions $\hat{f}_c(x_i)$, $i = 1, 2$ and $c = q, \bar{q}, g$ of colliding partons as follows:

$$\sigma^{H_1 H_2}(S, Q^2) = \int dx_1 \int dx_2 \hat{f}_a(x_1) \hat{f}_b(x_2) \hat{\sigma}_{ab}(\hat{s}, Q^2) \quad (2.18)$$

where $S = (P_1 + P_2)^2$ and $\hat{s} = (x_1 P_1 + x_2 P_2)^2$ are the center of mass energies of incoming hadrons and partons respectively. Q is the invariant mass of the final state particles. The bare parton distribution function $\hat{f}_c(x)$ describes the probability of finding a parton of type c which carries a momentum fraction x of the hadron. The ‘hat’ denotes the fact that the corresponding terms suffer from various divergences. The parton distribution functions describe the long distance part of the hadronic cross-section and hence they are not computable in perturbative QCD as the strong coupling constant is large at small energy. On the other hand, the bare partonic cross-sections $\hat{\sigma}_{ab}$ that describe the short distance part can be computed in the framework of perturbative QCD exploiting the asymptotic freedom of the strong coupling constant. The hadronic cross-section can be written in terms of convolution of these functions in the following,

$$\begin{aligned} \sigma^{H_1 H_2}(S, Q^2) &= \frac{1}{S} \hat{f}_a \otimes \hat{f}_b \otimes \hat{\Delta}_{ab}(Q^2) \\ &= \frac{1}{S} \int dx_1 \int dx_2 \int dz \hat{f}_a(x_1) \hat{f}_b(x_2) \hat{\Delta}_{ab}(z, Q^2) \delta(\tau - zx_1 x_2) \end{aligned} \quad (2.19)$$

where,

$$\hat{\Delta}(z, Q^2) \equiv \hat{s} \hat{\sigma}_{ab}(\hat{s}, Q^2), \quad z = \frac{Q^2}{\hat{s}} \quad \tau = \frac{Q^2}{S} \quad (2.20)$$

Beyond the leading order in perturbative QCD, additional subprocesses namely, loops with virtual partons as well as from emission of additional real partons contribute to the partonic cross-sections $\hat{\sigma}_{ab}$. The virtual diagrams suffer from the UV divergences when loop momenta becomes large. Due to the massless nature of the partons, the virtual diagrams also suffer from the soft and collinear divergences, which are known as Infra-red (IR) divergences. In the case of real emission processes,

the IR divergences come from the soft and collinear region of the phase space integrals. These divergences are regularised via the dimensional regularisation technique after analytically continuing the theory to $n = 4 + \varepsilon$ dimension, with ε being a complex number. As a result of it, the divergences of the partonic cross-sections appear as poles in $1/\varepsilon^k$ where k is an integer. The partonic cross-section is then renormalised by redefining the bare fields and parameters to remove the UV divergences present, thereby introducing an arbitrary scale, known as the renormalisation scale. The soft and final state collinear singularities, where the additional parton becomes collinear with a final state particle, arising from the virtual as well as real emission diagrams cancel among themselves upon the summation of all possible degenerate states, thanks to the Kinoshita-Lee-Nauenberg (KLN) theorem [21]. The initial state collinear singularities, where the additional parton becomes collinear with a initial state particle, do not cancel and this cancellation is achieved via mass factorisation where one redefines the bare parton distribution functions at a scale called factorisation scale μ_F in such a way that the collinear singularities in the bare partonic cross-sections are absorbed. Now, after this regularisation and the renormalisation in a particular scheme, we can express the hadronic cross-section as follows, generalising to all orders:

$$\begin{aligned} \Delta^{H_1 H_2}(S, Q^2) &= f_a(\tau, \mu_F^2) \otimes f_b(\tau, \mu_F^2) \otimes \Delta_{ab}(Q^2, \mu_F^2) \\ &= \sum_{a,b=q,\bar{q},g} \int_{\tau}^1 \frac{dx_1}{x_1} \int_{\tau/x_1}^1 \frac{dx_2}{x_2} f_a(x_1, \mu_F^2) f_b(x_2, \mu_F^2) \Delta_{ab}\left(\frac{\tau}{x_1 x_2}, Q^2, \mu_F^2\right) \end{aligned} \quad (2.21)$$

with,

$$f_a(\tau, \mu_F^2) = \Gamma_{ab}(\tau, \mu_F^2, \varepsilon) \otimes \hat{f}_b(\tau) \quad (2.22)$$

$$\Delta_{ab}(z, Q^2, \mu_F^2) \equiv [\Gamma^{-1}(\mu_F^2, \varepsilon)]^T \otimes \hat{\Delta}(Q^2) \otimes \Gamma^{-1}(\mu_F^2, \varepsilon) \quad (2.23)$$

The $f_a(\tau, \mu_F^2)$ is the renormalised parton distribution function which is renormalised by the $\Gamma_{ab}(\tau, \mu_F^2, \varepsilon)$ kernel containing the right poles in $1/\varepsilon$ to cancel the residual initial collinear singularities in the bare partonic cross-sections. This procedure is called mass factorisation. $\Delta(z, Q^2, \mu_F^2)$ is the renor-

malised partonic cross-section which is now free of all the divergences. and can be expanded in terms of the strong coupling constant as following.

$$\Delta_{ab}(z, Q^2, \mu_F^2) = \sum_{i=0}^{\infty} \frac{\alpha_s^i(\mu_R^2)}{4\pi} \Delta_{ab}^{(i)}(z, Q^2, \mu_F^2, \mu_R^2) \quad (2.24)$$

Here, $i = 0$ corresponds to Leading order (LO), $i = 1$ corresponds to Next-to leading order (NLO) and so on. In principle, we should take into account of all the terms in this perturbative series. However, it is not feasible process to calculate each term due to technical difficulties and also as the values of the strong coupling constant is small, the higher powers of it become further small, thereby making it meaningful to consider a few terms in the expansion for predicting any observable. The factorisation scale μ_F and the renormalisation scale μ_R , introduced in the procedure to obtain the finite hadronic cross-section, parametrises the theoretical uncertainties present in the partonic cross-section due to the absence of the higher order terms. Depending on the accuracy of the prediction, which in turn is estimated by the variation of the unphysical scales μ_F and μ_R , we can have fixed order predictions, fixed order prediction matched with Parton Shower (PS) and approximate fixed order prediction. In case of the fixed order prediction one calculates the i^{th} term in the Eq. 2.24 and obtains the NⁱLO prediction. Here we show these procedure of calculating these precise predictions in detail in the following. we start with the discussion of the bits and pieces of a generic NLO calculation.

2.4 Anatomy of NLO Calculation

$$\begin{aligned} d\hat{\sigma}_{ab}^{NLO} &= \int dPS_n S(\{p\}_{1,n+2}) d\hat{\sigma}_{ab}^{(0)} \\ &+ \frac{\alpha_s(\mu_R)}{4\pi} \left[\int dPS_n S(\{p\}_{1,n+2}) d\hat{\sigma}_{ab}^{V,(1)} + \int dPS_n S(\{p\}_{1,n+2}) d\hat{\sigma}_{ab}^{CT,(1)} \right. \\ &\left. + \int dPS_{n+1} S(\{p\}_{1,n+3}) d\hat{\sigma}_{ab}^{R,(1)} + \int dPS_n S(\{p\}_{1,n+2}) d\hat{\sigma}_{ab}^{MF,(1)} \right] \quad (2.25) \end{aligned}$$

Any NLO cross-section for $2 \rightarrow n$ process can be written as above. The first term is the Born contribution; dPS_n is the phase space measure of the final state particles and $S(\{p\}_{1,m})$ is the observable function which depends on the kinematic variables through the momenta of the external particles *i.e.*, p_1, p_2, \dots, p_m . The second term corresponds to the one loop virtual contributions. The UV divergences due to the large loop momentum are first regularised and then renormalized as discussed in the previous Sect. 2.1 using the counter terms given in the third term. The fourth term refers to the real emission contributions due to additional parton emission. The fifth term is the mass factorisation term required to cancel the initial state collinear singularities as discussed previously in the Sect. 2.3. As discussed earlier, both virtual and real emission contributions encounter soft and collinear divergences, namely the IR divergences. The soft and final state collinear divergences get canceled after summing the virtual as well as the real emission processes. In case of the virtual processes the divergence shows up as poles due to dimensional regularization, which can remove both UV and IR divergences at the same time. After the removal of UV divergences the IR divergences remain explicitly as poles. However, for the real emission processes the poles will only be explicit after the phase space integration and this integral faces divergence at the phase space points giving rise to soft and collinear configuration. In the next section we discuss the reduction of one loop tensor integrals required for the virtual corrections and the procedure to extract the singularities in case of real emission amplitudes.

2.4.1 Virtual correction

The reduction of tensor integrals to scalar ones in n dimensions is done using the standard procedure Passarino-Veltman [22–24]. The tensor integrals that appear at one loop level are of the form

$$I_n^{\mu_1 \dots \mu_m} = \int \frac{d^n l}{(2\pi)^n} \frac{l^{\mu_1} \dots l^{\mu_m}}{((l - q_1)^2 + i\epsilon) \dots ((l - q_n)^2 + i\epsilon)} \quad , \quad (2.26)$$

where

$$q_1 = p_1, q_2 = p_1 + p_2, \dots, q_n = \sum_{i=1}^n p_i \quad . \quad (2.27)$$

One can decompose the above tensor integral in terms of scalar coefficients as follows:

$$I_n^{\mu_1 \dots \mu_n} = \sum_{i_1, \dots, i_m}^n q_{i_1}^{[\mu_1} \dots q_{i_m}^{\mu_m]} F_{i_1 \dots i_m}^{(n)} + \sum_{i_3, \dots, i_m}^n g^{[\mu_1 \mu_2} q_{i_3}^{\mu_3} \dots q_{i_m}^{\mu_m]} F_{00 i_3 \dots i_m}^{(n)} \quad , \quad (2.28)$$

where the square bracket implies the non-equivalent symmetrisation by giving the full set of non-equivalent permutations. As described in [25], these co-efficients are related to the scalar integrals in different space-time dimensions in the following way,

$$I_{n, i_1, i_2, \dots}^{[2i], s_1, s_2, \dots} = \int \frac{d^{n+2i}l}{(2\pi)^{n+2i}} \prod_{r=1}^n \frac{1}{((l - q_r)^2 + i\epsilon)^{1 + \delta_{r i_1} + \delta_{r i_2} + \dots - \delta_{r s_1} - \delta_{r s_2} - \dots}} \quad , \quad (2.29)$$

where $I_{n, i_1, i_2, \dots}^{[2i], s_1, s_2, \dots}$ is a generalized scalar integral in shifted space-time dimension. These integrals in the shifted dimensions can be expressed in terms of integrals in n dimensions using the dimensional recurrence relations discussed in [26, 27]. In this approach, inverse Gram determinants that result from the recurrence relations, often spoil the numerical stability of the integral. There exists a handful of solutions to this problem in the literature [28–38]. Recently, an elegant approach has been put forward in [39], where the authors have found signed minor algebraic relation, which avoids the appearance of inverse Gram determinants and thereby introducing a set of higher dimensional scalar integrals to cope with the small Gram determinants. These higher dimensional scalar integrals have been evaluated numerically after employing a series expansion in the small Gram region. This whole algorithm has been implemented in the numerical package, named PJFry [40, 41], which we have used in this thesis to evaluate numerically the scalar co-efficients of the tensor integral for every phase space point in n dimensions. PJFry reduction library uses QCDLoop [42] and OneLOop [43] to evaluate the scalar integrals in 4 dimensions.

2.4.2 Real emission correction

To make the IR poles explicit in case of real emission processes we adopt the subtraction techniques, where we add and subtract a counter term with both the virtual and real, having the same point wise singular behavior like the real emission part. Furthermore, this has to be chosen such that it can be integrated analytically over the one-particle phase space dPS_1 , i.e. the form has to be chosen such that this integration is feasible. This term is then subtracted and added in Eq. 2.25 as follows:

$$\begin{aligned}
d\hat{\sigma}_{ab}^{NLO} = & \int dPS_n S(\{p\}_{1,n+2}) d\hat{\sigma}_{ab}^{(0)} \\
& + \frac{\alpha_s(\mu_R)}{4\pi} \left[\int dPS_n S(\{p\}_{1,n+2}) \left[d\hat{\sigma}_{ab}^{V',(1)} + \int dPS_1 d\hat{\sigma}_{ab}^{S,(1)} \right] \right. \\
& \left. + \int dPS_{n+1} S(\{p\}_{1,n+3}) \left[d\hat{\sigma}_{ab}^{R,(1)} - d\hat{\sigma}_{ab}^{S,(1)} \right] + \int dPS_n S(\{p\}_{1,n+2}) d\hat{\sigma}_{ab}^{MF,(1)} \right] \quad (2.30)
\end{aligned}$$

Hence the total NLO result is left unaltered by these additional terms. Here, in the Eq. 2.30 $d\hat{\sigma}_{ab}^{V',(1)}$ is the UV renormalized virtual expression with the IR divergences remaining as the poles in terms of the regulator of the dimensional regularization. Likewise, the analytical integration of the subtraction term over the one-particle emission phase space, $\int dPS_1 d\hat{\sigma}_{ab}^{S,(1)}$, is performed in d dimensions. With this approach the IR divergences can be extracted analytically as poles and cancel the corresponding poles occurring in the virtual contributions and the integration over the n-particle phase space can be performed numerically. The integral $\int dPS_{n+1} S(\{p\}_{1,n+3}) \left[d\hat{\sigma}_{ab}^{R,(1)} - d\hat{\sigma}_{ab}^{S,(1)} \right]$ is integrable by construction, as the IR divergences are canceled point wise, hence this term can be evaluated numerically, too. The explicit construction of this counter term is based on the factorization of the QCD amplitudes in the soft/collinear limit. There are several methods differing in the organization of the actual subtraction. The most widely used approaches are the dipole subtraction formalism introduced by Catani and Seymour [44] and the method by Frixione, Kunszt and Signer (FKS) [45]. We have used the FKS subtraction procedure in this thesis. This subtraction procedure

has been already implemented in an automated fashion in MADFKS package [46]. We will discuss the FKS subtraction in detail in the following.

2.4.2.0.1 FKS Subtraction Now we show the details of the FKS subtraction procedure. The contribution from the real emission part can be written as:

$$d\sigma^{Real} = |M_{ab}^{n+1}|^2 dPS_{n+1} \quad (2.31)$$

where $|M_{ab}^{n+1}|^2$ is the matrix element squared for the real emission part and dPS_{n+1} the differential phase-space. The squared matrix element blows up like $\frac{1}{\xi_i^2} \frac{1}{1-y_{ij}}$, where ξ_i is the fraction of the energy of final state particle i with respect to the total partonic energy in the center of mass frame, $\xi_i = \frac{E_i}{\sqrt{s}}$, and y_{ij} is the cosine of the angle between particle i and j . The basic idea of the FKS method consists in a partition of the real contributions into a sum of terms such that each summand contains at most one soft and one collinear singularity which is done by partitioning the phase space through the introduction of a set of positive-definite S functions. The S -functions are defined in such a way that they vanish in all singular limits not related to particle i becoming soft or particles i and j becoming collinear and also the sum over all pairs gives one.

$$d\sigma^{Real} = \sum_{ij} S_{ij} |M_{ab}^{n+1}|^2 d\phi_{n+1} \quad , \quad \sum_{ij} S_{ij} = 1 \quad (2.32)$$

In the consequence, each term of the sum is finite over all of phase space except if the energy of particle i goes to zero or particles i and j become collinear. Now, with the information of the exact position of the singularities for a given partition the generalized plus distributions are used to regulate the divergences.

$$d\tilde{\sigma}^R = \sum_{ij} \left(\frac{1}{\xi_i} \right)_{\xi_{cut}} \left(\frac{1}{1-y_{ij}} \right)_{\delta_0} \xi_i (1-y_{ij}) |M^{n+1}|^2 d\phi_{n+1} \quad (2.33)$$

where the plus distributions are defined as below:

$$\int d\xi_i \left(\frac{1}{\xi} \right)_{\xi_{cut}} f(\xi) = \int d\xi_i \frac{f(\xi) - f(0)\Theta(\xi_{cut} - \xi)}{\xi} \quad (2.34)$$

This defines the subtraction terms required for the calculation of the real emission parts. This method has been implemented already in an automated fashion in the MADFKS [46], which is a part of the full AMC@NLO [47] package. This completes the description of a NLO calculation in perturbative QCD. In the next section, we show the way of improving these fixed order results further, namely NLO calculation matched with parton shower (PS).

2.5 NLO correction matched to Parton Shower

In order to improve the theoretical predictions in a consistent way, one can take into account the effect of all possible radiations from the final and initial states, which are important in the complementary kinematic regions of phase space corresponding to the phase space relevant for the fixed order evaluation. These radiations are called parton showers, which not only give a reasonable estimate of these effects in the collinear kinematic regions of the phase space, but also provide a very realistic final state configuration. In other words, parton level predictions have to go through such showering of multi partons and recombination of these partons into hadrons through a hadronisation mechanism in order to compare them against the experimental data. Thus, fixed order SM results supplemented with parton showering can provide a more reliable as well as realistic predictions that can serve as a testing ground for various BSM scenarios. This parton shower algorithm only exists at the level of NLO, till now. Many processes of interest at LHC are being produced at this accuracy. However, there are ongoing works to obtain partons shower algorithm at higher order. In this section, we describe the basics of the parton shower and the way of obtaining a NLO calculation matched to PS results.

Generally, the hadronic collision consists of quarks and gluons in the initial state and also in the fi-

nal state depending on the process of interest. These partons can in principle radiate further partons i.e. quarks and gluons can emit further gluons whereas gluons also can split to quark-antiquark pairs. These produced partons can split further more, leading to a whole cascade of partons. The fixed-order calculations based on hard matrix elements provide an accurate description for a certain fixed final state parton multiplicity, in particular for hard emissions, i.e. in the phase space regions of well-separated final state partons. In the LHC, where large phase space is available, the fixed order only predictions can not capture all of the available phase space. However, by taking the complementary phase space available to the parton showers, one can capture the whole phase space available, thus improving the fixed order results by combining it with the parton shower. Formally all these branchings are suppressed by the strong coupling constant α_s , but for specific kinematic configurations where a parton is soft and/or collinear to another parton there can be logarithmic enhancement. These logarithms have to be resummed to all orders to obtain reliable results. A simulation of these exclusive final states and a resummation of the (leading) logarithmic terms can be achieved by applying a parton shower to the fixed-order result.

Let us start with the basic description of the parton shower. we consider the splitting of a parton i , produced in a hard process, into two partons j and k . In the collinear limit, when the angle between the partons j and k goes to zero, the cross-section can be imagined as those for the production of a parent parton i with small virtuality, that decays into the two collinear partons i.e. j and k . In this limit, the divergence occurs due to the vanishing denominator in the propagator of the parent parton i . In perturbative QCD there are three possible decays of this parent parton: $q \rightarrow qg, g \rightarrow q\bar{q}$ and $g \rightarrow gg$.

In the limit of such collinear splitting the squared amplitude can be factorized for an arbitrary hard process \mathcal{M}_{n+1} involving $n + 1$ external partons in terms of amplitudes for the production of the parent parton times a splitting factor, that does only depend on the particular splitting involved, and on its kinematics. For example, it can be written as follows:

$$|\mathcal{M}_{n+1}|^2 = |\mathcal{M}_n|^2 \frac{\alpha_s}{2\pi} \frac{dt}{t} dz P_{ij}(z) \quad (2.35)$$

where the splitting kernels are defined as follows:

$$P_{qq}(z) = C_F \frac{1+z^2}{1-z}, \quad (2.36)$$

$$P_{qg}(z) = C_F \left[\frac{1+(1-z)^2}{z} \right], \quad (2.37)$$

$$P_{gq}(z) = T_F [z^2 + (1-z)^2], \quad (2.38)$$

$$P_{gg}(z) = C_A \left[\frac{z}{(1-z)} + \frac{1-z}{z} + z(1-z) \right] \quad (2.39)$$

and \mathcal{M}_n corresponds to the amplitude of the n -particle process. P_{ij} symbolises that the parton i corresponds to the emitting particle and j is the emitted, resolved parton. The azimuthal angle ϕ has been integrated out here and is not stated explicitly in the following. The evolution variable t , has the dimension of mass and vanishes in the collinear limit. Several choices of the variable t is possible, thereby paving the way of different shower algorithms. The usual choices for t are

- the virtuality: $t = E^2 z(1-z)\theta^2$
- the transverse momentum: $t = E^2 z^2(1-z)^2\theta^2$
- the angular variable: $t = E^2\theta^2$

The variable z denotes the momentum fraction carried away by the outgoing resolved parton with respect to the parent parton after branching (E_j/E_i), in the collinear limit. The splitting functions P_{qq}, P_{qg} and P_{gg} are divergent for $z \rightarrow 1$ and/or $z \rightarrow 0$, which happens to be the soft limit i.e. the energy of the parton k goes to zero after branching. We will discuss the consequences of these soft divergences at the end of this section. The factorization described in Eq. 2.35 is valid as long as the variable t between the two collinear partons is the smallest of the whole amplitude. In order to obtain the most singular terms in the perturbative series, the splitting described in Eq. 2.35 can be iterated in a ordered sequence. For n splittings of partons strictly ordered in t , the total contribution

of the process goes as:

$$\sigma_0 \alpha_s^n \int \frac{dt_1}{t_1} \frac{dt_2}{t_2} \dots \frac{dt_n}{t_n} \Theta(Q^2 > t_1 > t_2 > \dots > t_n > Q_{cut}^2) = \sigma_0 \frac{1}{n!} \alpha_s^n \log^n \frac{Q^2}{Q_{cut}^2} \quad (2.40)$$

where σ_0 is the lowest order cross-section and the Θ function is equal to 1 if the argument is true, zero otherwise. Q is the hard scale of the process, and Q_{cut} denotes an infrared cutoff, below which no further splitting is possible, which can be related to the Λ_{QCD} . This integrand $\frac{dt}{t}$ is divergent as the collinear configurations come up. To remove these we have to consider the similar terms coming from the virtual corrections also, which will render this finite. Hence, in order to get sensible results, leading logarithmic virtuals are also included in the computation of the most singular contributions to cross-sections. The inclusion of both leading logarithmic real and virtual contributions are achieved by means of the shower, which is developed through a Monte Carlo program. In order to describe the development of all subsequent splittings in a shower through a Monte Carlo program, a probabilistic interpretation of these branchings is required. The probability to create a splitting of the parton i in a range between t and $t + dt$ for the ordering variable can be interpreted by defining the splitting factor in Eq. 2.35 as the weight factor for elementary branching in the phase space defined by dt, dz . Hence, the branching probability in the interval dt can be written as

$$d\mathcal{P}_{branching} = \frac{\alpha_s(t)}{2\pi} \frac{dt}{t} \int_0^1 dz P_{ij}(z) \quad (2.41)$$

Now, if we take into account the unitarity, i.e. the fact that either a branching occurs or not, the probability that no branching occurs is simply $(1 - d\mathcal{P}_{branching})$ between the interval $[t, t + dt]$, which is constituted from the sum of all leading-log virtuals. Now, for a finite interval for the evolution from a high scale t_1 to a lower one t_2 , the non-branching probability can be expressed in

terms of N infinitesimal subintervals:

$$\mathcal{P}_{nobraunching} = \lim_{N \rightarrow \infty} \prod_{n=1}^N \left(1 - \frac{\alpha_s(t'_n)}{2\pi} \frac{dt'_n}{t'_n} \int_0^1 P_{ij}(z) dz \right) \quad (2.42)$$

$$= \exp \left[- \int_{t_2}^{t_1} \frac{dt}{t} \frac{\alpha_s(t)}{2\pi} \int_0^1 P_{ij}(z) dz \right] \quad (2.43)$$

$$\equiv \Delta_i(t_1, t_2) \quad (2.44)$$

The quantity $\Delta_i(t_1, t_2)$ is known as Sudakov form factor corresponding to the non-emission probability in the given $[t_1, t_2]$ interval. It, being the main building block for the shower evolution, is by construction an all-order quantity which resums the leading virtual contributions. Hence, the probability of the first emission starting from a scale t_1 without any splitting between the range $[t_1, t]$ is

$$d\mathcal{P}_{first} = \Delta_i(t_1, t) \frac{\alpha_s(t)}{2\pi} \frac{dt}{t} \int_0^1 P_{ij}(z) dz \quad (2.45)$$

which is clearly the product of the no emission probability times the branching probability at t . Using this as the weight factor, a monte carlo program can be written to simulate the final-state shower.

The initial state shower can be constructed following the same approach of the final state shower. However, there are certain differences between these two as the parton taking part in the hard process is not the origin, but the result of many branchings already. The shower can be constructed using the space-like virtuality i.e. starting from a scale $-Q_0$ and evolving to lower scales, until the parton entering the hard process at the scale $-Q$ is produced. However, this forward evolution is very inefficient as most of the generated configurations would not result in the required one with a specific parton entering the hard process at a given scale. So, to construct an efficient initial state shower, the backward evolution i.e. starting the shower from the hard process itself at $-Q$ and then going backwards to the lower scale $-Q_0$.

There are also soft divergences associated with the QCD amplitudes during the construction of

a shower algorithm, which we have not discussed till now. The soft singularities can also arise with the collinear singularities at the same time leading to a double-logarithmic structure. In full analogy with the collinear singularity the large logarithms also appear during the soft branching. However, the only difference is that the factorization of the matrix element in the collinear limit happens at the amplitude square level whereas in case of soft emissions the factorization takes place at the amplitude level, thus leading to interferences between partons emitted from different parts of an event at the time of squaring the amplitude. So, it seems that a sequential construction of the exclusive final states, treating the QCD emissions independently like the collinear case, will not be possible. But, with the help of choosing the ordering variable t one can reconcile independent parton evolution and soft QCD radiation through color coherence. If t is taken to be the angular variable then it automatically takes care of soft QCD radiations consistently. In this thesis we have used the HERWIG [48–50] and PYTHIA [51] showers for the analysis.

The HERWIG shower takes the evolution variable t to be $E^2\theta^2/2$, where E is the energy of the incoming parton, and θ is the angle of the two branched partons. So, HERWIG takes care of the soft singularities properly, being an angular ordered shower. In contrast to it the PYTHIA shower takes the variable t as virtuality, which fails to yield the correct soft gluons behavior due to lack of the angular ordering in the algorithm. As a result of it, PYTHIA causes an unphysical increase in the number of soft partons.

Now, the next step should be retaining the virtues of the matrix element corrections at NLO and also the correct soft and collinear behavior due to large number of QCD radiations i.e. NLO results matched to PS.

One of the problem of matching the NLO calculations with parton shower is the double-counting problem, which is taken care by two algorithms mainly. MC@NLO and POWHEG can take care of the double counting to give a consistent description of the parton shower matched at NLO. We will discuss the MC@NLO method here as we we have used this in our works. In the MC@NLO approach, this is achieved by evaluating the differences of the Shower Monte Carlo simulation relative to the exact NLO result. A modified FKS subtraction framework is used where the difference

between the exact NLO and shower algorithms at approximate NLO is used. In this way the integrated quantities are calculate with NLO accuracy. However, one has to calculate the difference between the shower NLO approximation and the exact NLO result every time with a change in the shower algorithm and at the time of removing the double counting via the modified subtraction procedure, the subtraction terms give rise to negative weights for the events produced spoiling the probabilistic approximation.

2.5.1 AMC@NLO framework

AMC@NLO [47, 52, 53] is a wonderful tool for producing this NLO matched PS results completely in an automated way. In particular, the underlying tree-level computations are performed with MadGraph [54, 55] and one-loop amplitudes are evaluated via MadLoop, depending on the OPP integrand reduction method, whereby MADFKS [46] takes care of the real emission contributions and the corresponding phase-space subtractions, according to the FKS subtraction formalism [45, 56]. It is also combined with the one-loop and Born results and after the cancellation of the IR poles the subsequent integration is done in MADFKS to get fixed order results for a specific scattering process. It also does the job of the MC@NLO matching at the time of generating the events, afterwards which has to be showered to get the physical results. Utilising this framework, we have studied the three photon production in SM at LHC, which has been discussed in chapter 3 as well as the DY, ZZ, WW production in SM and ADD model at LHC, which has been shown in chapter 4.

2.6 Approximate fixed order calculation

There are certain difficulties to calculate beyond fixed order NNLO or to obtain results at NNLO+PS accuracy, at the moment. Even, very few processes has been reported at complete NNLO level till now. Given this scenario, one can obtain approximate fixed order predictions at higher perturbative order by considering the soft limit of the QCD radiations. Any partonic cross-section at the fixed

order consists of some distributions and finite pieces when written in terms of the partonic energy fraction (z). In the soft limit of the QCD radiations these distributions become large due to logarithmic enhancement and we can neglect other regular pieces in the expression. These are called threshold correction, which constitutes a certain part of the complete correction. There can be two type of thresholds namely hadronic and partonic threshold. When the hadronic ratio $\tau = Q^2/S$ is close to threshold, i.e. $\tau \rightarrow 1$, all contributions to the cross-section come from the threshold region. But in phenomenologically interesting process, this region $\tau \rightarrow 1$ is irrelevant due to the strong suppression of the PDFs near the endpoint implying a very low parton luminosity in this case. However, it has been pointed out since long [57, 58] that the threshold could be relevant even far from the hadronic threshold depending on the fact that the hadronic cross-sections are obtained after convoluting a hard cross-section with the parton luminosity. The hard partonic cross-section depends on the partonic center-of-mass energy and the dimensionless ratio of the latter to the final state invariant mass and as a result of it threshold correction are important when the partonic subprocess is close to threshold i.e. the partonic threshold. As a result of it all the QCD radiations are necessarily soft. The partonic center-of-mass energy in turn can take any value from threshold up to the hadronic center-of-mass energy, and its mean value is determined by the shape of the PDFs. So, we expect threshold correction to be relevant if the average partonic center-of-mass energy is small, i.e. if the relevant PDFs are peaked at small Bjorken x e.g. such as gluons and sea quarks. So, inspite of being very far from the hadronic threshold the partonic threshold can contribute a dominant part in the complete correction. As there is a huge theoretical uncertainty involved with the Higgs boson production so it is worthwhile to calculate these threshold corrections in case of Higgs boson production. Below we discuss the recent status of the Higgs boson production differing in the level of precision and how we paved the way of further precise results has been described in chapter 6 and chapter 5. In the SM, the production of Higgs boson is mainly through gluon fusion channel whereas the alternative channels include vector boson fusion process, Higgs-strahlung process wherein the Higgs is produced in association with vector bosons (W/Z), bottom quark annihilation process etc. In the gluon fusion channel via a top quark loop [59–67],

the Higgs production cross-sections are known up to next-to-next-to leading order (NNLO) in the literature for a long time. The sub-dominant channels for the production comprising of the vector boson fusion [68, 69] and associated production with vector bosons [70, 71] are also known up to NNLO accuracy in QCD. The bottom-antibottom ($b\bar{b}$) annihilation process for inclusive Higgs production is also available at NNLO accuracy considering five active flavours i.e. including the bottom quarks in the parton distribution functions [72–77].

While the theoretical predictions at NNLO and next-to-next-to leading log (NNLL) [78] QCD corrections and of two loop electroweak effects [79–84] played an important role in the discovery of the Higgs boson, the theoretical uncertainties resulting from the unphysical factorization and renormalisation scales are not convincingly negligible. In addition, the interpretation of the experimental data with higher accuracy from the upcoming run at the LHC demands the inclusion of higher order terms in QCD in the theoretical computation. Hence there is a constant pursuit of increasing the accuracy of the results with the systematic inclusion of higher order terms in QCD and there are on going efforts to go beyond the existing NNLO level. The computation of N^3 LO corrections is underway and some of the crucial ingredients, like the quark and gluon form factors [85–89], the mass factorization kernels [90] and the renormalisation constant [91] for the effective operator describing the coupling between the Higgs boson and the SM fields in the infinite top quark mass limit are available up to three loop level in dimensional regularization. In addition, NNLO soft contributions are also known [92] in n dimensions. These results were already used to compute the partial threshold contributions at N^3 LO to the production cross-section of di-leptons in Drell-Yan (DY) and of the Higgs boson in gluon fusion as well as in $b\bar{b}$ annihilation, see [93–97]. The reported threshold corrections, which manifest themselves through the delta function and the plus distributions, were partial results as the contribution from the delta function was not available completely. Since then, there have been several advances [98–101] towards obtaining the complete N^3 LO result for the inclusive Higgs production. The milestone in this direction was achieved by Anastasiou et al. in [102] to obtain the complete threshold N^3 LO corrections. This result provided a crucial input in [103] to obtain the corresponding N^3 LO threshold corrections to DY production.

Independently, in [104], using light-like Wilson lines threshold corrections to the Higgs boson as well as Drell-Yan productions up to N³LO were obtained. Catani et al. in [105] used the universality of soft gluon contributions near threshold and the results of [102] to obtain general expression of the hard-virtual coefficient relevant for N³LO threshold as well as threshold resummation at next- to-next-to-next-to-leading-logarithmic (N³LL) accuracy for the production cross-section of a colorless heavy particle at hadron colliders. There have been also several attempts to go beyond threshold corrections [106, 107] for the inclusive Higgs production at N³LO. Recently, [108], the full next to soft as well as the exact results for the coefficients of the first three leading logarithms at this order have been obtained for the first time. In this context we computed the threshold corrections at third order in QCD for the inclusive cross-section of the Higgs boson production associated with a vector boson, which has been reported in details in chapter 5. Like the inclusive one, the differential rapidity distributions are computed for the di-lepton pair in DY [109] and the Higgs boson produced through gluon fusion in [110, 111], the Higgs boson through $b\bar{b}$ annihilation in [112] and associated production of the Higgs with vector boson in [113, 114] to NNLO in QCD. Using the formalism developed in [96, 97], the partial N³LO threshold correction to the rapidity distributions of the di-leptons in DY and the Higgs boson in gluon fusion as well as bottom quark annihilation were computed in [115]. Following the same technique, the complete N³LO threshold correction to the rapidity distributions of both di-lepton pair in DY and the Higgs boson in gluon fusion has been reported in [116]. The dominance of the threshold contribution to the rapidity distribution in these processes is evident from the results. A significant amount of reduction in the dependence on the unphysical renormalisation and factorization scale of the rapidity distribution takes place upon inclusion of the N³LO threshold corrections. In addition, these computations provide first results beyond NNLO level and will serve as a non-trivial check for a complete N³LO results. Keeping these motivations in mind, we extend the existing result of the rapidity distribution of the Higgs boson produced through $b\bar{b}$ annihilation to higher accuracy, namely the inclusion of complete N³LO threshold correction, which we discuss in detail in chapter 6.

Chapter 3

Three photon production

3.1 Introduction

The field of triboson studies is required as the LHC experiments are beginning to probe these channels with the data set accumulated in Run 1, and will study the various channels in detail in Run 2. Since tri photon production is nominally that with the highest rate, it will be one of the first (and most accurately) studied of the processes. For this reason precise theory predictions, such as those obtained using NLO+PS accuracy are extremely desirable to the LHC community. Here, we revisit the three photon production process at the LHC at NLO in QCD and study the consequences of matching it with the parton shower. Triple-photon production provides a background to techni-pion production in association with a photon, where the techni-pion decays into a photon pair [117]. This process has already been studied at LO [118, 119], as well as at NLO level [120] in QCD. We extend the analysis including the effect of parton shower to get a realistic estimate of various kinematical distributions. We quantify the improvement in the predictions at small transverse momentum regions of the final state particles and the stabilisation of cross-section against the variation of the factorisation and renormalisation scales.

In Sect. 3.2, we have described the details of the calculation, mainly the virtual as well as the real emission contribution. The numerical results of the fixed order calculation together with the

NLO+PS accurate results have been discussed in Sect. 3.3 and finally, we conclude in Sect. 3.4.

3.2 Computational Details

LO ($\mathcal{O}(\alpha^3)$) contributions to the production of three photons at the LHC come from quark anti-quark annihilation processes. At NLO $\mathcal{O}(\alpha^3\alpha_s)$ in QCD, we encounter virtual as well as real emission contributions resulting from an additional parton, namely quark or anti-quark or gluon. Virtual amplitudes are already at $\mathcal{O}(\alpha^{3/2}\alpha_s)$, hence only the interference of them with the LO Born amplitudes will contribute to the NLO level. The real emission processes at NLO level come from two types of processes namely gluon emissions from the LO processes and scattering of a quark (anti-quark) and a gluon producing three photons along with a quark (anti-quark). The ultra-violet (UV) divergences coming from the virtual contributions and the infra-red (IR) divergences originated from the virtual as well as real emission contributions, need to be removed through the addition of proper counter terms. Following the discussions in the Sect. 2.4, the resulting IR-safe parton level cross-section up to NLO can be written as,

$$\begin{aligned}
d\hat{\sigma}_{ab}^{NLO} = & \int dPS_{3\gamma} S(\{p\}_{1,5}) d\hat{\sigma}_{ab}^{(0)} \\
& + \frac{\alpha_s(\mu_R)}{4\pi} \left[\int dPS_{3\gamma} S(\{p\}_{1,5}) d\hat{\sigma}_{ab}^{V,(1)} + \int dPS_{3\gamma} S(\{p\}_{1,5}) d\hat{\sigma}_{ab}^{CT,(1)} \right. \\
& \left. + \int dPS_{3\gamma+parton} S(\{p\}_{1,6}) d\hat{\sigma}_{ab}^{R,(1)} + \int dPS_{3\gamma} S(\{p\}_{1,5}) d\hat{\sigma}_{ab}^{MF,(1)} \right] \quad (3.1)
\end{aligned}$$

The first term is the Born contribution; $dPS_{3\gamma}$ is the phase space measure of the three photon final states and $S(\{p\}_{1,m})$ is the observable function which depends on the kinematic variables through the momenta of the external particles *i.e.*, p_1, p_2, \dots, p_m . The second term corresponds to virtual corrections to the Born process. They are often divergent when the loop momentum becomes very large and these UV divergences are first regularised and then renormalised using the counter terms given in the third term. The fourth term represents the real emission contributions

at the NLO level come from parton emissions from the initial and/or final state partons. Due to massless quarks, anti-quarks and gluons participating in the hard processes, both virtual and real emission contributions encounter soft and collinear divergences. The divergences coming from soft gluons and from collinear partons in the final state of the real emission processes get cancelled with those coming from the virtual processes. The remaining collinear divergences from the initial states are removed by adding mass counter terms given in the last term of Eq. 3.1. The details of obtaining UV renormalised virtual contributions have already been discussed in the Sect. 2.4. The real emission contributions and the corresponding mass counter terms are obtained with the help of MADFKS [46], a set of routines available in the AMC@NLO [47, 52, 53], which along with our in-house FORTRAN routines for calculating virtual contributions, can provide results on an event-by-event basis in terms of four momenta of all the particles involved in the scattering process and we use them to obtain the observables that we require to study. In the following sub-sections, we sketch a systematic outline of the complete computational procedure.

3.2.1 Virtual contribution

Virtual contribution comes from the interference between the Born diagrams and the one loop corrected virtual diagrams. The number of virtual diagrams to order $\alpha^{3/2}\alpha_s$ for the three photon production is forty eight. Up to permutations of the final state photons, we find 1 pentagon diagram, 2 box diagrams, 3 triangle diagrams and 2 bubble diagrams. We have used QGRAF [121] to generate both LO and NLO amplitudes. It generates the symbolic description of the Feynman diagrams in terms of propagators and vertices. We have written a FORM [122] code, which translates the output of QGRAF into a suitable format, that can be used for further symbolic manipulations. We have supplied Feynman rules, identities for Dirac gamma matrices, equations of motion through this code and performed various simplifications at the amplitude level. The loop integrals are regulated using dimensional regularisation. Both Lorentz contractions and Dirac gamma matrix simplifications are done in $n = 4 + \epsilon$ space-time dimensions. Both UV and IR divergences appear as poles in

ε and they have been calculated using $\overline{\text{MS}}$ scheme. Writing the virtual contribution in the following way:

$$\sum_{\text{col spin}} \sum \mathcal{M}^{V,(1)} \left(\mathcal{M}^{(0)} \right)^* = \sum_{\Gamma} \left[\sum_{\text{col spin}} \sum \mathcal{M}^{V,(\Gamma)} \left(\mathcal{M}^{(0)} \right)^* \right] , \quad (3.2)$$

where $\mathcal{M}^{(0)}$ is the born amplitude and $\mathcal{M}^{V,(\Gamma)}$ s' are the distinct topologies of virtual diagrams, we compute only one particular topology and then the permutations of photon momenta and their polarisations gave us the remaining contributions. The tensor integrals are reduced via our own in-house FORM codes and the scalar coefficients are evaluated via PJFry as discussed in Sect. 2.4.1. In order to validate our FORM codes, namely those ones that perform conversion of output of QGRAF to FORM readable symbolic expressions, reduction of tensor integrals to scalar coefficients and also to validate FORTRAN routines, which evaluate the virtual contributions numerically using PJFry, we re-calculated the virtual corrections of the di-photon production process in both SM and BSM to order α_s . We compared our results thoroughly against the results presented in [123–125] and found an excellent agreement between these two. Using our FORM codes and FORTRAN routines along with the publicly available packages, *viz.* QGRAF, PJFry, QCDLoop and OneLoop, we have evaluated the virtual contributions to the three photon production process at $\mathcal{O}(\alpha_s)$ level. We find that after UV renormalisation, the IR poles namely double and single poles in ε are in accordance with the expectation. We express the virtual contribution of the three photon production in a form suitable for further analysis as follows:

$$d\hat{\sigma}_{q\bar{q}}^{V,(1)} = \frac{\alpha_s}{2\pi} \frac{1}{\Gamma(1 + \frac{\varepsilon}{2})} \left(\frac{s}{4\pi\mu_R^2} \right)^{\frac{\varepsilon}{2}} C_F \left(-\frac{8}{\varepsilon^2} + \frac{6}{\varepsilon} \right) d\hat{\sigma}_{q\bar{q}}^{(0)} + d\hat{\sigma}_{q\bar{q}}^{V,(1),fin}(\mu_R) , \quad (3.3)$$

where α_s is the strong coupling evaluated at the the renormalisation scale μ_R , s is the partonic center of mass energy and the colour factor is: $C_F = 4/3$ for $SU(3)$. $d\hat{\sigma}_{q\bar{q}}^{(0)}$ comes from the colour-linked Born amplitude $\mathcal{M}_{q\bar{q}}^{(0)}$, whereas $d\hat{\sigma}_{q\bar{q}}^{V,(1),fin}$ denotes the finite virtual contribution that has been computed numerically. Note that the IR poles in ε are in agreement with the universal behaviour of soft and collinear partons.

3.2.2 Real emission contribution

Real emission contributions come from gluon emission from the Born processes as well as from the scattering of a quark/anti-quark and a gluon producing a quark/anti-quark and three photons. We use the AMC@NLO [47, 52, 53] framework not only to compute these contributions along with the mass factorisation terms required to remove the initial state collinear singularities, but also to obtain the NLO results matched with PS. We have explicitly checked the cancellation of the soft and collinear divergences among the virtual, real and mass factorisation terms at different regions of the phase space thereby confirming the perfect implementation of all the above mentioned external inputs within the AMC@NLO framework. The events, that are generated using AMC@NLO, also include the Monte Carlo counter terms to take care of the MC@NLO matching and thereby preventing the occurrence of any double counting at the time of matching to PS. These events are then showered by HERWIG [48–50], PYTHIA [51] parton shower to get the realistic events.

Photons are produced not only at the partonic level, but also through the fragmentation of partons into photons and a jet of hadrons can often be collinear to them. This necessitates the inclusion of non-perturbative fragmentation functions. At NLO level, the QED collinear divergence can arise when one of the final state parton becomes collinear to a photon. This can be factorised in a universal manner and then removed by adding counter terms, which renormalise the fragmentation functions, thereby bringing in a scale dependence at the partonic cross sections through the fragmentation functions, which is known as fragmentation scale. An alternate isolation criteria has been proposed in [126], using which one can obtain an observable in which fragmentation contribution is minimised and at the same time, the IR safety of that observable is guaranteed. We call it Frixione isolation here after and use this isolation for our analysis. It works in the following way: define a cone centered around each photon with a radius R in the rapidity-azimuthal angle $(\eta - \phi)$ plane, where $R = \sqrt{(\eta - \eta_\gamma)^2 + (\phi - \phi_\gamma)^2}$. Now, it is demanded that the sum of hadronic transverse energy $H(R)$ inside any concentric circle of radius $R < R_\gamma$ would be less than an amount given by the function $H(R)_{max}$. This function can be chosen in such a way that lesser and lesser

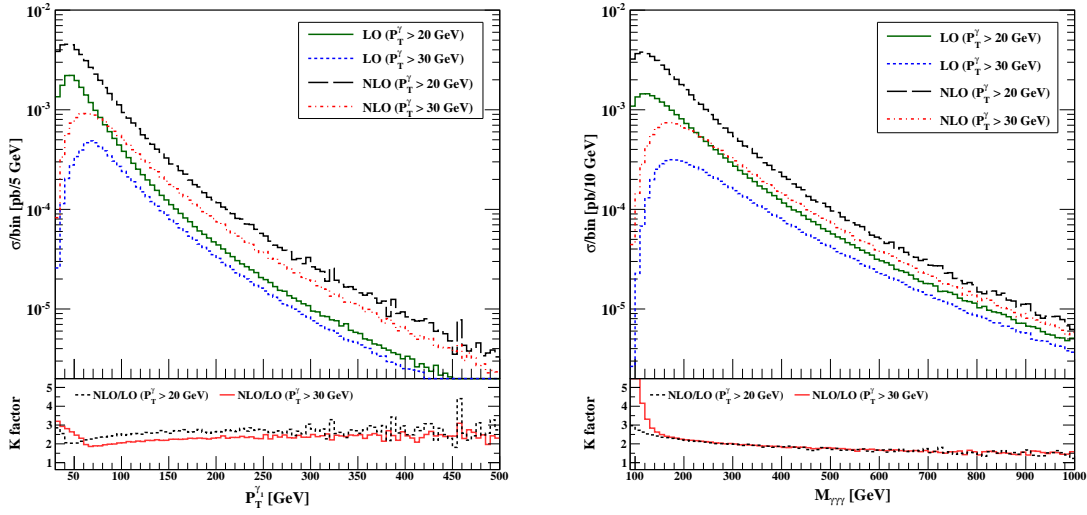


Figure 3.1: Transverse momentum distribution of the hardest photon $P_T^{\gamma_1}$ (left panel) and invariant mass distribution $M_{\gamma\gamma\gamma}$ of the three photon (right panel) for the fixed order NLO and LO.

hadronic energy is allowed as we move closer to a given photon. Because of the fact that $H(R)$ goes to zero as $R \rightarrow 0$, the partons that are collinear to photon are removed while the soft partons are kept intact thereby guaranteeing the QCD IR safety. For our analysis, we have taken the following canonical choice for $H(R)_{max}$, *i.e.*,

$$H(R)_{max} = \varepsilon_\gamma E_T^\gamma \left(\frac{1 - \cos R}{1 - \cos R_\gamma} \right)^n, \quad (3.4)$$

where E_T^γ is the transverse energy of the photon and R_γ , ε_γ , n are three parameters that are to be set while applying this isolation criteria.¹

3.3 Numerical Results

In this section, we present the results for various kinematic distributions relevant to the production of three photon in SM at the LHC with the center-of-mass energy $\sqrt{S} = 14$ TeV. Here we list the

¹Effects of photon fragmentation and different isolation prescriptions have very recently been studied [127]

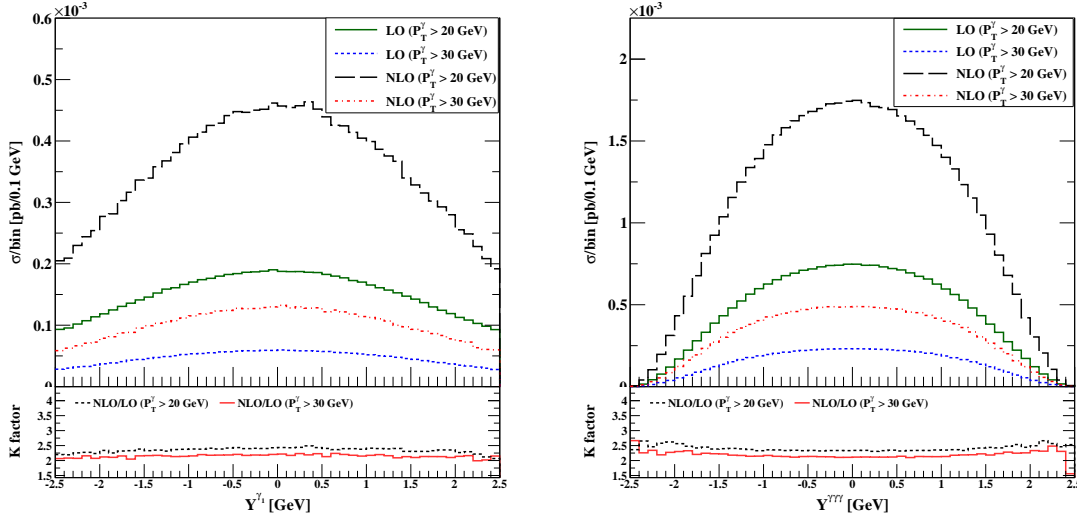


Figure 3.2: Rapidity distribution of the hardest photon Y^{γ_1} (left panel) and the three photon system $Y^{\gamma\gamma\gamma}$ (right panel) for the fixed order NLO and LO.

input parameters used for the whole computation:

$$\begin{aligned}
 M_Z &= 91.188 \text{ GeV}, & \alpha_{em}^{-1} &= 132.507, \\
 G_F &= 1.16639 \times 10^{-5} \text{ GeV}^{-2}. & & (3.5)
 \end{aligned}$$

These values of α_{em} , G_F and M_Z ensure that the mass of the W-boson ($M_W = 80.419 \text{ GeV}$) and the value of $\sin^2 \theta_W$ ($\sin^2 \theta_W = 0.222$) remain closer to the experimental values. We have considered massless quarks with five flavours ($n_f = 5$) throughout our calculation. In our present study, we have used MSTW2008(N)LO parton distribution function with errors estimated at 68% CL for the (N)LO and it also sets the value of the strong coupling $\alpha_s(M_Z)$ at (N)LO in QCD. The factorisation scale (μ_F) and the renormalisation scale (μ_R) are set equal to a central scale, which is the invariant mass of the three photon final states *i.e.*, $\mu_F = \mu_R = M_{\gamma\gamma\gamma} \equiv \sqrt{(P_{\gamma_1} + P_{\gamma_2} + P_{\gamma_3})^2}$.

For the fixed order (N)LO calculation, we have taken the following choices of cuts: rapidity of each photon $|\eta^\gamma| < 2.5$, separation between any two photons in the $(\eta - \phi)$ plane $\Delta R^{\gamma\gamma} > 0.4$, where $\Delta R^{\gamma\gamma} = \sqrt{(\Delta\eta)^2 + (\Delta\phi)^2}$. In addition, we have studied a variety of differential distributions

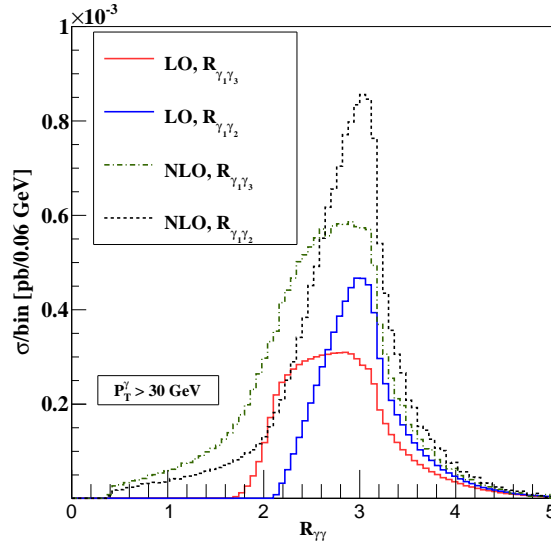


Figure 3.3: Separation of the softer photons (γ_2, γ_3) in comparison with the hardest one (γ_1) at LO and NLO.

applying two types of cuts on the transverse momentum of each photon *i.e.*, $P_T^\gamma > 20$ GeV and $P_T^\gamma > 30$ GeV in the fixed order analysis. Unless stated otherwise, we consider $P_T^\gamma > 30$ GeV as the generic choice of cut on photons transverse momenta. Parameters involved in the Frixione isolation are set as: $R_\gamma = 0.7$, $\varepsilon_\gamma = 1$ and $n = 2$.

LHC	LO [pb]	NLO [pb]	K-factor
$P_T^\gamma > 20$ GeV	2.257×10^{-2}	5.336×10^{-2}	2.36
$P_T^\gamma > 30$ GeV	7.050×10^{-3}	1.519×10^{-2}	2.16

Table 3.1: Total cross sections for the 3-photon production at the LHC. The results are shown for two different cuts at LO, NLO, and the associated K-factor. Relative statistical errors of the Monte Carlo are below 10^{-5} .

3.3.1 Fixed order Analysis

In table 3.1, we have shown the results of total cross sections for fixed order LO and NLO using the central choice of μ_F and μ_R for two different P_T^γ cuts. To begin with, we present some distributions of few selective kinematical variables at fixed order LO and NLO. Photons are ordered according to

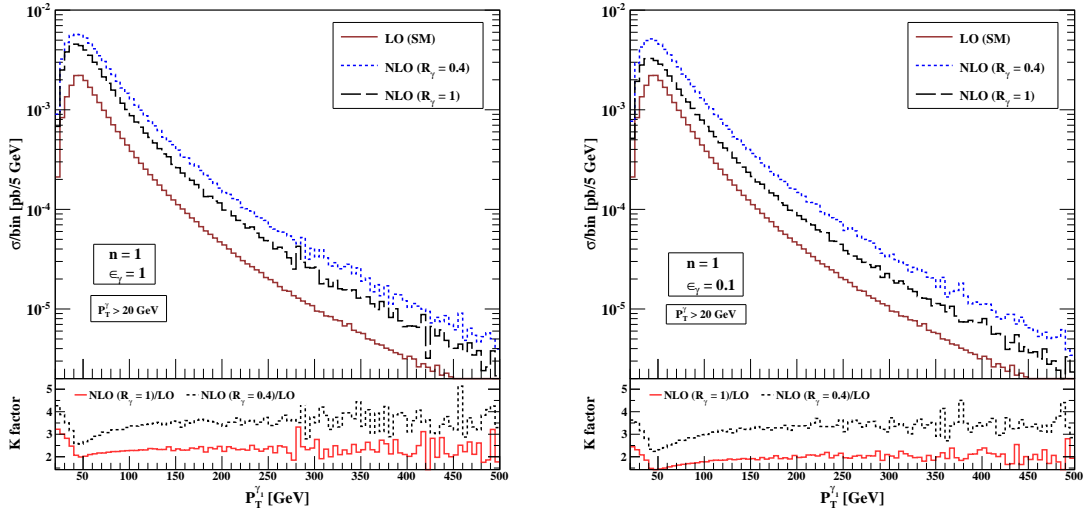


Figure 3.4: Transverse momentum distribution of the hardest photon ($P_T^{\gamma_1}$) with R_γ variation for a fixed value of $n=1$ and $\epsilon_\gamma=1$ (left panel) and for another fixed value of $n=1$ and $\epsilon_\gamma=0.1$ (right panel).

their transverse momentum. The hardest photon with maximum transverse momentum is denoted by γ_1 . Like wise, γ_2 represents the second hardest photon and the softest photon is labelled as γ_3 . In fig. 3.1, we have shown transverse momentum distribution of γ_1 at LO and NLO in the left panel and in the right panel, distribution of invariant mass of the three photon system has been plotted. The lower insets show the bin-by-bin distribution of the K-factor for the corresponding observable. We find that, for low transverse momentum, the K-factor is large as it is due to the fact that the recoil against the extra parton helps to fulfil the transverse momentum cut, which was not possible at LO. The left panel of the fig. 3.2 shows the distribution of the rapidity of the hardest photon, whereas the rapidity of the three photon system is shown in the right panel. The distribution of the K-factor is shown for the corresponding variables in the lower insets. Unlike fig. 3.1, the K-factors in fig. 3.2 appear to be mostly steady indicating the affinity of these observables towards the photons having fairly high transverse momenta.

All the above distributions show a substantial effect of radiative corrections on this process. This is mainly because of the inclusion of new subprocesses at the NLO, as quark-gluon subprocesses begin to contribute at this order and due to the enhancement in the phase space. In fig. 3.3, we

R_γ	n	σ_{NLO} [pb]		
		$\varepsilon_\gamma = 1$	$\varepsilon_\gamma = 0.5$	$\varepsilon_\gamma = 0.1$
0.4	1	6.896×10^{-2}	6.550×10^{-2}	6.154×10^{-2}
	2	6.489×10^{-2}	6.291×10^{-2}	6.045×10^{-2}
1	1	5.090×10^{-2}	4.620×10^{-2}	3.825×10^{-2}
	2	4.454×10^{-2}	4.110×10^{-2}	3.462×10^{-2}

Table 3.2: Total cross sections for the 3-photon production at the LHC for various Frixione isolation parameters. We have taken $p_T^\gamma > 20$ GeV at NLO.

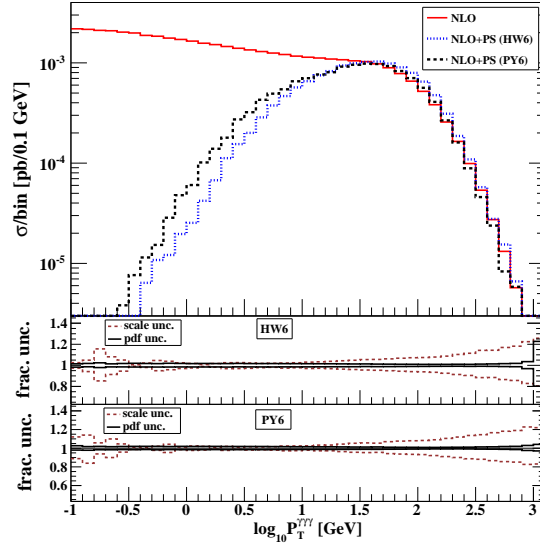


Figure 3.5: Three photon transverse momentum distribution $P_T^{\gamma\gamma\gamma}$ for the fixed order NLO and NLO+PS.

have plotted the separation between the ordered photons in the $(\eta - \phi)$ plane obeying the selection cut: $\Delta R^{i\gamma_j} > 0.4$, where $i, j = 1, 2, 3$. We have checked the rapidity differences between these photons are quite small. Therefore, the peaks arising in these distributions near the angle π (180), suggest that the emitted photons are mostly back-to-back. The hardest photon γ_1 is separated from the softest one *i.e.*, γ_3 , by at least $\Delta R^{\gamma_1\gamma_3} = 1.6$ at LO, whereas at NLO they can be very close as permitted by the selection cut due to the emission of an extra radiation at this level.

Besides, we have checked the effect of variation of Frixione isolation parameters *i.e.*, R_γ , ε_γ and n. Though Frixione isolation has no effect on the LO cross-section, the dependency of the NLO cross-section on these isolation parameters is shown in table 3.2. From Eq. (3.4), it is evident that

the NLO cross-section increases when R_γ decreases and it also increases with increasing ε_γ . In fig. 3.4, we have shown the transverse momentum distribution of the hardest photon by varying the value of R_γ (left panel) from 0.4 to 1 for a fixed value of $n = 1$ and $\varepsilon_\gamma = 1$, where the K-factors vary from 3.06 to 2.26. The right panel shows the same distribution for a fixed value of $n = 1$ and $\varepsilon_\gamma = 0.1$ and in this case, K-factors vary from 2.72 to 1.69. It is evident from table 3.2, as well as from fig. 3.4 that, for a fixed choice of n value, the NLO cross-section is large for $R_\gamma = 0.4$ and $\varepsilon_\gamma = 1$, whereas it becomes much smaller for $R_\gamma = 1$ and $\varepsilon_\gamma = 0.1$ indicating the fact that smaller R_γ increases the cross-section when ε_γ is larger [128]. It is also clear from table 3.2, that the effect of varying ε_γ , keeping n and R_γ fixed, is quite minimal. Similar studies with changing the value $n = 2$, provide same kind of distributions analogous to fig. 3.4.

3.3.2 Discussion on NLO+PS

In this section, we compare the fixed order NLO result with the NLO results matched with PS (NLO+PS) with two different showering algorithm, namely HW6 and PY6. For the showering purpose, parton level events are generated using very loose cuts: $P_T^\gamma > 15$ GeV, $|\eta^\gamma| < 2.7$, $\Delta R^{\gamma\gamma} > 0.3$ with the following Frixione isolation parameters: $R_\gamma = 0.4$, $\varepsilon_\gamma = 1$ and $n = 2$. We have explicitly checked that the events thus produced, remain unbiased in total rates and differential distributions after showering and hadronisation for this choice of kinematical cuts and Frixione isolation parameters. These events are then showered with HERWIG6 (HW6) and PYTHIA6 (PY6) and we have imposed the same set of analysis cuts that we used in the fixed order analysis along with the generic P_T^γ cut on the transverse momentum of the photon at the time of showering.

The scale dependencies of the results are calculated by varying μ_F and μ_R independently around the central value $\mu_F = \mu_R = M_{\gamma\gamma\gamma}$ via the following assignment: $\mu_F = \xi_F M_{\gamma\gamma\gamma}$ and $\mu_R = \xi_R M_{\gamma\gamma\gamma}$, where ξ_F and ξ_R are varied between the range $[1/2, 2]$ independently. Various ratios of μ_F , μ_R and $M_{\gamma\gamma\gamma}$ that appear as arguments of logarithms in the perturbative expansion to NLO are within the range $[1/2, 2]$. The scale uncertainty band is the envelope of the results obtained by varying this ξ_F

and ξ_R within this range [125]. The PDF uncertainties are estimated with the Hessian method, as given by the MSTW [129] collaboration. We have plotted fractional uncertainty, which is defined as the ratio of the variation about the central value divided by the central value, being a good indicator of the uncertainties. These uncertainty bands can be generated automatically at the time of parton level event generation by storing additional information, sufficient to determine via a reweighting technique, at no extra CPU cost within the AMC@NLO framework as described in [130].

We have shown $\log_{10} P_T^{\gamma\gamma\gamma}$ distribution for HW6 and PY6 together the fixed order NLO result, in fig. 3.5. It is clear that at low $P_T^{\gamma\gamma\gamma}$ values, NLO+PS (for both HW6 and PY6) result shows the effect of all order resummation of the large logarithms, hereby suppressing the cross-section leading to a meaningful value, while the fixed order NLO result diverges for $P_T^{\gamma\gamma\gamma} \rightarrow 0$. At low $P_T^{\gamma\gamma\gamma}$, PY6 result is different from the HW6 result as the soft and collinear emissions constituting the parton shower are treated differently. PYTHIA generates more softer spectra than HERWIG in this region and as a result of this, these two showers show different behaviour as expected [131]. At high $P_T^{\gamma\gamma\gamma}$, the NLO fixed order and NLO+PS (for both HW6 and PY6) results are in agreement as in this region, the hard emissions are dominant and they are correctly described by the NLO hard cross-section. In the middle and lower insets of fig. 3.5, we have presented the fractional scale and PDF uncertainties of the NLO+PS result for HW6 and PY6 respectively which increase with increasing $P_T^{\gamma\gamma\gamma}$ [131]. We do not find any significant differences in case of studying fractional uncertainties using these two different showers. Therefore, in the rest of the figures, we present the fractional uncertainty plots only for HW6.

We now present the results for various kinematical distributions to NLO accuracy, matched with PS (labelled as NLO+PS), for both HW6 and PY6 with the specified analysis cuts. We have adopted a consistent pattern for all the rest of the distributions. In each case, within the main frame, three curves corresponding to the distributions in fixed order NLO (solid red) and NLO+PS using HW6 (dashed blue) and NLO+PS using PY6 (dotted black) are shown. The middle inset shows fractional scale uncertainty (dashed cyan) and fractional pdf uncertainty (solid violet), while the lower inset shows the ratio between NLO+PS and NLO for HW6 (dashed blue) and for PY6 (solid

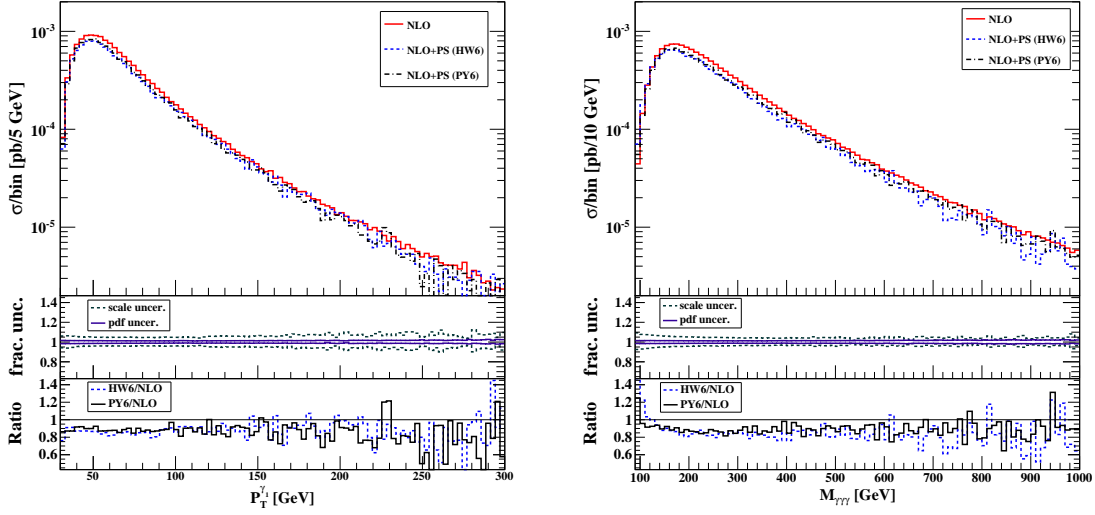


Figure 3.6: Transverse momentum distribution P_T^γ of the hardest photon (left panel) and invariant mass distribution $M_{\gamma\gamma\gamma}$ of the three photon system (right panel) for the fixed order NLO and NLO+PS.

black). In the left panel of fig. 3.6, we have shown the plots for transverse momentum distribution of the hardest photon and the right panel shows the distribution of the invariant mass distribution of the three photons. We do not find much difference in the results of two showers HW6 and PY6. In both distributions, NLO results are very little larger than the NLO+PS results and this is due to the fact that the QCD radiation becomes softer when we demand all the photons to satisfy a high P_T^γ cut (*i.e.* $P_T^\gamma > 30$ GeV) and damping of PDFs at large Bjorken x values further subdue its effect at the parton level, whereas AMC@NLO produces more events with hard and central jets resulting in the suppression of these distributions after showering. In fig 3.7, we have depicted the plot showing rapidity distribution of the three photon system and as expected, we observe that the NLO result is slightly harder than the NLO+PS result. However, the ratio in the lower inset shows that PY6 generated events give larger contribution than HW6 in the large rapidity region indicating that PY6 produces significantly large number of radiations than HW6 in the full kinematically available phase space.

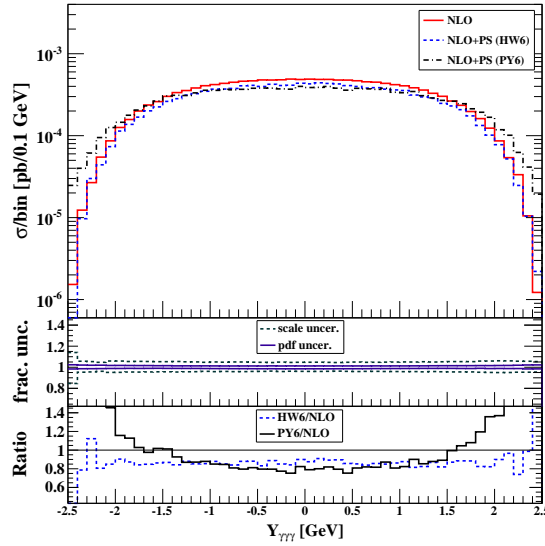


Figure 3.7: Three photon rapidity distribution for the fixed order NLO and NLO+PS.

3.4 Conclusion

Precise and realistic predictions of both signal and background processes at hadron colliders are now possible due to tremendous developments in the computational methods and the availability of the state of the art computational tools. We have used packages, namely QGRAF, PJFry, AMC@NLO to study the three photon production process at the NLO level in QCD for the LHC taking into account the parton shower effects and realistic experimental cuts. In addition, we have developed some codes that build the interfaces among these different analytical and numerical tools. We have plotted different kinematic observables and discussed the consequences of showering the fixed order NLO results with two different showering algorithm HERWIG and PYTHIA. We have also discussed the effects of scanning over the Frixione isolation parameters on the NLO cross-section. We find our predictions are less sensitive to scale uncertainties and choice of PDFs and hence more suited for direct comparison with the data from the experiments.

Chapter 4

DY, ZZ and WW production

4.1 Introduction

Wealth of data from the Large Hadron Collider (LHC) and the Tevatron involving large number of leptons, gauge bosons and hadrons in the final state not only have provided ample opportunity to test the predictions of the Standard Model (SM), but also constrained various physics scenarios in the beyond standard model (BSM). In this chapter, we will study the large extra dimensional models (ADD). With more accumulated data at the LHC, extra dimension searches at different energies have yielded stringent bounds [132, 133] on the model parameters [11–13]. This has also been facilitated by improved theoretical calculations to next-to-leading order (NLO) in QCD that have been available for this model for various processes *viz.* di-lepton [134–136], di-boson ($\gamma\gamma$ [123, 124], ZZ [137, 138], WW [139, 140] (W^+W^- is denoted as WW)). As we have discussed in Sect. 1.2.1 the production rate and potentially certain kinematical distributions may get modified as compared to the SM predictions due to the exchange of virtual Kaluza-Klein (KK) modes in scattering processes. Moreover, it is essential that higher order QCD corrections are included as it leads to reduction in scale uncertainties which in turn improves the theoretical predictions.

One important recent development has been the implementation of the di-photon production to NLO including Parton Shower (PS) in the `AMC@NLO` environment for the ADD model [125]. This

allows for the generation of fully exclusive events that are NLO accurate for observables inclusive in QCD radiation. If required, these events can be directly passed through a detector simulation. In this chapter, we discuss the implementation of the rest of the pair production processes ($\ell^+\ell^-$, ZZ and WW) that could contribute to the ADD model, to NLO+PS accuracy in the `AMC@NLO` environment. For our present analysis, using the various bounds given by ATLAS and CMS, we choose the following values of $M_S = 3.7$ TeV (d=2), 3.8 TeV (d=3), 3.2 TeV (d=4), 2.9 TeV (d=5), 2.7 TeV (d=6). We briefly describe the framework for matching the NLO results with Parton Shower Monte Carlo again in Sect. 4.2. A selection of the numerical results are presented in Sect. 4.3 and finally we present our conclusions in Sect. 4.4.

4.2 NLO+PS

In order to provide a more realistic description of a process at the LHC, it is unavoidable to match the NLO QCD results with Parton Shower Monte Carlo. We adopt the automated `AMC@NLO` framework, discussed in Sect. 2.5.1, again to calculate this.

The virtual contributions are implemented separately in this environment for each of these processes, using the analytically calculated results for $\ell^+\ell^-$ [134–136], ZZ [137, 138] and WW [139, 140] production processes. We have also incorporated an algorithm that takes care of the summation of the KK modes in the ADD model (Eq. 1.7); this has been made possible by appropriate changes in the spin-2 HELAS routine [125]. The exact numerical cancellations of double and single poles coming from the real and virtual terms in all the subprocesses, for each of the production processes have been checked.

For the Drell-Yan (DY) process, we have generated the events for the process $PP \rightarrow e^+e^- X$, which is phenomenologically same as $PP \rightarrow \mu^+\mu^- X$, except for the experimental identification of the final state particles. The leading order (LO) partonic contribution comes from the $q\bar{q} \rightarrow e^+e^-$ in both the SM and ADD model, whereas at LO $gg \rightarrow e^+e^-$ contributes only to the ADD model. Emission of real gluon and one loop correction due to the virtual gluon, together with the partonic

subprocess $q(\bar{q}) g \rightarrow q(\bar{q}) e^+ e^-$, give all the $\mathcal{O}(\alpha_s)$ contributions. The interference between the SM and ADD diagrams also give $\mathcal{O}(\alpha_s)$ contribution at the NLO. For the di-boson final states, in addition to similar partonic sub processes, there are contributions due to the interference between the gg initiated box diagrams in SM and the gg initiated Born diagrams in the ADD which is of $\mathcal{O}(\alpha_s)$. We have considered all the above contributions in each of these processes of interest for our present analysis.

After generation of events following the above procedure, we let the Z and W^\pm bosons to decay to leptons at the time of showering. For the ZZ events, we let one Z boson to decay to $e^+ e^-$ and the other one to $\mu^+ \mu^-$, while for WW events we let the W^+ decay to $e^+ \nu_e$ and the W^- to $\mu^- \bar{\nu}_\mu$. Alternatively, the W^\pm and Z bosons can be decayed using MadSpin [141] at the time of event generation itself, which retains nearly all spin correlations. We have not chosen to do this, because the inclusion of the sum over the KK modes is non-trivial in this way.

4.3 Numerical Result

In this section, we present some of the kinematical distributions for the production of $\ell^+ \ell^-$, ZZ , WW , both in the SM and ADD to NLO+PS accuracy for the LHC center of mass energy $\sqrt{S} = 8$ TeV. Events are generated using the following input parameters: $\alpha_{EW}^{-1} = 132.507$, $G_F = 1.16639 \times 10^{-5}$ GeV $^{-2}$, $m_z = 91.188$ GeV. Using these electro-weak parameters as inputs, the mass of W boson $m_w = 80.419$ GeV and $\sin^2 \theta_w = 0.222$ are obtained. The (N)LO events are generated using MSTW(n)lo2008cl68 parton distribution functions (PDF) for the (N)LO and the value of strong coupling constant α_s is solely determined by the corresponding MSTW PDF [129] at (N)LO. The factorisation scale μ_F and the renormalisation scale μ_R are set equal to the invariant mass of the corresponding di-final state. The number of active quark flavor is taken to be five and are treated as massless. We use the following loose cuts at the time of event generation for the DY production: (a) transverse momentum of the lepton $P_T^\ell > 15$ GeV, (b) rapidity $|\eta^\ell| < 2.7$, (c) the separation of two particles in the rapidity-azimuthal angle plane $\Delta R^{e^+ e^-} > 0.3$ (where $\Delta R = \sqrt{(\Delta\eta)^2 + (\Delta\phi)^2}$)

and (d) the invariant mass $M_{e^+e^-} < 1.1 \times M_S$. For ZZ and WW event generation, we use no cut at the generation level except on the invariant mass *i.e.*, $M_{ZZ}, M_{W^+W^-} < 1.1 \times M_S$. For WW event generation, the following CKM matrix elements are used: $|V_{ud}| = 0.97425$, $|V_{us}| = 0.2252$, $|V_{ub}| = 4.15 \times 10^{-3}$, $|V_{cd}| = 0.230$, $|V_{cs}| = 1.006$, $|V_{cb}| = 40.9 \times 10^{-3}$. All the CKM matrix elements associated with the top quark are taken to be zero.

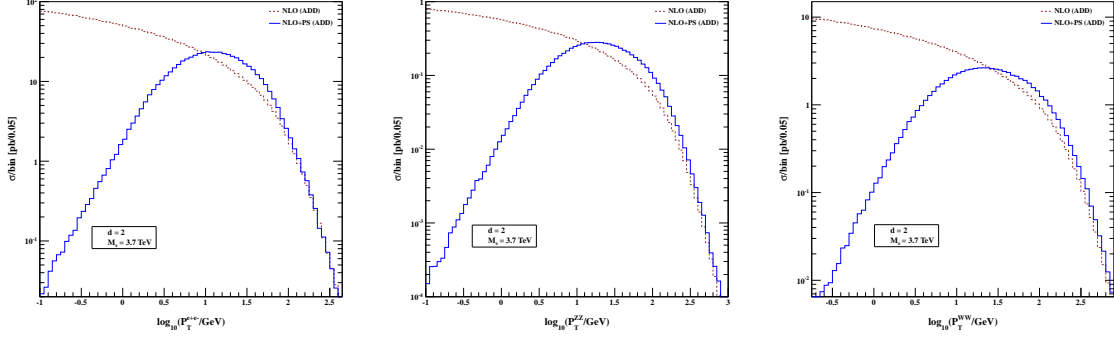


Figure 4.1: Fixed order NLO results (dashed brown) along with the NLO+PS results (solid blue) for the $\log_{10}(P_T)$ distribution of the e^+e^- (left), ZZ (middle) and W^+W^- (right) pair.

For showering the DY events, HERWIG6 in MC@NLO formalism is used. Using the following analysis cuts: $P_T^l > 20$ GeV ($l = e^+, e^-$), $|\eta^l| < 2.5$, $M_{e^+e^-} < M_S$, $\Delta R^{ll} > 0.4$ for showering, the hardest (with maximum P_T) e^+ and e^- are collected. In order to separate leptons from jets, $\Delta R^{lj} > 0.7$ is used. For both ZZ and WW showering, we have identified those final state, stable lepton-pair, whose mother is one of the Z boson (for ZZ showering) or the final state stable lepton-neutrino pair whose mother is one of the W boson (for WW showering) and that is the reason we avoid the cut which is commonly used to reconstruct the $Z(W)$ boson mass from the invariant mass of the lepton-lepton (lepton-neutrino) pair. For decay products of Z/W , we use the same analysis cuts to plot various differential distributions and they are the following: invariant mass $M_{ZZ/W^+W^-} < M_S$, $P_T^l > 20$ GeV (where, $l = e^+, e^-, \mu^+, \mu^-$ for ZZ and $l = e^+, \mu^-$ for W^+W^-), $|\eta^l| < 2.5$. In addition, we have collected only those leptons whose separation from other leptons and jets are greater than 0.4 and 0.7 respectively in the rapidity-azimuthal angle plane.

Here, we describe few selected differential distributions for some of the kinematical observ-

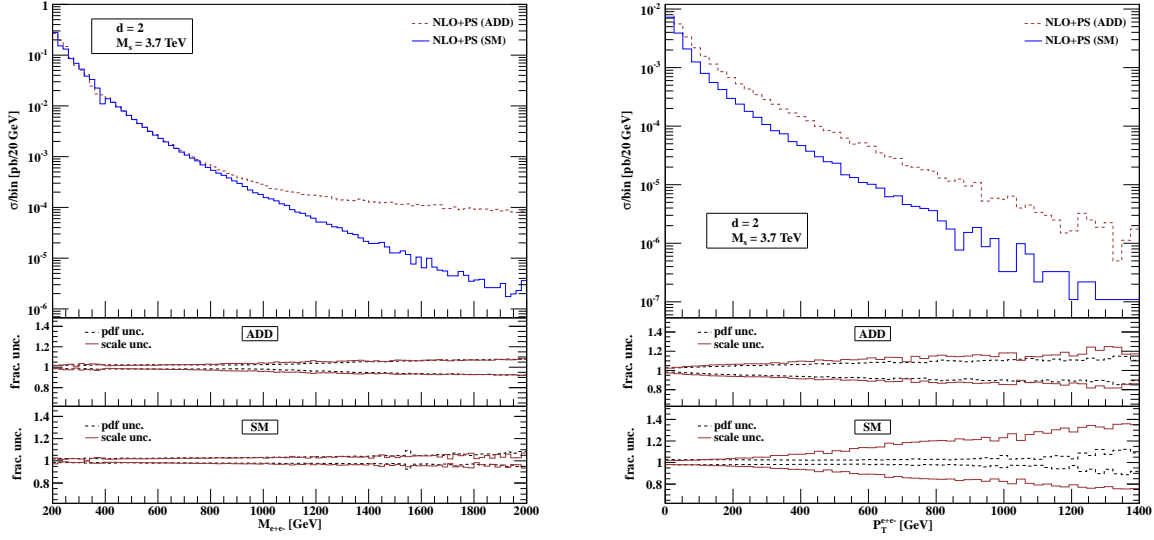


Figure 4.2: Invariant mass ($M_{e^+e^-}$) distribution (left) and transverse momentum distribution (right) of the e^+e^- pair for ADD ($d = 2$) and SM in Drell-Yan process. The right one is in $M_{e^+e^-} > 600$ GeV region.

ables. To start with, we study the effect of parton shower over the fixed order NLO correction. Fixed order NLO results (dashed brown) along with the NLO+PS results (solid blue) for the $\log_{10}(P_T)$ distribution of the e^+e^- (left), ZZ (middle) and WW (right) pair are plotted in fig. 4.1, using their specific analysis cuts detailed above for extra dimensions $d = 2$ and its corresponding M_S value. In all these plots, the fixed order cross section diverges for $P_T \rightarrow 0$, while the NLO+PS result shows a converging behavior in the low P_T region. The effect of parton shower ensures correct resummation of the Sudakov logarithmic terms which appear in the collinear region leading to a suppression of the cross section in the low P_T region. There is no significant deviation in the high P_T region as expected.

In the subsequent plots, we have included fractional scale and PDF uncertainties corresponding to the SM and ADD model distributions. By fractional uncertainty we mean the central value of a particular distribution divided by its extremum value. The scale uncertainties are calculated by considering independent variation of the renormalisation and the factorisation scales in the following way: $\mu_R = \xi_R M$ and $\mu_F = \xi_F M$. Here, M denotes the invariant mass of the di-final state *i.e.*,

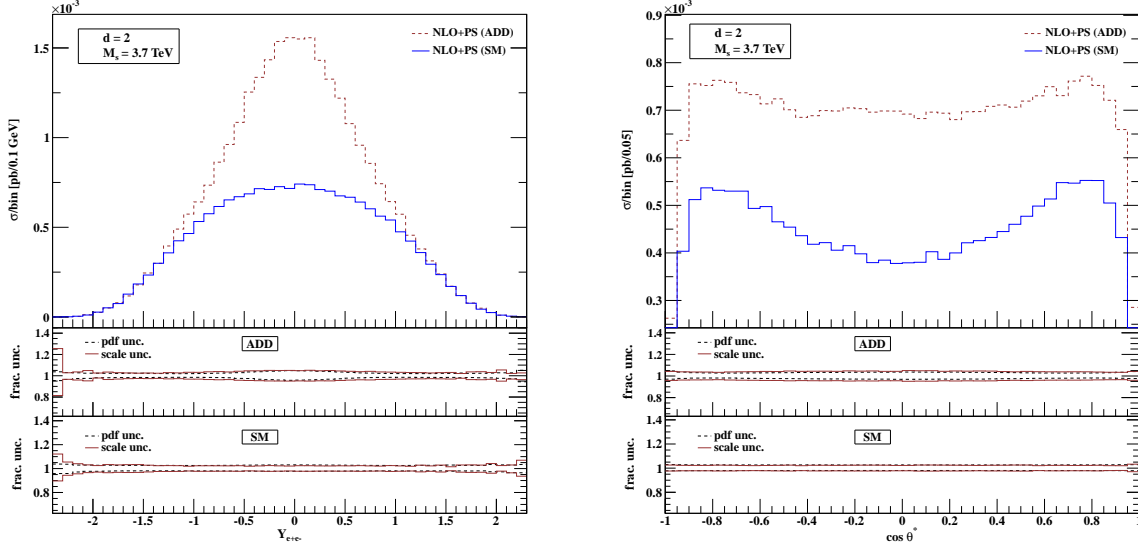


Figure 4.3: Rapidity distribution (left) of e^+e^- pair and the angular distribution (right) are given for $d = 2$ in ADD and also for SM in Drell-Yan process for $M_{e^+e^-} > 600$ GeV.

$M_{e^+e^-}, M_{ZZ}, M_{WW}$ as required and ξ_R, ξ_F can take either of the following values (1, 1/2, 2) independently. The scale uncertainty band is the envelope of the following (ξ_F, ξ_R) combinations [125] as described below: (1,1), (1/2,1/2), (1/2,1), (1,1/2), (1,2), (2,1), (2,2). Estimation of the PDF uncertainty is done in the Hessian method as prescribed by the MSTW [129] collaboration. All these uncertainties are determined automatically by following the re-weighting procedure [130] built in $\Delta\text{MC@NLO}$ which stores sufficient information in the parton level Les Houches events for this purpose.

In all the plots ADD represents the full contribution of the SM and ADD model contributions including interference. We use a consistent graphical representation for the rest of the kinematic distributions. In each case, the upper inset gives the distribution in SM (solid blue) as well as in ADD model (dashed brown) to NLO+PS accuracy. For the same distribution, the middle (ADD) and lower (SM) insets provide fractional scale (solid brown) and PDF (dashed black) uncertainties.

Various kinematical observable in the DY process are given in fig. 4.2, 4.3, 4.4 and 4.5. In fig. 4.2, we have shown the invariant mass distribution (left) and transverse momentum distribution

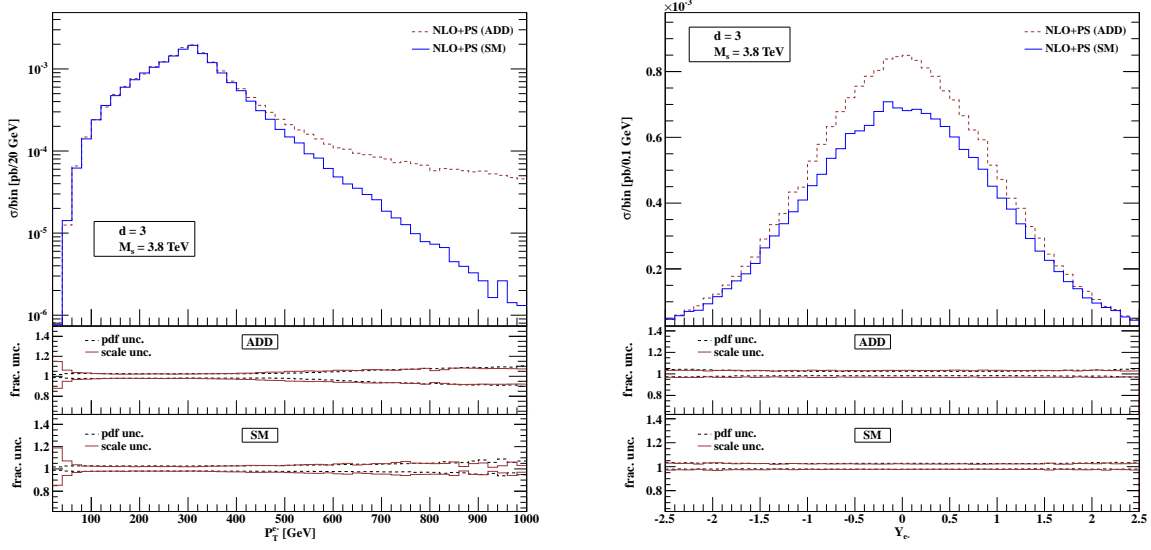


Figure 4.4: Transverse momentum (left) and rapidity (right) distribution of final state positron in ADD ($d = 3$) and SM for Drell-Yan process for $M_{e^+e^-} > 600$ GeV.

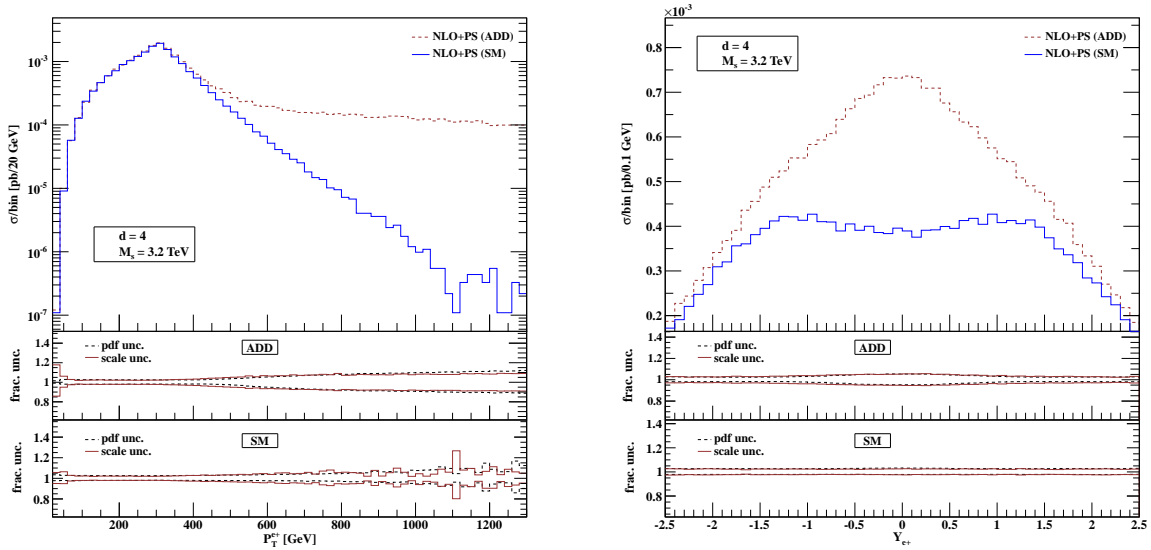


Figure 4.5: Transverse momentum (left) and rapidity (right) distribution of final state electron in ADD ($d = 4$) and SM for Drell-Yan process for $M_{e^+e^-} > 600$ GeV.

(right) of the e^+e^- pair for $d = 2$ with its associated M_S value. The effect of large extra dimension is dominant in the high invariant mass region and hence we focus in the region $M_{e^+e^-} > 600$ GeV to study the other distribution *viz.* P_T , rapidity, angular distribution of the e^+e^- pair and also look at some of the distributions of the individual leptons. In fig. 4.2, note that there is an increase in the scale and PDF uncertainties with increase in P_T as is well known, see for example [131]. In fig. 4.3, the rapidity distribution of e^+e^- pair (left) and the angular distribution (right) are given for $d = 2$. For the rapidity distribution the deviation from the SM is only prominent in the central region. The angle made by the lepton pair in its center of mass frame with respect to one of the incoming hadron is denoted by θ^* . The angular distribution is a good discriminator for the full range to distinguish the ADD from the SM. fig. 4.4 describes the behavior of P_T (left) and rapidity (right) distribution of final state positron for $d = 3$ extra dimensions. Similarly, in fig. 4.5, transverse momentum distribution (left) is presented along with the rapidity distribution (right) of the final state electron for $d = 4$. The difference in the SM rapidity distribution for e^- (fig. 4.4) compared to e^+ (fig. 4.5), can be attributed to the fact that Z boson couples differently to left and right handed fermions and the high invariant mass cut used to zoom into the region of interest for the ADD model, enhances this effect.

The plots associated with the decay products of ZZ process are presented in fig. 4.6, 4.7, 4.8. For $d = 2$ we see deviations from the SM in the high invariant mass region in the case of four-lepton invariant mass (M_{4l}) distribution as shown in fig. 4.6. Except for the invariant mass distribution, all other kinematical observable are studied above the region where the four lepton invariant mass is greater than 600 GeV, which is the ADD dominant region. In fig. 4.7, we have shown transverse momentum (left) and rapidity (right) distribution of the e^+e^- pair for $d = 3$. Similarly, the transverse momentum (left) and rapidity (right) distribution for the $\mu^+\mu^-$ pair are presented in fig. 4.8 for $d = 4$. The ADD distributions are fairly distinguishable for $d = 4$ compared to $d = 3$, as bounds on M_S value for larger number of extra dimension is a bit lower.

For the WW production process, the relevant plots are presented in fig. 4.9 and fig. 4.10, wherein the decays of W^\pm bosons to leptons and neutrinos are included at the stage of showering. For

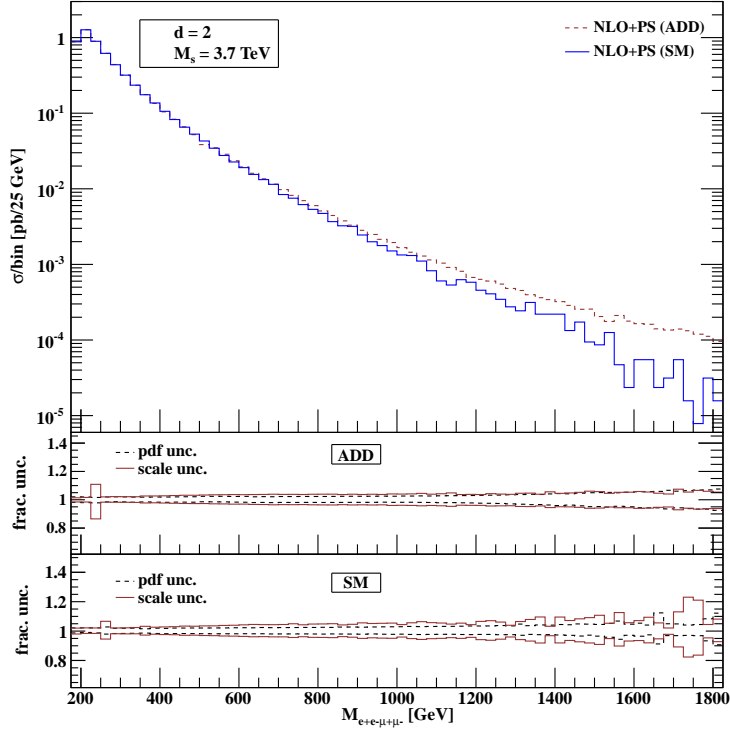


Figure 4.6: Four-lepton invariant mass (M_{4l}) distribution for ADD ($d = 2$) and SM for decay products coming from the ZZ process.

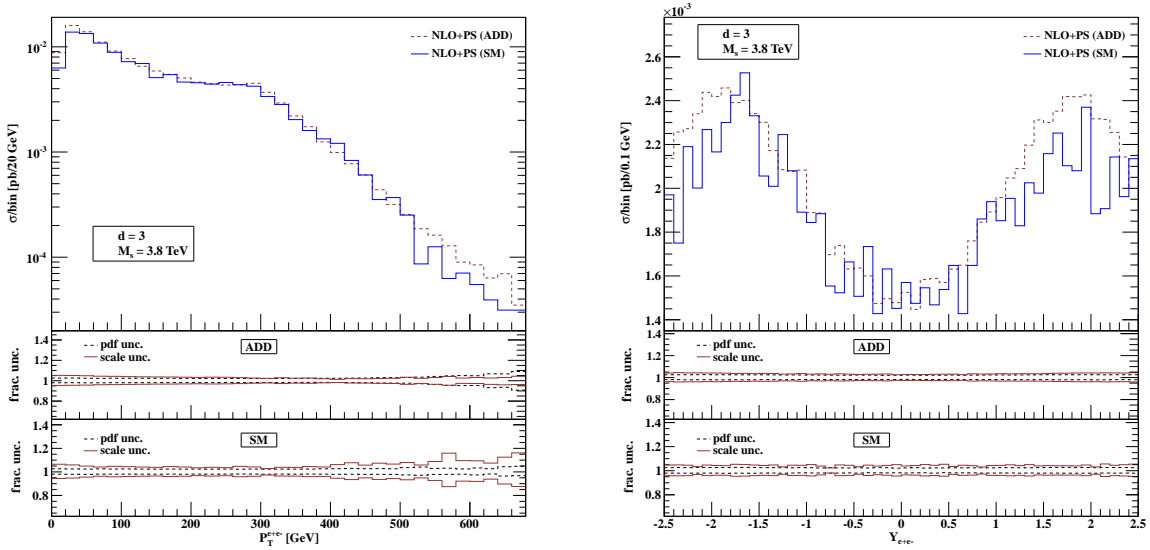


Figure 4.7: Transverse momentum (left) and rapidity (right) distribution of the e^+e^- pair coming from ZZ decay for ADD ($d = 3$) and SM, when $M_{4l} > 600$ GeV.

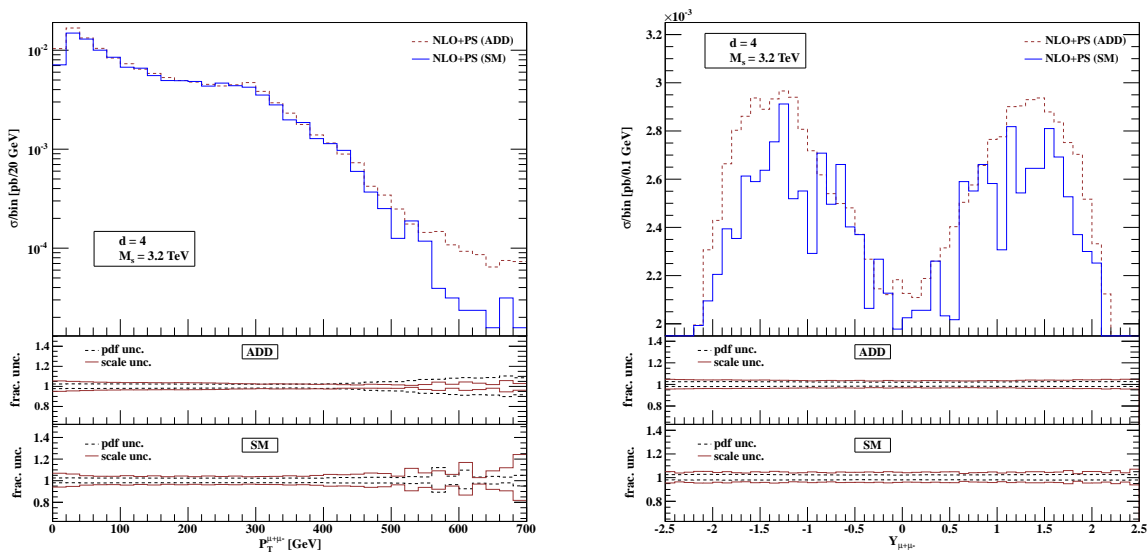


Figure 4.8: Transverse momentum (left) and rapidity (right) distribution of the $\mu^+\mu^-$ pair coming from ZZ decay for ADD ($d = 4$) and SM, when $M_{AI} > 600$ GeV.

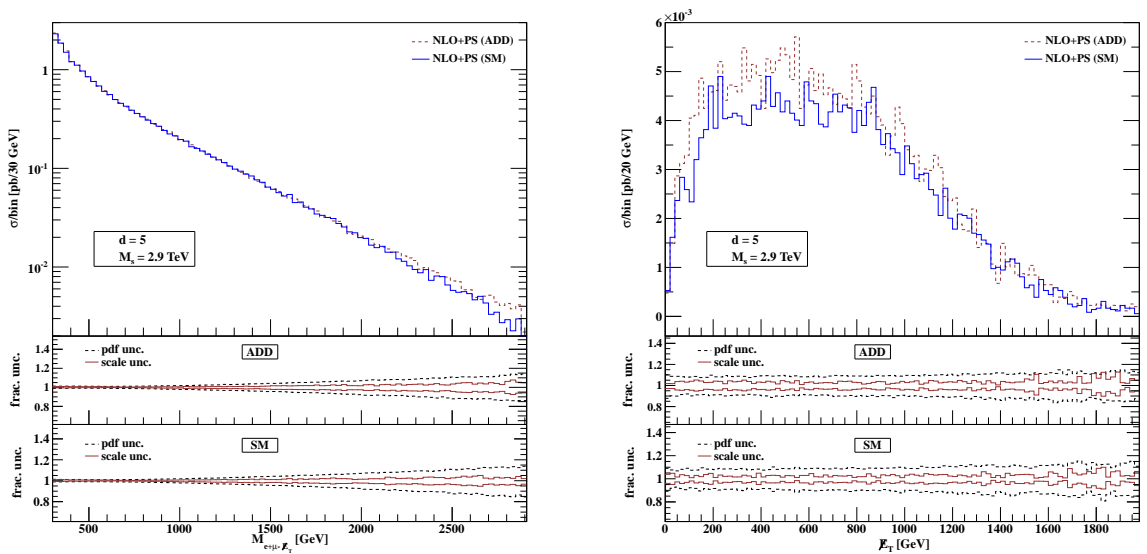


Figure 4.9: Invariant mass ($M_{e^+\mu^-E_T}$) distribution (left) of all the final state decay products of WW and the total missing transverse energy distribution (right) for $d = 5$ and SM. The right one is restricted within $2000 < M_{e^+\mu^-E_T} < M_S$ GeV.

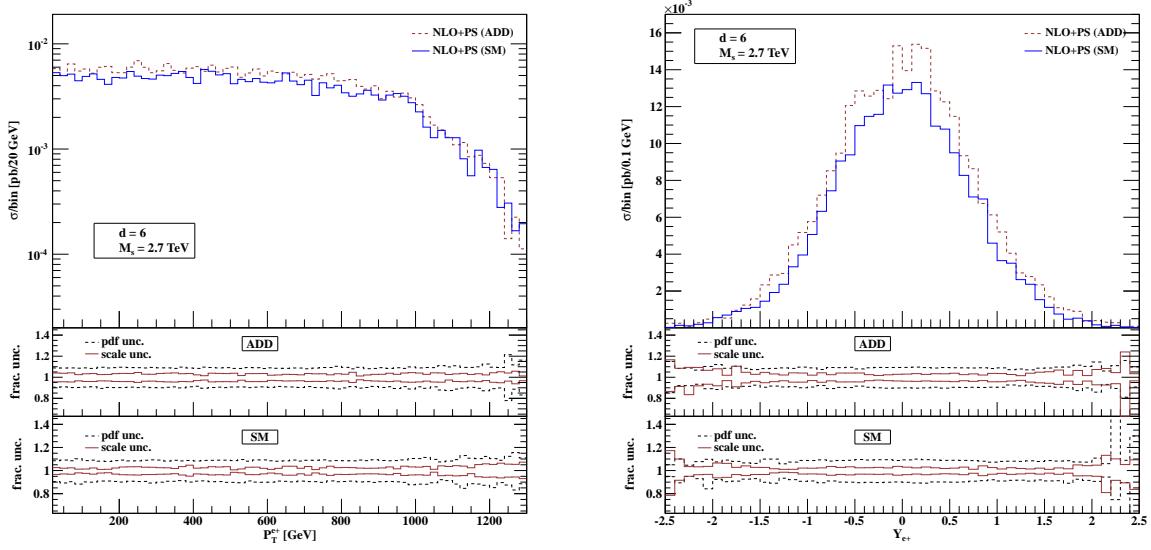


Figure 4.10: Transverse momentum distribution (left) and rapidity distribution (right) of the final state positron which comes from W^+ decay for WW production process in both ADD ($d = 6$) and SM when, $2000 < M_{e^+\mu^-E_{\cancel{\nu}}} < M_S$ GeV.

the choice of M_S values associated with specific number of extra dimensions, we do not find any significant deviation from the SM. In the very high invariant mass region of the four-body final state for $d = 5, 6$ there is some deviation from the SM. In fig. 4.9, we have given the invariant mass ($M_{e^+\mu^-E_{\cancel{\nu}}}$) distribution (left) of the final state decay products of W^\pm and the total missing transverse energy distribution (right) which comes from the final state neutrinos for $d = 5$. For completeness in fig. 4.10, we also provide the transverse momentum distribution of the final state positron (left) along with its rapidity distribution (right) for $d = 6$. Only mild difference between the SM and ADD in the high invariant mass region is observed. We zoom into this very high invariant mass region to look for deviations from the SM for these exclusive observable. We have studied $d\sigma/dE_{\cancel{\nu}}$, $d\sigma/dP_T^{e^+}$ and $d\sigma/d\eta_{e^+}$ in the region when the invariant mass lies between 2 TeV and M_S .

Using the dilepton process, we present the search sensitivity for the extra dimensions $d = 2 - 6$, for 14 TeV LHC. The total cross section σ is calculated using the invariant mass distribution of the di-lepton pair for signal plus background and the background only. For a particular choice of extra dimension d , we find the minimum luminosity by varying the scale M_S at 3-

d	2	3	4	5	6
$M_S^{(3\sigma)}$ (TeV)	12.3	13.7	13.5	11.3	10.5
$M_S^{(5\sigma)}$ (TeV)	10.8	11.3	11.1	11.2	10.1

Table 4.1: Lower bounds on M_S for various extra dimensions d at the 14 TeV LHC with integrated luminosity of 10 fb^{-1} at 3-sigma and 5-sigma signal significance.

sigma (3σ) and 5-sigma (5σ) signal significance. We define the required minimum luminosity as $L = \max\{L_{3\sigma(5\sigma)}, L_{3N_S(5N_S)}\}$, where $L_{3\sigma(5\sigma)}$ is the integrated luminosity at 3-sigma (5-sigma) signal significance and $L_{3N_S(5N_S)}$ describes the integrated luminosity to get at least 3(5) signal events. Now we can get the corresponding M_S value for 10 fb^{-1} luminosity by inversion which is tabulated in table 4.1. Of course, a full analysis including the effects of detector simulation, non-reducible backgrounds *etc.* can be better performed by the experimental collaborations.

4.4 Conclusion

We have made available, the $\ell^+\ell^-$, ZZ , W^+W^- production results to NLO+PS accuracy for the large extra dimension model which is implemented in the `AMC@NLO` framework. All the subprocesses that contribute to NLO in QCD have been included for each of these processes. A selection of results for 8 TeV LHC has been presented for various distributions in an attempt to identify region of interest for extra dimension searches. Scale and PDF uncertainties for each of these distributions have also been studied. In addition, we have presented the search sensitivity for the extra dimensions $d = 2 - 6$, for 14 TeV LHC at 10 fb^{-1} . With the earlier implementation of the di-photon final state to the same accuracy [125], this work completes the rest of the di-final state process (but for di-jet) in large extra dimension searches. In the ADD model, these codes can be used to generate events of the di-final states discussed in this chapter to NLO+PS accuracy and are available on the website <http://amcatnlo.cern.ch>.

Chapter 5

VH production

5.1 Introduction

The Higgs-Strahlung process is one of the potential channels for the Higgs boson production at the LHC. Precise theory predictions for this process are useful in measuring the Higgs-gauge boson couplings accurately. At LO, it is an electroweak process and hence the higher order QCD corrections enter only in the initial state comprising of a quark and an antiquark. This fact prompted this process to be represented in terms of the convolution of the production of a virtual vector boson (W/Z) (DY like) with its decay to a real vector boson and the Higgs boson, at every order in QCD. Therefore, the available higher order QCD corrections to DY process can be used to study the QCD effects in Higgs-Strahlung process. The QCD corrections to DY at next-to leading order (NLO) [81] as well as at NNLO [65, 84] are known for a long time and they have already been used for the Higgs-Strahlung process [70, 71, 142–148]. At NNLO, for the associated production of the Higgs boson with Z boson, there are additional corrections coming from the gluon fusion subprocess via box diagrams and also from the quark antiquark initiated subprocesses where the Higgs boson is coupled to top quark loops. These corrections have been obtained in [71, 145, 146]. In [149], the threshold logarithms have been resummed to NNNLL accuracy matched to NNLO fixed order results, while the transverse momentum logarithms are resummed to NLL accuracy

matched to NLO results. In the gluon fusion channel, the associated Higgs boson production cross sections have also been reported at NLO [150] and the threshold resummation has been achieved at NLL accuracy [151]. However, the final state not being charge neutral, there are no such additional corrections for the associated production of the Higgs with the W -boson.

The `vh@nnlo` [152] program includes all these contributions for the associated productions of ZH and WH separately up to NNLO. The electroweak (EW) corrections reported in [153, 154] have also been incorporated in this program as a multiplicative factor based on the fact that the EW corrections for these processes do not depend on any of the QCD parameters. For LHC8, the NLO corrections have been found to enhance the total inclusive rate by 31% whereas the NNLO DY like corrections contribute towards an additional 3% correction for the ZH production. The numerical values for the WH production are also very similar to the DY like corrections up to NNLO. The top loop effects can be counted for about 1% correction for both the processes. The additional gluon fusion subprocesses generate 5% correction in the case of ZH associated production. These numerical values show that the corrections at NNLO are small in size. Besides, these NNLO corrections are found to reduce the scale dependence significantly. However, the inclusion of higher order terms is important to assess the reliability of the perturbative calculations as well as to have a better understanding of the pattern of these corrections at higher orders.

The chapter is organized as follows. In the Sect. 5.2 we present the results contributing at N³LO in the threshold limit. We then discuss the numerical impact of these corrections at the LHC in Sect. 5.3. Finally, we conclude with our findings in Sect. 6.3.

5.2 Threshold Corrections Beyond NNLO

The inclusive production of Higgs boson in association with vector boson comes from factorizable and non factorizable partonic subprocesses. The factorizable ones can be written as convolution of the production of virtual vector boson with its decay to Higgs and a real vector boson. They are often called DY like. The hadronic cross section for this DY like process $P(p_1) + P(p_2) \rightarrow$

$V(p_V) + H(p_H)$ can be expressed as

$$\sigma(S, M_V^2, M_H^2) = \int_{(M_H+M_V)^2}^S dq^2 \sigma^{V^*}(q^2, S) \frac{d\Gamma(M_V^2, M_H^2, q^2)}{dq^2} \quad (5.1)$$

where p_1 and p_2 are the incoming hadronic momenta and $S = (p_1 + p_2)^2$ is the hadronic center of mass energy squared. The corresponding one for the incoming partons is given as $\hat{s} = (k_1 + k_2)^2$ and the momentum of the virtual gauge boson V^* is $q = (p_V + p_H)$. The parton level cross section for the production of virtual vector boson V^* is denoted by σ^{V^*} and $\frac{d\Gamma}{dq^2}$ represents its decay rate to a real vector boson and the Higgs boson as given by:

$$\frac{d\Gamma(M_V^2, M_H^2, q^2)}{dq^2} = \frac{G_F M_V^4}{2\sqrt{2}\pi^2} \frac{\lambda^{1/2}(M_V^2, M_H^2; q^2)}{(q^2 - M_V^2)^2} \left(1 + \frac{\lambda(M_V^2, M_H^2; q^2)}{12M_V^2/q^2} \right) \quad (5.2)$$

where $\lambda(x, y; z) = \left(1 - \frac{x}{z} - \frac{y}{z}\right)^2 - 4\frac{xy}{z^2}$ is the usual phase-space function for the two body final state.

Now the DY like production cross-section can further be written as:

$$\sigma^{V^*}(q^2, S) = \frac{1}{S} \sum_{a,b} \int_0^1 dx_1 \int_0^1 dx_2 \int_\tau^1 dz f_a(x_1, \mu_F^2) f_b(x_2, \mu_F^2) \Delta_{ab}^{V^*}(z, q^2, \mu_F^2) \delta(\tau - x_1 x_2 z) \quad (5.3)$$

Here f_a and f_b are the parton distribution functions renormalized at the scale μ_F . We have defined $\Delta_{ab} \equiv \hat{s}\hat{\sigma}$ with $\tau = q^2/S$ and $z = q^2/\hat{s}$. This finite Δ_{ab} can be expanded in terms of the strong coupling constant as follows:

$$\Delta_{ab}(z, q^2, \mu_F^2) = \sum_{i=0}^{\infty} (a_s(\mu_R^2))^i \Delta_{ab}^{(i)}(z, q^2, \mu_F^2, \mu_R^2), \quad (5.4)$$

where $a_s(\mu_R^2) = \frac{g_s(\mu_R^2)^2}{16\pi^2}$.

Beyond LO (i.e. $i = 0$) the perturbative coefficients $\Delta_{ab}^{(i)}$ can be split into two parts.

$$\Delta_{ab}^{(i)}(z, q^2, \mu_F^2, \mu_R^2) = \Delta_{ab}^{\text{hard},(i)}(z, q^2, \mu_F^2, \mu_R^2) + \delta_{aq}\delta_{b\bar{q}}\Delta_{q\bar{q}}^{\text{SV},(i)}(z, q^2, \mu_F^2, \mu_R^2) \quad (5.5)$$

The hard part $\Delta_{ab}^{\text{hard},(i)}$ contains the regular terms in the variable z and the part $\Delta^{\text{SV},(i)}$ is simply proportional to $\delta(1-z)$ and \mathcal{D}_k terms resulting from the soft plus virtual (SV) corrections i.e.

$$\Delta_{ab}^{\text{SV},(i)}(z) = \Delta_{ab}^{\text{SV},(i),\delta} \delta(1-z) + \sum_{k=0}^{\infty} \Delta_{ab}^{\text{SV},(i),(k)} \mathcal{D}_k \quad (5.6)$$

with

$$\mathcal{D}_k = \left(\frac{\ln^k(1-z)}{(1-z)} \right)_+ \quad (5.7)$$

As we have already discussed, the hard and soft parts of $\Delta_{ab}^{(i)}$ are known up to NNLO level in QCD. At N³LO level, only $\Delta_{q\bar{q}}^{\text{SV},(3)}$ is known, see [103–105]. The computation of SV part of $\Delta_{q\bar{q}}^{(3)}$ in [103] uses the factorization property of the QCD amplitudes and the Sudakov resummation of soft gluons. At N³LO level in QCD, SV part requires quark form factor as well as the diagonal terms of the mass factorization kernels up to three loop level and the contributions of soft gluon radiations in the single, double and triple gluon emission subprocesses to third order in the strong coupling constant. While the form factor and the kernels are available to desired accuracy for quite some time, the third order soft gluon effects from real emission subprocesses have been missing to get N³LO results till recently. A spectacular achievement by Anastasiou et al. [102] in obtaining the contributions of the third order soft gluon radiations for the inclusive Higgs production process and for the better understanding of the soft gluon resummation paved the way to obtain several third order results as has been discussed earlier in the Sect. 5.1. Along this direction, the results of [103–105] can be used for the Higgs-Strahlung processes to get an estimate of the threshold N³LO corrections as is the case for the pure DY process where these corrections are found to be significant. Up to NNLO, DY like corrections can be found in [65, 84]. At N³LO, the analytic result for the threshold corrections is identical to that of DY process. At this order, the threshold contributions from plus distributions \mathcal{D}_i can be found in [93–97] while for $\delta(1-z)$ term, see [103–105]. For completeness,

we give the full result for the scale choice of $\mu_R = \mu_F = Q$ as follows:

$$\begin{aligned}
\Delta_{q\bar{q}}^{\text{SV},(3)} = & \delta(1-z) \left(C_A^2 C_F \left(\frac{13264}{315} \zeta_2^3 + \frac{14611}{135} \zeta_2^2 - \frac{884}{3} \zeta_2 \zeta_3 + 843 \zeta_2 - \frac{400}{3} \zeta_3^2 \right. \right. \\
& + \left. \frac{82385}{81} \zeta_3 - 204 \zeta_5 - \frac{1505881}{972} \right) + C_A C_F^2 \left(-\frac{20816}{315} \zeta_2^3 - \frac{1664}{135} \zeta_2^2 + \frac{28736}{9} \zeta_2 \zeta_3 \right. \\
& - \left. \frac{13186}{27} \zeta_2 + \frac{3280}{3} \zeta_3^2 - \frac{20156}{9} \zeta_3 - \frac{39304}{9} \zeta_5 + \frac{74321}{36} \right) + C_A C_{Fn_f} \left(-\frac{5756}{135} \zeta_2^2 \right. \\
& + \left. \frac{208}{3} \zeta_2 \zeta_3 - \frac{28132}{81} \zeta_2 - \frac{6016}{81} \zeta_3 - 8 \zeta_5 + \frac{110651}{243} \right) + C_F^3 \left(-\frac{184736}{315} \zeta_2^3 + \frac{412}{5} \zeta_2^2 \right. \\
& + \left. 80 \zeta_2 \zeta_3 - \frac{130}{3} \zeta_2 + \frac{10336}{3} \zeta_3^2 - 460 \zeta_3 + 1328 \zeta_5 - \frac{5599}{6} \right) + C_F^2 n_f \left(\frac{272}{135} \zeta_2^2 \right. \\
& - \left. \frac{5504}{9} \zeta_2 \zeta_3 + \frac{2632}{27} \zeta_2 + \frac{3512}{9} \zeta_3 + \frac{5536}{9} \zeta_5 - \frac{421}{3} \right) + C_{Fn_f, v} \left(\frac{N^2 - 4}{N} \right) \left(-\frac{4}{5} \zeta_2^2 \right. \\
& + \left. 20 \zeta_2 + \frac{28}{3} \zeta_3 - \frac{160}{3} \zeta_5 + 8 \right) + C_F n_f^2 \left(\frac{128}{27} \zeta_2^2 + \frac{2416}{81} \zeta_2 - \frac{1264}{81} \zeta_3 - \frac{7081}{243} \right) \\
& + C_A^2 C_F \mathcal{D}_0 \left(-\frac{2992}{15} \zeta_2^2 - \frac{352}{3} \zeta_2 \zeta_3 + \frac{98224}{81} \zeta_2 + \frac{40144}{27} \zeta_3 - 384 \zeta_5 - \frac{594058}{729} \right) \\
& + C_A^2 C_F \mathcal{D}_1 \left(\frac{704}{5} \zeta_2^2 - \frac{12032}{9} \zeta_2 - 704 \zeta_3 + \frac{124024}{81} \right) + C_A^2 C_F \mathcal{D}_2 \left(\frac{704}{3} \zeta_2 - \frac{28480}{27} \right) \\
& + C_A^2 C_F \mathcal{D}_3 \left(\frac{7744}{27} \right) + C_A C_F^2 \mathcal{D}_0 \left(\frac{1408}{3} \zeta_2^2 - 1472 \zeta_2 \zeta_3 - \frac{12416}{27} \zeta_2 + \frac{26240}{9} \zeta_3 \right. \\
& + \left. \frac{25856}{27} \right) + C_A C_F^2 \mathcal{D}_1 \left(\frac{3648}{5} \zeta_2^2 - \frac{11648}{9} \zeta_2 - 5184 \zeta_3 - \frac{35572}{9} \right) \\
& + C_A C_F^2 \mathcal{D}_2 \left(\frac{11264}{3} \zeta_2 + 1344 \zeta_3 - \frac{4480}{9} \right) + C_A C_F^2 \mathcal{D}_3 \left(\frac{17152}{9} - 512 \zeta_2 \right) \\
& + C_A C_F^2 \mathcal{D}_4 \left(-\frac{7040}{9} \right) + C_A C_{Fn_f} \mathcal{D}_0 \left(\frac{736}{15} \zeta_2^2 - \frac{29392}{81} \zeta_2 - \frac{2480}{9} \zeta_3 + \frac{125252}{729} \right) \\
& + C_A C_{Fn_f} \mathcal{D}_1 \left(384 \zeta_2 - \frac{32816}{81} \right) + C_A C_{Fn_f} \mathcal{D}_2 \left(\frac{9248}{27} - \frac{128}{3} \zeta_2 \right) \\
& + C_A C_{Fn_f} \mathcal{D}_3 \left(-\frac{2816}{27} \right) + C_F^3 \mathcal{D}_0 \left(-6144 \zeta_2 \zeta_3 - 4096 \zeta_3 + 12288 \zeta_5 \right)
\end{aligned}$$

$$\begin{aligned}
& + C_F^3 \mathcal{D}_1 \left(-\frac{14208}{5} \zeta_2^2 + 2976 \zeta_2 - 960 \zeta_3 + 2044 \right) + C_F^3 \mathcal{D}_2 \left(10240 \zeta_3 \right) \\
& + C_F^3 \mathcal{D}_3 \left(-3072 \zeta_2 - 2048 \right) + C_F^3 \mathcal{D}_5 \left(512 \right) + C_F^2 n_f \mathcal{D}_0 \left(-\frac{1472}{15} \zeta_2^2 + \frac{1952}{27} \zeta_2 \right. \\
& \left. - \frac{5728}{9} \zeta_3 - 6 \right) + C_F^2 n_f \mathcal{D}_1 \left(\frac{2048}{9} \zeta_2 + 1280 \zeta_3 + \frac{4288}{9} \right) + C_F^2 n_f \mathcal{D}_2 \left(\frac{544}{9} \right. \\
& \left. - \frac{2048}{3} \zeta_2 \right) + C_F^2 n_f \mathcal{D}_3 \left(-\frac{2560}{9} \right) + C_F^2 n_f \mathcal{D}_4 \left(\frac{1280}{9} \right) + C_F n_f^2 \mathcal{D}_0 \left(\frac{640}{27} \zeta_2 \right. \\
& \left. + \frac{320}{27} \zeta_3 - \frac{3712}{729} \right) + C_F n_f^2 \mathcal{D}_1 \left(\frac{1600}{81} - \frac{256}{9} \zeta_2 \right) - C_F n_f^2 \mathcal{D}_2 \frac{640}{27} \\
& + C_F n_f^2 \mathcal{D}_3 \left(\frac{256}{27} \right), \tag{5.8}
\end{aligned}$$

where ζ_i are the Riemann zeta functions, $C_F = (N^2 - 1)/2N$ and $C_A = N$ are the casimirs for $SU(N)$ gauge theory, n_f is the number of active quark flavours and $n_{f,v}$ is the effective number of flavours resulting from some special class of diagrams at three loop level [89].

5.3 Numerical Results

E_{CM}	LO	NLO _{SV}	NLO	NNLO _{SV}	NNLO	N ³ LO _{SV}
7	0.2415	0.2987	0.3183	0.3203	0.3257	0.3254
8	0.2977	0.3667	0.3901	0.3932	0.3993	0.3991
13	0.6120	0.7363	0.7788	0.7900	0.7975	0.7970
14	0.6801	0.8150	0.8604	0.8730	0.8808	0.8807

Table 5.1: DY like contributions (in pb) to ZH production cross sections at the LHC for different center of mass energies (TeV) with MSTW2008 PDFs. The factorization and renormalization scales are set to $\mu_F = \mu_R = Q$.

In what follows we present the numerical results for associated production of the Higgs boson with vector boson at the LHC for the proton-proton center of mass energies of 7, 8, 13 and 14 TeV. The hadronic cross sections are obtained by folding the respective LO, NLO and NNLO partonic

cross sections with the parton distribution functions (PDFs) measured at the same order in the perturbation theory and by using the corresponding strong coupling constant $\alpha_s(\mu_R)$. For N³LO threshold corrections, however, we use NNLO PDFs and the $\alpha_s(\mu_R)$ obtained from the 4-loop β function. Unless mentioned otherwise, we use MSTW2008 PDFs for our results. Except for the scale uncertainties, both the renormalization and the factorization scales are set to $\mu_R = \mu_F = Q$, where $Q^2 = (p_V + p_H)^2$ is the invariant mass of the vector boson and the Higgs boson.

For the numerical implementation of the N³LO threshold corrections, we have included the additional subroutines for the contributions coming from the $\delta(1-z)$ term and the logarithmic contributions \mathcal{D}_k , in the code `vh@nnlo` in a similar fashion as at the 2-loop level. This easily enables one to compute the N³LO threshold corrections using the PDFs supplied by LHAPDF and the strong coupling constant as in the code `vh@nnlo`.

First, we present the DY like contributions to the ZH associated production up to N³LO in QCD for different LHC energies in table 5.1. Here $\text{NLO}_{\text{SV}} = \text{LO} + a_s \Delta_{q\bar{q}}^{\text{SV},(1)}$, $\text{NNLO}_{\text{SV}} = \text{NLO} + a_s^2 \Delta_{q\bar{q}}^{\text{SV},(2)}$ and $\text{N}^3\text{LO}_{\text{SV}} = \text{NNLO} + a_s^3 \Delta_{q\bar{q}}^{\text{SV},(3)}$. The first and second order SV corrections are found

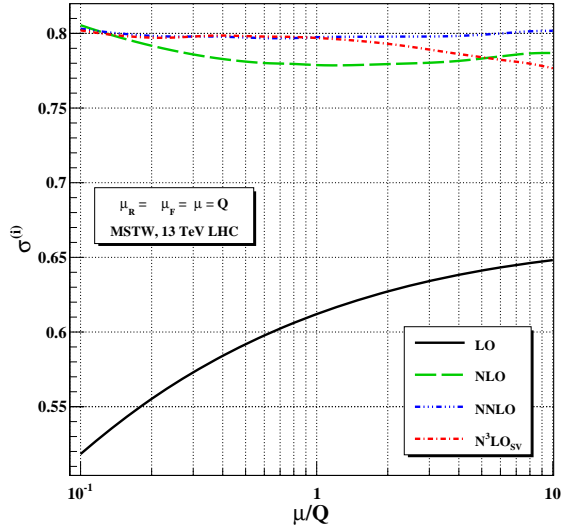


Figure 5.1: Scale uncertainties of DY like contributions to ZH production cross sections for LHC13 by varying the factorization and renormalization scales in the range $0.1 < \mu/Q < 10.0$, where $\mu = \mu_F = \mu_R$.

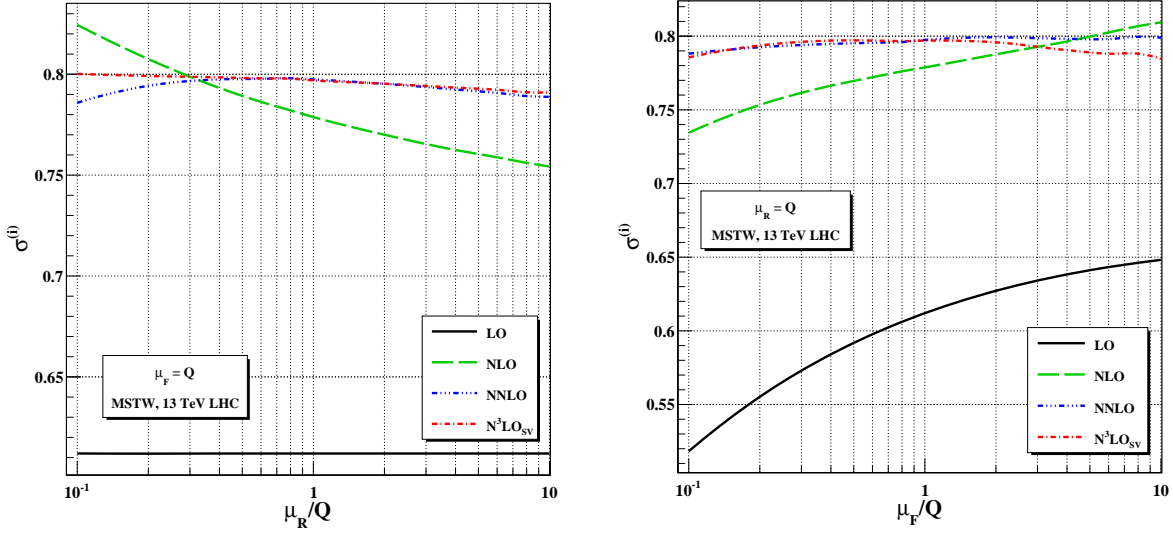


Figure 5.2: Scale uncertainties of DY like contributions to ZH production cross sections for LHC13. In the left panel, we show the renormalization scale uncertainty for $0.1 < \mu_R/Q < 10.0$ keeping $\mu_F = Q$ fixed. In the right panel, we show the factorization scale uncertainty for the similar range variation as μ_R .

to be positive and enhance the cross sections while the third order ones are found to be negative for all different energies. We also observe here that at 3-loop level the $\delta(1-z)$ term can contribute as much as the \mathcal{D}_k terms in magnitude.

For LHC14 we observe that the SV contributions make up to 75% of the exact QCD correction at NLO level while they are about 60% at NNLO level, showing the significant contribution of the large logarithms that arise in the threshold limit. At NNLO, for DY type processes, there will be many more subprocesses exhausting almost all possible combinations of the initial state partons, that will contribute to the beyond threshold corrections. Such is not the case at NLO. Hence, naively one would expect that the contributions of the beyond threshold corrections to the total cross section will increase from NLO to NNLO. At $N^3\text{LO}$ level, as the full result including the beyond threshold corrections is yet to be available, it is not possible to make such a quantitative estimation of the SV contributions and also it is not clear if a similar behavior will continue. However, they constitute an important component of the full $N^3\text{LO}$ result and hence we investigate their numerical impact. In addition, the trend of their contributions at previous orders indicates that they can be numerically

E_{CM}	LO	NLO	NNLO	$\text{N}^3\text{LO}_{\text{SV}}$
7	0.2292	0.3021	0.3230	0.3227
8	0.2826	0.3702	0.3984	0.3982
13	0.5797	0.7377	0.8146	0.8141
14	0.6440	0.8148	0.9037	0.9035

Table 5.2: Total cross sections (in pb) for ZH production at the LHC for different center of mass energies (in TeV).

PDFs	LO	NLO	NNLO	$\text{N}^3\text{LO}_{\text{SV}}$
MSTW2008	0.5797	0.7377	0.8146	0.8141
ABM11	–	0.7716	0.8308	0.8305
NNPDF	0.6199	0.7234	0.7997	0.7994
CT10	0.6307	0.7312	0.8132	0.8128

Table 5.3: Total cross sections (in pb) for ZH production at LHC13 for different PDFs.

non-negligible and can compete with the beyond threshold effects. We also notice, from the results in table 5.1, that the QCD corrections in general increase with the decrease in the proton-proton collision energy.

Next, we study the scale uncertainties by varying the arbitrary factorization and renormalization scales. In fig.5.1, we show the scale dependence of the DY like cross sections up to $\text{N}^3\text{LO}_{\text{SV}}$ by varying the scales in the range $0.1 < \mu/Q < 10.0$, where $\mu = \mu_R = \mu_F$. The scale uncertainties are found to decrease with the order in the perturbation theory. Here, at N^3LO only the soft plus virtual corrections are available. However, with the availability of the respective hard functions and the PDFs, the scale uncertainty is expected to improve further.

E_{CM}	LO	NLO	NNLO	$\text{N}^3\text{LO}_{\text{SV}}$
7	0.4254	0.5590	0.5785	0.5779
8	0.5208	0.6809	0.7043	0.7038
13	1.0474	1.3306	1.3803	1.3800
14	1.1607	1.4671	1.5220	1.5218

Table 5.4: Total cross sections (in pb) for WH production at the LHC for different center of mass energies (in TeV).

In the right panel of fig.5.2, we show only the factorization scale dependence of the DY like cross sections by varying μ_F in the range $0.1 < \mu_F/Q < 10.0$ and keeping $\mu_R = Q$ fixed. The observations are similar to those found in fig.5.1. In the left panel of fig.5.2, we show the renormalization scale dependence by varying it in the range $0.1 < \mu_R/Q < 10.0$ and keeping $\mu_F = Q$ fixed. Here the N³LO threshold results are found to be more stable than the lower order ones as expected.

Apart from the DY like contributions, there will also be other subprocess contributions such as $gg \rightarrow ZH$ via quark loops (σ^{gg}), $q\bar{q} \rightarrow ZH$ via *top*-loops (σ^{top}) at NNLO level. Moreover, the $\mathcal{O}(\alpha)$ electroweak corrections to the DY like processes are already available. These electroweak corrections are assumed to be factorizable from the QCD corrections and hence they are included as a multiplicative factor at each order in the QCD perturbation theory. For consistency, we include in our analysis all these contributions as in [71, 145, 152, 154] and the corresponding third order result is given by

$$\sigma_{N^3LO}^{\text{tot}} = \sigma_{N^3LO}^{DY} (1 + \delta_{EW}) + \sigma^{gg} + \sigma^{\text{top}} \quad (5.9)$$

Here, the δ_{EW} is given at percent level and is the same as defined in the `vh@nnlo` package. In table 5.2, we present the total cross sections up to N³LO in QCD for different center of mass energies. For LHC7 and LHC8, the gluon initiated subprocess contributions are about 5% of DY like at NNLO while the EW corrections are of the same size but with opposite sign. Consequently, the total NNLO cross sections here are almost the same as those of pure DY contributions. However, for LHC13 and LHC14, the gluon initiated subprocess contributions rises to about 9% making the total cross sections larger than those of the DY like processes. In all these cases, the third order QCD corrections are about 0.1% but negative. In table 5.3, we present the total cross sections up to N³LO for LHC13 for different parton distribution functions, namely, ABM11, CT10, NNPDFs and MSTW2008 PDFs.

Finally, we give the total cross sections as defined above for the associated production of *W*-boson and Higgs in table 5.4. The *WH* production cross sections are found to be higher than those of

ZH process. As mentioned previously, there will be no gluon fusion contribution for this process at NNLO owing to the electric charge conservation. However, there will be top-loop contributions at NNLO from quark initiated subprocesses. The threshold N³LO corrections are found to be negative similar to the case of ZH production. For both ZH and WH productions, however, the impact of QCD corrections are found to be similar at each order in the perturbation theory. Moreover, the electroweak corrections here are found to decrease the cross sections by about 6.7% in contrast to the ZH case where they decrease the cross sections by about 5%.

5.4 Conclusion

In this work we have computed the N³LO QCD threshold corrections to the associated production of the Higgs with vector boson using the third order threshold corrections for inclusive DY process, which became available very recently. With both the threshold logarithms \mathcal{D}_k and the $\delta(1-z)$ term, these results are expected to augment the previously available exact NNLO results for this process. For the numerical computation, we have incorporated these corrections in the code `vh@nnlo` to obtain the state of the art results. We gave predictions for ZH as well as WH processes and found that the effects of higher order QCD corrections are similar in both the cases. We have also estimated the theory uncertainties from the factorization and renormalization scales and also from the choice of the parton distribution functions. While the hard part at the N³LO level is yet to be computed, we believe that these results, providing the first predictions in this direction towards the computation of the full N³LO for Higgs-Strahlung processes, will be useful for the phenomenological studies related to Higgs Physics at the LHC.

Chapter 6

Rapidity distribution of the Higgs boson production

6.1 Introduction

Within the framework of SM, the production mechanism of the Higgs boson is dominated by gluon fusion, whereas one of the alternative channels, namely, bottom quark annihilation is severely suppressed by the small Yukawa coupling of bottom quark to the Higgs boson. However, in extensions of the SM with an enlarged spectrum of Higgs sector, as in the case of two-Higgs doublet model, the Yukawa coupling of bottom quark to some of the Higgs bosons can be enhanced significantly, such that the production channel of bottom quark annihilation could be the dominant one. Moreover, the contribution from gluon fusion channel decreases due to enhanced negative top-bottom interference diagrams. Furthermore, the bottom quark initiated processes at hadron colliders are of much theoretical interest on account of the freedom in treating the initial state bottom-quarks. In the four flavor scheme (4FS), alternatively known as the fixed flavor number scheme (FFS), the mass of the bottom quarks is considered to be non-zero throughout and they are excluded from the proton constituents, whereas, in the framework of five flavor scheme (5FS), also known as the variable flavor number scheme (VFS), the bottom quarks are considered as massless partons, except in

the Yukawa coupling, with their own parton distribution functions (PDF).

For the Higgs boson production through $b\bar{b}$ annihilation, the recent results of the Higgs form factor with bottom-antibottom by Gehrmann and Kara [155] and the universal soft distribution obtained for the Drell-Yan production [103] enabled us to obtain the missing $\delta(1-z)$ contribution (see [96, 97, 156] for the partial results to this order) to the production cross-section at threshold at N³LO [157].

The chapter is organized as follows. In Sect. 6.2.1, we perform an explicit calculation of threshold correction to the rapidity distribution of the Higgs boson in $b\bar{b}$ annihilation at NLO, using the factorization properties of QCD amplitude, Sudakov resummation of soft gluons and renormalization group invariance. This helps us to build an elegant framework to calculate the rapidity distribution at threshold, of a colorless state produced at hadron colliders, to all orders in QCD perturbation theory. In Sect. 6.2.2, we use that general framework to achieve the goal of computing the complete analytic expression for the threshold corrections beyond NLO and provide the result up to N³LO. Sect. 6.2.3 contains the discussion on the numerical impacts of our results. Finally, we conclude with our findings in Sect. 6.3.

6.2 Differential Distribution with Respect to Rapidity

The interaction of bottom quarks and the Higgs boson is encapsulated in the following action

$$S_I^b = -\frac{\lambda}{\sqrt{2}} \int d^4x \phi(x) \bar{\psi}_b(x) \psi_b(x) \quad (6.1)$$

where, $\psi_b(x)$ and $\phi(x)$ denote the bottom quark and scalar field, respectively. The Yukawa coupling λ is given by $\sqrt{2}m_b/v$, with the bottom quark mass m_b and the vacuum expectation value $v \approx 246$ GeV. Throughout our calculation, we consider five active flavours (VFS scheme), hence except in the Yukawa coupling, m_b is taken to be zero like other light quarks in the theory.

We study infrared safe differential distribution, namely rapidity distribution of the Higgs bo-

son at hadron colliders, in particular those produced through bottom anti-bottom annihilation. Our findings are very well suited for similar observables where the rapidity distribution is for any colorless state produced at hadron colliders. We will set up a framework that can provide threshold corrections to rapidity distribution of the Higgs boson to all orders in perturbation theory. It is then straightforward to obtain fixed order perturbative results in the threshold limit.

The general framework that we set up for the computation of threshold corrections beyond leading order in the perturbation theory for such observables is based on the factorization property of the QCD amplitudes. Sudakov resummation of soft gluons, renormalization group equations and most importantly the infrared safety of the observable play important role in achieving this task. QCD amplitudes that contribute to hard scattering cross sections exhibit rich infra-red structure through cusp and collinear anomalous dimensions due to the factorization property of soft and collinear configurations. Massless gluons and light quarks are responsible for soft and collinear singularities in these amplitudes and also in partonic subprocesses. Singularities resulting from soft gluons cancel between virtual and real emission diagrams in infrared safe observables. While the final state collinear singularities cancel among themselves if the summation over degenerate states are appropriately carried out in such observables, the initial state collinear singular configurations remain until they are absorbed into bare parton distribution functions. In the upcoming section, we present one loop computation for the rapidity distribution in order to demonstrate how the various soft singularities cancel and also to give a pedagogical derivation of how the most general resummed threshold correction to the rapidity distribution can be obtained.

6.2.1 Threshold Correction at NLO

The process under consideration is the production of the Higgs boson through bottom quark annihilation in hadron colliders. The leading order process is

$$b(k_1) + \bar{b}(k_2) \rightarrow H(q) \tag{6.2}$$

where, k_i 's are the momenta of the incoming bottom and anti-bottom quarks involved in partonic reaction and q is the momentum of the Higgs boson. The hadronic center of mass energy squared is defined by $S \equiv (p_1 + p_2)^2$, where p_i 's are the hadronic momenta and the corresponding one for the incoming partons is given as $\hat{s} = (k_1 + k_2)^2$. The fraction of the initial state hadron momentum carried by the parton is denoted by x_i *i.e.* $k_i = x_i p_i$. The rapidity of the Higgs boson is defined through

$$y = \frac{1}{2} \ln \left(\frac{p_2 \cdot q}{p_1 \cdot q} \right). \quad (6.3)$$

The differential distribution with respect to rapidity of the Higgs boson can be expressed as

$$\frac{d}{dy} \sigma^b(\tau, q^2, y) = \sigma^{b,(0)}(\tau, q^2, \mu_R^2) W^b(\tau, y, q^2, \mu_R^2), \quad \sigma^{b,(0)} = \frac{\pi}{4SN} \lambda^2(\mu_R^2) \quad (6.4)$$

with $\tau \equiv q^2/S$, $q^2 = m_H^2$, m_H -the mass of the Higgs boson. $\lambda(\mu_R^2)$ is the Yukawa coupling defined at the renormalization scale μ_R , $N = 3$ is the number of QCD colors and $\sigma^{b,(0)}$ is the leading order cross-section. Defining $z \equiv q^2/\hat{s}$, we find

$$\begin{aligned} W^b(\tau, y, q^2, \mu_R^2) &= \frac{(Z^b(\mu_R^2))^2}{\sigma^{b,(0)}} \sum_{a,c=b,\bar{b},g} \int_0^1 dx_1 \int_0^1 dx_2 \hat{\mathcal{H}}_{ac}(x_1, x_2) \int_0^1 dz \delta(\tau - zx_1 x_2) \\ &\times \int dPS_{1+X} |\mathcal{M}_{ac \rightarrow H+X}|^2 \delta \left(y - \frac{1}{2} \ln \left(\frac{p_2 \cdot q}{p_1 \cdot q} \right) \right). \end{aligned} \quad (6.5)$$

In this expression, X is the remnants other than the Higgs boson, $Z^b(\mu_R^2)$ is the ultraviolet (UV) renormalization constant for the Yukawa coupling λ and dPS_{1+X} is the phase space element for the $H + X$ system. $\mathcal{M}_{ac \rightarrow H+X}$ denotes the scattering amplitude at partonic level. The function $\hat{\mathcal{H}}_{ac}(x_1, x_2)$ is the product of unrenormalized parton distribution functions (PDF) $\hat{f}_a(x_1)$ and $\hat{f}_c(x_2)$,

$$\hat{\mathcal{H}}_{ac}(x_1, x_2) \equiv \hat{f}_a(x_1) \hat{f}_c(x_2). \quad (6.6)$$

The PDF $f_a(x_1, \mu_F^2)$, renormalized at the factorization scale μ_F , is related to the unrenormalized ones through Altarelli-Parisi (AP) kernel Γ_{ad} as follows:

$$f_a(x_i, \mu_F^2) = \sum_{d=b, \bar{b}, g} \int_{x_i}^1 \frac{dz}{z} \Gamma_{ad}(\hat{a}_s, \mu^2, \mu_F^2, z, \varepsilon) \hat{f}_d\left(\frac{x_i}{z}\right), \quad a = b, \bar{b}, g \quad (6.7)$$

where, the scale μ is introduced to keep the strong coupling constant \hat{g}_s dimensionless in space-time dimensions $n = 4 + \varepsilon$, regulating the theory and $\hat{a}_s \equiv \hat{g}_s^2/16\pi^2$. Expanding the AP kernel in powers of \hat{a}_s , we get

$$\Gamma_{ad}(\hat{a}_s, \mu^2, \mu_F^2, z, \varepsilon) = \delta_{ad} \delta(1-z) + \hat{a}_s S_\varepsilon \left(\frac{\mu_F^2}{\mu^2} \right)^{\frac{\varepsilon}{2}} \frac{1}{\varepsilon} P_{ad}^{(0)}(z) + \mathcal{O}(\hat{a}_s^2) \quad (6.8)$$

where, $P_{ad}^{(0)}(z)$ is the leading order AP splitting function. $S_\varepsilon = \exp\left(\left(\gamma_E - \ln 4\pi\right)\frac{\varepsilon}{2}\right)$ where γ_E is the Euler-Mascheroni constant. Using Γ_{ad} , W^b can be written in terms of renormalized \mathcal{H} , given by

$$\begin{aligned} \mathcal{H}_{ac}(x_1, x_2, \mu_F^2) &\equiv f_a(x_1, \mu_F^2) f_c(x_2, \mu_F^2) \\ &= \int_{x_1}^1 \frac{dy_1}{y_1} \int_{x_2}^1 \frac{dy_2}{y_2} \Gamma_{aa'}(\hat{a}_s, \mu^2, \mu_F^2, y_1, \varepsilon) \hat{\mathcal{H}}_{a'c'}\left(\frac{x_1}{y_1}, \frac{x_2}{y_2}\right) \Gamma_{cc'}(\hat{a}_s, \mu^2, \mu_F^2, y_2, \varepsilon). \end{aligned} \quad (6.9)$$

The LO contribution arises from the Born process $b + \bar{b} \rightarrow H$ and the NLO ones are from one loop virtual contributions to born process and from the real emission processes, namely $b + \bar{b} \rightarrow H + g$, $b(\bar{b}) + g \rightarrow H + b(\bar{b})$. For LO and virtual contributions, $dPS_{1+X} = dPS_1$ and for real emission processes we have two body phase space element $dPS_{1+X} = dPS_2$. In order to define the threshold limit at the partonic level and to express the hadronic cross-section in terms of the partonic one through convolution integrals, we choose to work with the symmetric scaling variables x_1^0 and x_2^0 instead of y and τ which are related through

$$y = \frac{1}{2} \ln\left(\frac{x_1^0}{x_2^0}\right), \quad \tau = x_1^0 x_2^0. \quad (6.10)$$

In terms of these new variables, the partonic subprocess contributions can be shown to depend on the ratios $z_j = \frac{x_j^0}{x_j}$ which take the role of scaling variables at the partonic level. The dimensionless partonic differential cross-section denoted by $\hat{\Delta}_{d,ac}^b$ through

$$\begin{aligned} \frac{1}{x_1 x_2} \hat{\Delta}_{d,ac}^b \left(\frac{x_1^0}{x_1}, \frac{x_2^0}{x_2}, \hat{a}_s, \mu^2, q^2, \mu_R^2 \right) &= \frac{(Z^b(\mu_R^2))^2}{\sigma^{b,(0)}} \int dPS_{1+X} \int dz |\mathcal{M}_{ac \rightarrow H+X}|^2 \\ &\times \delta(\tau - zx_1 x_2) \delta \left(y - \frac{1}{2} \ln \left(\frac{p_2 \cdot q}{p_1 \cdot q} \right) \right) \end{aligned} \quad (6.11)$$

is UV finite. Here subscript d stands for differential distribution. The collinear singularities that arise due to the initial state light partons are removed through the AP kernels resulting in the following finite $\Delta_{d,ac}^b$

$$\begin{aligned} \Delta_{d,ac}^b(z_1, z_2, a_s(\mu_R^2), q^2, \mu_F^2, \mu_R^2) &= \int_{z_1}^1 \frac{dy_1}{y_1} \int_{z_2}^1 \frac{dy_2}{y_2} \Gamma_{ad'}^{-1}(\hat{a}_s, \mu^2, \mu_F^2, y_1, \epsilon) \\ &\times \hat{\Delta}_{d,a'c'}^b \left(\frac{z_1}{y_1}, \frac{z_2}{y_2}, \hat{a}_s, \mu^2, q^2, \mu_R^2, \epsilon \right) \Gamma_{c'c}^{-1}(\hat{a}_s, \mu^2, \mu_F^2, y_2, \epsilon). \end{aligned} \quad (6.12)$$

Therefore, expressing W^b in terms of renormalized \mathcal{H}_{ac} and finite $\Delta_{d,ac}^b$, we get

$$\begin{aligned} W^b(x_1^0, x_2^0, q^2, \mu_R^2) &= \sum_{ac=b, \bar{b}, g} \int_{x_1^0}^1 \frac{dz_1}{z_1} \int_{x_2^0}^1 \frac{dz_2}{z_2} \mathcal{H}_{ac} \left(\frac{x_1^0}{z_1}, \frac{x_2^0}{z_2}, \mu_F^2 \right) \\ &\times \Delta_{d,ac}^b(z_1, z_2, a_s(\mu_R^2), q^2, \mu_F^2, \mu_R^2). \end{aligned} \quad (6.13)$$

Since, W^b involves convolutions of various functions, it becomes normal multiplication in the Mellin space of the Mellin moments of renormalized PDFs, AP kernels and bare differential partonic cross-section. The double Mellin moment of $W^b(x_1^0, x_2^0)$ is defined by

$$\tilde{W}^b(N_1, N_2) \equiv \int dx_1^0 (x_1^0)^{N_1-1} \int dx_2^0 (x_2^0)^{N_2-1} W^b(x_1^0, x_2^0)$$

$$= \widetilde{\mathcal{H}}_{ac}(N_1, N_2) \widetilde{\Delta}_{d,ac}^b(N_1, N_2) \quad (6.14)$$

where

$$\widetilde{\Delta}_{d,ac}^b(N_1, N_2) = \widetilde{\Gamma}_{ae}^{-1}(N_1) \widetilde{\Gamma}_{cf}^{-1}(N_2) \widetilde{\Delta}_{d,ef}^b(N_1, N_2). \quad (6.15)$$

The threshold limit is defined by $N_i \rightarrow \infty$, which in z_j variables corresponds to $z_j \rightarrow 1$. In this limit, only diagonal terms in the AP kernel $\widetilde{\Gamma}^{-1}$ and $\widetilde{\Delta}_d^b$ contribute to the differential cross-section. Hence, $\ln \widetilde{\Delta}_d^b$ is simply a sum of the contributions from 1) diagonal terms of the AP kernels and 2) bare differential partonic cross-section. Due to the born kinematics, the form factor contribution can be further factored out from the differential partonic cross sections to all orders in perturbation theory. Hence, the remaining part of the differential partonic cross-sections contains contributions from only real emission processes, namely those involving only soft gluons. Taking into account the renormalization constant of the Yukawa coupling $\hat{\lambda}$, we find

$$\begin{aligned} \ln \widetilde{\Delta}_d^b(N_1, N_2, q^2, \mu_R^2, \mu_F^2) &= \ln \left(Z^b(\mu_R^2) \right)^2 - \ln \widetilde{\Gamma}_{bb}(N_1, \mu_F^2) - \ln \widetilde{\Gamma}_{bb}(N_2, \mu_F^2) \\ &\quad + \ln |\hat{F}^b(q^2)|^2 + \ln \widetilde{S}^b(N_1, N_2, q^2) \end{aligned} \quad (6.16)$$

where \hat{F}^b and $\widetilde{S}^b(N_1, N_2)$ are bare form factor and real emission contributions of partonic subprocesses, respectively. The inverse Mellin transform will bring back the expressions in terms of the variables z_j and they will contain besides regular functions, the distributions namely $\delta(1 - z_j)$, \mathcal{D}_i and $\overline{\mathcal{D}}_i$, defined as

$$\mathcal{D}_i = \left[\frac{\ln^i(1 - z_1)}{(1 - z_1)} \right]_+, \quad \overline{\mathcal{D}}_i = \left[\frac{\ln^i(1 - z_2)}{(1 - z_2)} \right]_+, \quad i = 0, 1, \dots \quad (6.17)$$

The subscript ‘+’ denotes the customary ‘plus-distribution’ $f_+(z)$ which acts on functions regular in $z \rightarrow 1$ limit as

$$\int_0^1 dz f_+(z) g(z) = \int_0^1 dz f(z) (g(z) - g(1)) \quad (6.18)$$

where, $g(z)$ is any well behaved function in the region $0 \leq z \leq 1$. In the threshold limit, we drop all the regular terms and keep only these distributions.

In the following, we perform NLO computation in the threshold limit. The overall renormalization constant $(Z^b)^2$ is found to be

$$(Z^b(\mu_R^2))^2 = 1 + \hat{a}_s S_\epsilon \left(\frac{\mu_R^2}{\mu^2} \right)^\epsilon C_F \left(\frac{12}{\epsilon} \right) + \mathcal{O}(\hat{a}_s^2). \quad (6.19)$$

The form factor contribution $|\hat{F}^b|^2$ at one loop level gives

$$|\hat{F}^b(q^2)|^2 = 1 + \hat{a}_s S_\epsilon \left(\frac{q^2}{\mu^2} \right)^\epsilon C_F \left(-\frac{16}{\epsilon} - 4 + 14\zeta_2 + \mathcal{O}(\epsilon) \right) + \mathcal{O}(\hat{a}_s^2) \quad (6.20)$$

The contribution from Γ_{bb} in the threshold limit is found to be

$$\begin{aligned} \int_{z_1}^1 \frac{dy_1}{y_1} \int_{z_2}^1 \frac{dy_2}{y_2} \Gamma_{bb}^{-1}(y_1, \mu_F^2) \delta\left(1 - \frac{z_1}{y_1}\right) \delta\left(1 - \frac{z_2}{y_2}\right) \Gamma_{bb}^{-1}(y_2, \mu_F^2) &= \delta(1 - z_1) \delta(1 - z_2) \\ -\hat{a}_s S_\epsilon \left(\frac{\mu_F^2}{\mu^2} \right)^\epsilon C_F \frac{1}{\epsilon} \left[\left(8 \frac{1}{(1 - z_1)_+} + 6\delta(1 - z_1) \right) \delta(1 - z_2) \right. \\ \left. + \left(8 \frac{1}{(1 - z_2)_+} + 6\delta(1 - z_2) \right) \delta(1 - z_1) \right] &+ \mathcal{O}(\hat{a}_s^2). \end{aligned} \quad (6.21)$$

Note that the regular terms in the limit $z_j \rightarrow 1$ in Γ_{bb} do not contribute in the threshold limit and hence dropped.

The inverse Mellin transform of $\tilde{S}^b(N_1, N_2)$, namely $S^b(z_1, z_2)$ can be obtained directly from the real gluon emission processes in bottom anti-bottom annihilation processes: $b + \bar{b} \rightarrow H + g$. The

two body phase space is given by

$$dPS_{H+g} = \frac{1}{8\pi x_1 x_2} \frac{1}{\Gamma(1 + \frac{\epsilon}{2})} \left(\frac{m_H^2}{4\pi} \right)^{\frac{\epsilon}{2}} \frac{2z_1 z_2 (1 + z_1 z_2)}{(z_1 + z_2)^{2-\epsilon}} \left((1 - z_1^2)(1 - z_2^2) \right)^{\frac{\epsilon}{2}}. \quad (6.22)$$

The phase space in the limit $z_j \rightarrow 1$ becomes

$$dPS_{H+g}|_{z_i \rightarrow 1} = \frac{1}{8\pi x_1 x_2} \frac{1}{\Gamma(1 + \frac{\epsilon}{2})} \left(\frac{m_H^2}{4\pi} \right)^{\frac{\epsilon}{2}} \left((1 - z_1^2)(1 - z_2^2) \right)^{\frac{\epsilon}{2}}. \quad (6.23)$$

The spin and color averaged matrix element square in threshold limit is found to be

$$|\overline{M}_{b\bar{b} \rightarrow H+g}|_{z_j \rightarrow 1}^2 = \sigma_0^b \frac{\hat{a}_s}{\mu^\epsilon} C_F \left[\frac{32}{(1 - z_1)(1 - z_2)} + \mathcal{O}(\epsilon^3) \right] \quad (6.24)$$

where terms that are regular in z_j as $z_j \rightarrow 1$ have been dropped. It is then straightforward to obtain the threshold contribution resulting from the real gluon emission process:

$$\begin{aligned} S^b(z_1, z_2) &= \delta(1 - z_1)\delta(1 - z_2) + \hat{a}_s \left(\frac{q^2}{4\pi\mu^2} \right)^{\frac{\epsilon}{2}} \frac{1}{\Gamma(1 + \frac{\epsilon}{2})} \\ &\quad \times 4C_F \left[\frac{(1 - z_1)^{\frac{\epsilon}{2}}(1 - z_2)^{\frac{\epsilon}{2}}}{(1 - z_1)(1 - z_2)} + \mathcal{O}(\epsilon^3) \right]. \end{aligned} \quad (6.25)$$

Using the identity

$$\frac{(1 - z_j)^{a\frac{\epsilon}{2}}}{(1 - z_j)} = \frac{2}{a\epsilon} \delta(1 - z_j) + \left(\frac{(1 - z_j)^{a\frac{\epsilon}{2}}}{(1 - z_j)} \right)_+, \quad (6.26)$$

it can be shown that $\Delta_d^b(z_1, z_2)$ in the threshold limit contains only the distributions such as $\delta(1 - z_j)$, \mathcal{D}_i and $\overline{\mathcal{D}}_i$. Decomposing $\Delta_{d,ac}^b$ into hard and soft parts,

$$\Delta_{d,ac}^b(z_1, z_2, q^2, \mu_F^2, \mu_R^2) = \Delta_{d,ac}^{b,\text{hard}}(z_1, z_2, q^2, \mu_F^2, \mu_R^2) + \delta_{ac} \Delta_{d,b}^{\text{SV}}(z_1, z_2, q^2, \mu_F^2, \mu_R^2), \quad (6.27)$$

and setting $\mu_F = \mu_R = m_H$, we find

$$\begin{aligned}
\Delta_{d,b}^{\text{SV},(0)} &= \delta(1-z_1)\delta(1-z_2), \\
\Delta_{d,b}^{\text{SV},(1)} &= \delta(1-z_1)\delta(1-z_2)C_F\left(-2+6\zeta_2\right) + \mathcal{D}_0\overline{\mathcal{D}}_0\left(2C_F\right) \\
&\quad + \mathcal{D}_1\delta(1-z_2)\left(4C_F\right) + \left\{z_1 \leftrightarrow z_2\right\}
\end{aligned} \tag{6.28}$$

At the hadronic level, decomposing W^b as

$$W^b(x_1^0, x_2^0, q^2, \mu_R^2, \mu_F^2) = W_b^{\text{hard}}(x_1^0, x_2^0, q^2, \mu_R^2, \mu_F^2) + W_b^{\text{SV}}(x_1^0, x_2^0, q^2, \mu_R^2, \mu_F^2), \tag{6.29}$$

similar to $\Delta_{d,b}$ and putting $\Delta_{d,b}^{\text{SV}}$ we get, to order $a_s = a_s(m_H^2)$

$$\begin{aligned}
W_b^{\text{SV}}(x_1^0, x_2^0, q^2, m_H^2) &= \mathcal{H}_{b\bar{b}}(x_1^0, x_2^0) + a_s 4C_F \left[\mathcal{H}_{b\bar{b}}(x_1^0, x_2^0) \left(-1 + \zeta_2 + li_2(x_1^0) + li_2(x_2^0) \right) \right. \\
&\quad + \frac{1}{2} \ln^2((1-x_1^0)(1-x_2^0)) + \ln\left(\frac{(1-x_1^0)}{x_2^0}\right) \ln\left(\frac{(1-x_2^0)}{x_1^0}\right) \\
&\quad + \int dx_1 \mathcal{H}_{b\bar{b},1}(x_1, x_2^0) \frac{1}{x_1 - x_1^0} \ln\left(\frac{(1-x_2^0)(x_1 - x_1^0)}{x_1 x_2^0}\right) \\
&\quad + \int dx_2 \mathcal{H}_{b\bar{b},1}(x_1^0, x_2) \frac{1}{x_2 - x_2^0} \ln\left(\frac{(1-x_1^0)(x_2 - x_2^0)}{x_1^0 x_2}\right) \\
&\quad \left. + \int dx_1 \int dx_2 \mathcal{H}_{b\bar{b},12}(x_1, x_2) \frac{1}{(x_1 - x_1^0)(x_2 - x_2^0)} \right].
\end{aligned} \tag{6.30}$$

where all the parton densities are defined at $\mu_F = m_H$. In general,

$$\begin{aligned}
\mathcal{H}_{b\bar{b},12}(x_1, x_2, \mu_F^2) &\equiv \mathcal{H}_{b\bar{b}}(x_1, x_2, \mu_F^2) - \mathcal{H}_{b\bar{b}}(x_1^0, x_2, \mu_F^2) - \mathcal{H}_{b\bar{b}}(x_1, x_2^0, \mu_F^2) + \mathcal{H}_{b\bar{b}}(x_1^0, x_2^0, \mu_F^2), \\
\mathcal{H}_{b\bar{b},1}(x_1, x_2, \mu_F^2) &\equiv \mathcal{H}_{b\bar{b}}(x_1, x_2, \mu_F^2) - \mathcal{H}_{b\bar{b}}(x_1^0, x_2, \mu_F^2),
\end{aligned}$$

$$\mathcal{H}_{b\bar{b},2}(x_1, x_2, \mu_F^2) \equiv \mathcal{H}_{b\bar{b}}(x_1, x_2, \mu_F^2) - \mathcal{H}_{b\bar{b}}(x_1, x_2^0, \mu_F^2) \quad (6.31)$$

The Spence function ($li_2(x)$) is defined as

$$li_2(x) \equiv - \int_0^x \frac{dz}{z} \ln(1-z). \quad (6.32)$$

The exact result computed at NLO level confirms our expectations, see for example [158] where the rapidity distribution of di-leptons in the Drell-Yan production for a physics beyond the SM (BSM) involving a generic Yukawa type interaction was obtained to NLO level. After the suitable replacement of the BSM coupling in [158], we obtain

$$\frac{d\sigma^b}{dy}(\tau, y, Q^2) = \sigma^{b,(0)}(\mu_F) \left[W_{b\bar{b}}(x_1^0, x_2^0, \mu_F^2) + W_{bg}(x_1^0, x_2^0, \mu_F^2) + W_{gb}(x_1^0, x_2^0, \mu_F^2) \right] \quad (6.33)$$

where W 's can be expanded in the strong coupling constant $a_s(\mu_F^2)$ as

$$W_{ac}(x_1^0, x_2^0, \mu_F^2) = W_{ac}^{(0)}(x_1^0, x_2^0, \mu_F^2) + a_s(\mu_F^2) W_{ac}^{(1)}(x_1^0, x_2^0, \mu_F^2) + \mathcal{O}(a_s^2) \quad (6.34)$$

and the corresponding coefficients are given by

$$\begin{aligned} W_{b\bar{b}}^{(0)}(x_1^0, x_2^0, \mu_F^2) &= \mathcal{H}_{b\bar{b}}(x_1^0, x_2^0, \mu_F^2) \\ W_{b\bar{b}}^{(1)}(x_1^0, x_2^0, \mu_F^2) &= 2 C_F \left\{ \varphi_0^{b\bar{b}} + \int dx_1 \varphi_1^{b\bar{b}} + \int dx_1 dx_2 \varphi_2^{b\bar{b}} \right\} + (1 \leftrightarrow 2) \\ W_{gb}^{(1)}(x_1^0, x_2^0, \mu_F^2) &= 2 T_f \int \frac{dx_1}{x_1^3} \left[\varphi_1^{g\bar{b}} + \int dx_2 \left\{ \varphi_2^{g\bar{b}} - \frac{\varphi_3^{g\bar{b}} \mathcal{H}_{gb}(x_1, x_2, \mu_F^2)}{x_2^2 (x_2 + x_2^0) (x_1 x_2^0 + x_2 x_1^0)^3} \right\} \right] \\ W_{bg}^{(1)}(x_1^0, x_2^0, \mu_F^2) &= W_{gb}^{(1)}(x_1^0, x_2^0, \mu_F^2)|_{(1 \leftrightarrow 2)} \end{aligned} \quad (6.35)$$

with

$$\begin{aligned}
\varphi_0^{b\bar{b}} &= \frac{1}{2} \mathcal{H}_{b\bar{b}}(x_1^0, x_2^0, \mu_F^2) \left(-2 + \kappa_{12}^2 + 6 \zeta_2 + 2 \kappa_{12} \ln \frac{q^2}{\mu_F^2} \right) \\
\varphi_1^{b\bar{b}} &= \frac{2\kappa_{b_1}}{x_1 - x_1^0} \mathcal{H}_{b\bar{b},1}(x_1, x_2^0, \mu_F^2) + \mathcal{H}_{b\bar{b}}(x_1, x_2^0, \mu_F^2) \left(\frac{1 - \kappa_{a_1}}{x_1} + \frac{2\kappa_{c_1}}{x_1 - x_1^0} - \frac{1 + \kappa_{a_1} x_1^0}{x_1^2} \right) \\
\varphi_2^{b\bar{b}} &= \frac{\mathcal{H}_{b\bar{b},12}(x_1, x_2, \mu_F^2)}{(x_1 - x_1^0)(x_2 - x_2^0)} - \frac{x_2 + x_2^0}{(x_1 - x_1^0)x_2^2} \mathcal{H}_{b\bar{b},1}(x_1, x_2, \mu_F^2) \\
&\quad + \frac{\mathcal{H}_{b\bar{b}}(x_1, x_2, \mu_F^2)}{2x_1^2 x_2^2} \left((x_1 + x_1^0)(x_2 + x_2^0) + \frac{x_1^2 x_2^2 + x_1^0 x_2^0}{(x_1 + x_1^0)(x_2 + x_2^0)} \right) \\
\varphi_1^{g\bar{b}} &= \mathcal{H}_{gb}(x_1, x_2^0, \mu_F^2) \left(2x_1^0(x_1 - x_1^0) + \kappa_{a_1} (x_1^0 + (x_1 - x_1^0)^2) \right) \\
\varphi_2^{g\bar{b}} &= \frac{\mathcal{H}_{gb,2}(x_1, x_2, \mu_F^2)}{x_2 - x_2^0} (x_1^0 + (x_1 - x_1^0)^2) \\
\varphi_3^{g\bar{b}} &= -x_1^5 x_2^2 x_2^0 + x_1^4 x_1^0 x_2^2 x_2^0 (3x_2 + 4x_2^0) + x_1^3 x_1^0 x_2 x_2^0 (3x_2^3 + 2x_2^0) + 2x_1^0 x_2^2 (x_2^3 + 2x_2^2 x_2^0 \\
&\quad + 2x_2 x_2^0 + 2x_2^0) + 2x_1 x_1^0 x_2 (-x_2^4 + x_2^3 x_2^0 + 4x_2^2 x_2^0 + 2x_2 x_2^0 + 2x_2^0) \\
&\quad + x_1^2 x_1^0 (x_2^5 - 4x_2^4 x_2^0 - 4x_2^3 x_2^0 + 2x_2^2 x_2^0 + 2x_2 x_2^0 + 2x_2^0)
\end{aligned} \tag{6.36}$$

and

$$\begin{aligned}
\kappa_{a_1} &= \ln \frac{2q^2(1-x_2^0)(x_1-x_1^0)}{\mu_F^2(x_1+x_1^0)x_2^0}, & \kappa_{b_1} &= \ln \frac{q^2(1-x_2^0)(x_1-x_1^0)}{\mu_F^2 x_1^0 x_2^0} \\
\kappa_{c_1} &= \ln \frac{2x_1^0}{x_1+x_1^0} & \kappa_{12} &= \ln \frac{(1-x_1^0)(1-x_2^0)}{x_1^0 x_2^0}.
\end{aligned} \tag{6.37}$$

In the threshold limit, after setting $\mu_F = m_H$, we find that the above result reduces to given in Eq. 6.30.

6.2.2 Threshold Corrections Beyond NLO

Following the factorization approach that we used in the previous section to obtain the threshold correction to NLO rapidity distribution, we now set up a framework to compute threshold correc-

tions to rapidity distribution to all orders in strong coupling constant. Our approach is based on the fact that the rapidity distribution in the threshold limit can be systematically factorized into 1) the exact form factor, 2) overall UV renormalization constant, 3) soft gluon contributions from real emission partonic subprocesses and 4) the diagonal collinear subtraction terms involving only $\delta(1-z)$ and $\mathcal{D}_0(z)$ terms of AP splitting functions. We call such a combination soft-virtual (SV) part of the rapidity distribution and the remaining part as hard. Hence, we propose that

$$\Delta_{d,b}^{\text{SV}}(z_1, z_2, q^2, \mu_R^2, \mu_F^2) = \mathcal{C} \exp \left(\Psi_d^b(q^2, \mu_R^2, \mu_F^2, z_1, z_2, \varepsilon) \right) \Big|_{\varepsilon=0}. \quad (6.38)$$

The symbol ‘ \mathcal{C} ’ means convolution with the following definition

$$\begin{aligned} \mathcal{C} e f(z_1, z_2) &= \delta(1-z_1)\delta(1-z_2) + \frac{1}{1!} f(z_1, z_2) + \frac{1}{2!} f(z_1, z_2) \otimes f(z_1, z_2) \\ &+ \frac{1}{3!} f(z_1, z_2) \otimes f(z_1, z_2) \otimes f(z_1, z_2) + \dots, \end{aligned} \quad (6.39)$$

where, \otimes indicates double Mellin convolution with respect to the variables z_1 and z_2 and the function $f(z_1, z_2)$ is a distribution of the kind $\delta(1-z_j)$ and/or $\mathcal{D}_i(z_j)$. The finite distribution Ψ_d^b in dimensional regularization contains $Hb\bar{b}$ unrenormalized form factor $\hat{F}^b(\hat{a}_s, q^2 = -Q^2, \mu^2, \varepsilon)$, UV overall operator renormalization constant $Z^b(\hat{a}_s, \mu_R^2, \mu^2, \varepsilon)$, soft distribution functions $\Phi_d^b(\hat{a}_s, q^2, \mu^2, z_1, z_2, \varepsilon)$ and the mass factorization kernels $\Gamma_{bb}(\hat{a}_s, \mu^2, \mu_F^2, z_j, \varepsilon)$:

$$\begin{aligned} \Psi_d^b &= \left(\ln \left(Z^b(\hat{a}_s, \mu_R^2, \mu^2, \varepsilon) \right)^2 + \ln |\hat{F}^b(\hat{a}_s, Q^2, \mu^2, \varepsilon)|^2 \right) \delta(1-z_1)\delta(1-z_2) \\ &+ 2 \Phi_d^b(\hat{a}_s, q^2, \mu^2, z_1, z_2, \varepsilon) - \mathcal{C} \ln \Gamma_{bb}(\hat{a}_s, \mu^2, \mu_F^2, z_1, \varepsilon) \delta(1-z_2) \\ &- \mathcal{C} \ln \Gamma_{bb}(\hat{a}_s, \mu^2, \mu_F^2, z_2, \varepsilon) \delta(1-z_1). \end{aligned} \quad (6.40)$$

We have expressed all the quantities in the above equation in terms of unrenormalized strong coupling constant \hat{a}_s related to the standard $\hat{\alpha}_s$ through $\hat{a}_s = \hat{\alpha}_s/4\pi$ and the dimensional regulariza-

tion scale μ . The UV renormalization of \hat{a}_s is done at the renormalization scale μ_R through $Z(\mu_R^2)$ giving the renormalized $a_s(\mu_R^2)$, that is

$$\hat{a}_s = \left(\frac{\mu}{\mu_R}\right)^\varepsilon Z(\mu_R^2) S_\varepsilon^{-1} a_s(\mu_R^2). \quad (6.41)$$

The renormalization group equation (RGE) for $a_s(\mu_R^2)$

$$\mu_R^2 \frac{da_s(\mu_R^2)}{d\mu_R^2} = \frac{\varepsilon a_s(\mu_R^2)}{2} + \beta(a_s(\mu_R^2)) \quad (6.42)$$

with

$$\beta(a_s(\mu_R^2)) = a_s(\mu_R^2) \mu_R^2 \frac{d \ln Z(\mu_R^2)}{d\mu_R^2} = - \sum_{i=0}^{\infty} a_s^{i+2}(\mu_R^2) \beta_i, \quad (6.43)$$

determines the structure of the $Z(\mu_R^2)$, up to $\mathcal{O}(a_s^3)$, we find

$$Z(\mu_R^2) = 1 + a_s(\mu_R^2) \frac{2}{\varepsilon} \beta_0 + a_s^2(\mu_R^2) \left(\frac{4}{\varepsilon^2} \beta_0^2 + \frac{1}{\varepsilon} \beta_1 \right) + a_s^3(\mu_R^2) \left(\frac{8}{\varepsilon^3} \beta_0^3 + \frac{14}{3\varepsilon^2} \beta_0 \beta_1 + \frac{2}{3\varepsilon} \beta_2 \right). \quad (6.44)$$

The first three coefficients of the QCD β function, β_0 , β_1 and β_2 are given by [159]

$$\begin{aligned} \beta_0 &= \frac{11}{3} C_A - \frac{4}{3} T_F n_f, \\ \beta_1 &= \frac{34}{3} C_A^2 - 4 T_F n_f C_F - \frac{20}{3} T_F n_f C_A, \\ \beta_2 &= \frac{2857}{54} C_A^3 - \frac{1415}{27} C_A^2 T_F n_f + \frac{158}{27} C_A T_F^2 n_f^2 \\ &\quad + \frac{44}{9} C_F T_F^2 n_f^2 - \frac{205}{9} C_F C_A T_F n_f + 2 C_F^2 T_F n_f \end{aligned} \quad (6.45)$$

with the $SU(N)$ color factors

$$C_A = N, \quad C_F = \frac{N^2 - 1}{2N}, \quad T_F = \frac{1}{2} \quad (6.46)$$

and n_f is the number of active flavours.

The overall operator renormalization constant Z^b renormalizes the bare Yukawa coupling $\hat{\lambda}$ resulting $\lambda(\mu_R^2)$ through the relation

$$\hat{\lambda} = \left(\frac{\mu}{\mu_R}\right)^{\frac{\varepsilon}{2}} Z^b(\mu_R^2) S_\varepsilon^{-1} \lambda(\mu_R^2). \quad (6.47)$$

In $\overline{\text{MS}}$ scheme, $Z^b(\mu_R^2)$ is identical to quark mass renormalization constant. The RGE for $\lambda(\mu_R^2)$ takes the form

$$\mu_R^2 \frac{d}{d\mu_R^2} \ln Z^b(\hat{a}_s, \mu_R^2, \mu^2, \varepsilon) = \sum_{i=1}^{\infty} a_s^i(\mu_R^2) \gamma_{i-1}^b, \quad (6.48)$$

with the anomalous dimensions γ_i^b given by [160–162]

$$\begin{aligned} \gamma_0^b &= 3C_F, \\ \gamma_1^b &= \frac{3}{2}C_F^2 + \frac{97}{6}C_F C_A - \frac{10}{3}C_F T_F n_f, \\ \gamma_2^b &= \frac{129}{2}C_F^3 - \frac{129}{4}C_F^2 C_A + \frac{11413}{108}C_F C_A^2 + \left(-46 + 48\zeta_3\right)C_F^2 T_F n_f \\ &\quad + \left(-\frac{556}{27} - 48\zeta_3\right)C_F C_A T_F n_f - \frac{140}{27}C_F T_F^2 n_f^2. \end{aligned} \quad (6.49)$$

Upon solving the above RGE in $4 + \varepsilon$ space-time dimensions, we obtain

$$\begin{aligned} \ln Z^b(\mu_R^2) &= a_s(\mu_R^2) \frac{1}{\varepsilon} \left(2\gamma_0^b\right) + a_s^2(\mu_R^2) \left[\frac{1}{\varepsilon^2} \left(2\beta_0\gamma_0^b\right) + \frac{1}{\varepsilon} \left(\gamma_1^b\right) \right] \\ &\quad + a_s^3(\mu_R^2) \left[\frac{1}{\varepsilon^3} \left(\frac{8}{3}\beta_0^2\gamma_0^b\right) + \frac{1}{\varepsilon^2} \left(\frac{4}{3}\beta_1\gamma_0^b + \frac{4}{3}\beta_0\gamma_1^b\right) + \frac{1}{\varepsilon} \left(\frac{2}{3}\gamma_2^b\right) \right] \end{aligned} \quad (6.50)$$

up to $\mathcal{O}(a_s^3)$.

The bare form factor $\hat{F}^b(\hat{a}_s, Q^2, \mu^2, \varepsilon)$ satisfies the following differential equation which follows

from the gauge as well as renormalization group invariances [163–166]

$$Q^2 \frac{d}{dQ^2} \ln \hat{F}^b = \frac{1}{2} \left[K^b(\hat{a}_s, \frac{\mu_R^2}{\mu^2}, \varepsilon) + G^b(\hat{a}_s, \frac{Q^2}{\mu_R^2}, \frac{\mu_R^2}{\mu^2}, \varepsilon) \right] \quad (6.51)$$

where, all the poles in ε are encapsulated within K^b and G^b contains the terms finite in ε . Renormalization group invariance of $\hat{F}^b(\hat{a}_s, Q^2, \mu^2, \varepsilon)$ leads

$$\mu_R^2 \frac{d}{d\mu_R^2} K^b = -\mu_R^2 \frac{d}{d\mu_R^2} G^b = -\sum_{i=1}^{\infty} \hat{a}_s^i (\mu_R^2) A_i^q, \quad (6.52)$$

where, A_i^q 's are the cusp anomalous dimensions, found to be [90, 167–170]

$$\begin{aligned} A_1^q &= 4C_F, \\ A_2^q &= 8C_F C_A \left\{ \frac{67}{18} - \zeta_2 \right\} + 8C_F n_f \left\{ -\frac{5}{9} \right\}, \\ A_3^q &= 16C_F C_A^2 \left\{ \frac{245}{24} - \frac{67}{9} \zeta_2 + \frac{11}{6} \zeta_3 + \frac{11}{5} \zeta_2^2 \right\} + 16C_F^2 n_f \left\{ -\frac{55}{24} + 2\zeta_3 \right\} \\ &\quad + 16C_F C_A n_f \left\{ -\frac{209}{108} + \frac{10}{9} \zeta_2 - \frac{7}{3} \zeta_3 \right\} + 16C_F n_f^2 \left\{ -\frac{1}{27} \right\}. \end{aligned} \quad (6.53)$$

Being flavor independent, A_i^b 's are same as A_i^q . Solving the RGE 6.52 satisfied by K^b we get

$$K^b(\hat{a}_s, \mu^2, \mu_R^2, \varepsilon) = \sum_{i=1}^{\infty} \hat{a}_s^i \left(\frac{\mu_R^2}{\mu^2} \right)^{i \frac{\varepsilon}{2}} S_\varepsilon^i K^{b,(i)}(\varepsilon) \quad (6.54)$$

with

$$\begin{aligned} K^{b,(1)}(\varepsilon) &= \frac{1}{\varepsilon} \left\{ -2A_1^b \right\}, \quad K^{b,(2)}(\varepsilon) = \frac{1}{\varepsilon^2} \left\{ 2\beta_0 A_1^b \right\} + \frac{1}{\varepsilon} \left\{ -A_2^b \right\}, \\ K^{b,(3)}(\varepsilon) &= \frac{1}{\varepsilon^3} \left\{ -\frac{8}{3} \beta_0^2 A_1^b \right\} + \frac{1}{\varepsilon^2} \left\{ \frac{2}{3} \beta_1 A_1^b + \frac{8}{3} \beta_0 A_2^b \right\} + \frac{1}{\varepsilon} \left\{ -\frac{2}{3} A_3^b \right\}. \end{aligned} \quad (6.55)$$

Similarly upon solving the RGE 6.52 for G^b , we obtain

$$\begin{aligned}
G^b(\hat{a}_s, \frac{Q^2}{\mu_R^2}, \frac{\mu_R^2}{\mu^2}, \varepsilon) &= G^b(a_s(\mu_R^2), \frac{Q^2}{\mu_R^2}, \varepsilon) \\
&= G^b(a_s(Q^2), 1, \varepsilon) + \int_{Q^2/\mu_R^2}^1 \frac{d\lambda^2}{\lambda^2} A^b(a_s(\lambda^2 \mu_R^2)) \\
&= G^b(a_s(Q^2), 1, \varepsilon) + \sum_{i=1}^{\infty} S_\varepsilon^i \hat{a}_s^i \left(\frac{\mu_R^2}{\mu^2}\right)^{i\varepsilon} \left[\left(\frac{Q^2}{\mu_R^2}\right)^{i\varepsilon} - 1 \right] K^{b,(i)}(\varepsilon). \tag{6.56}
\end{aligned}$$

Expanding the finite function $G^b(a_s(Q^2), 1, \varepsilon)$ in powers of $a_s(Q^2)$ as

$$G^b(a_s(Q^2), 1, \varepsilon) = \sum_{i=1}^{\infty} a_s^i(Q^2) G_i^b(\varepsilon), \tag{6.57}$$

one finds that G_i^b can be expressed in terms of collinear B_i^q and soft f_i^q anomalous dimensions through the relation [171–173]

$$G_i^b(\varepsilon) = 2(B_i^q - \gamma_i^b) + f_i^q + C_i^b + \sum_{k=1}^{\infty} \varepsilon^k g_i^{b,k}. \tag{6.58}$$

Note that the single pole term of the form factor depends on three different anomalous dimensions, namely the collinear anomalous dimension B_i^q , anomalous dimension of the coupling constant γ_i^b and the soft anomalous dimension f_i^q . B_i^q can be obtained from the $\delta(1-z)$ part of the diagonal splitting function known up to three loop level [90, 167] which are

$$\begin{aligned}
B_1^q &= 3C_F, \\
B_2^q &= \frac{1}{2} \left(C_F^2 \left\{ 3 - 24\zeta_2 + 48\zeta_3 \right\} + C_A C_F \left\{ \frac{17}{3} + \frac{88}{3}\zeta_2 - 24\zeta_3 \right\} + n_f T_F C_F \left\{ -\frac{4}{3} - \frac{32}{3}\zeta_2 \right\} \right), \\
B_3^q &= -16C_A^2 C_F \left\{ \frac{1}{8}\zeta_2^2 - \frac{281}{27}\zeta_2 + \frac{97}{9}\zeta_3 - \frac{5}{2}\zeta_5 + \frac{1657}{576} \right\} + 16C_A C_F^2 \left\{ -\frac{247}{60}\zeta_2^2 + \zeta_2 \zeta_3 \right. \\
&\quad \left. - \frac{205}{24}\zeta_2 + \frac{211}{12}\zeta_3 + \frac{15}{2}\zeta_5 + \frac{151}{64} \right\} + 16C_A C_F n_f \left\{ \frac{1}{20}\zeta_2^2 - \frac{167}{54}\zeta_2 + \frac{25}{18}\zeta_3 + \frac{5}{4} \right\}
\end{aligned}$$

$$\begin{aligned}
& + 16C_F^3 \left\{ \frac{18}{5} \zeta_2^2 - 2\zeta_2 \zeta_3 + \frac{9}{8} \zeta_2 + \frac{17}{4} \zeta_3 - 15\zeta_5 + \frac{29}{32} \right\} \\
& - 16C_F^2 n_f \left\{ -\frac{29}{30} \zeta_2^2 - \frac{5}{12} \zeta_2 + \frac{17}{6} \zeta_3 + \frac{23}{16} \right\} - 16C_F n_f^2 \left\{ -\frac{5}{27} \zeta_2 + \frac{1}{9} \zeta_3 + \frac{17}{144} \right\}. \quad (6.59)
\end{aligned}$$

The f_i^q for $i = 1, 2$ can be found in [171] and in [90] for $i = 3$. We list them below:

$$\begin{aligned}
f_1^q &= 0, \\
f_2^q &= C_A C_F \left\{ -\frac{22}{3} \zeta_2 - 28\zeta_3 + \frac{808}{27} \right\} + C_F n_f T_F \left\{ \frac{8}{3} \zeta_2 - \frac{224}{27} \right\}, \\
f_3^q &= C_A^2 C_F \left\{ \frac{352}{5} \zeta_2^2 + \frac{176}{3} \zeta_2 \zeta_3 - \frac{12650}{81} \zeta_2 - \frac{1316}{3} \zeta_3 + 192\zeta_5 + \frac{136781}{729} \right\} \\
& + C_A C_F n_f \left\{ -\frac{96}{5} \zeta_2^2 + \frac{2828}{81} \zeta_2 + \frac{728}{27} \zeta_3 - \frac{11842}{729} \right\} \\
& + C_F^2 n_f \left\{ \frac{32}{5} \zeta_2^2 + 4\zeta_2 + \frac{304}{9} \zeta_3 - \frac{1711}{27} \right\} + C_F n_f^2 \left\{ -\frac{40}{27} \zeta_2 + \frac{112}{27} \zeta_3 - \frac{2080}{729} \right\}. \quad (6.60)
\end{aligned}$$

Since B_i^q and f_i^q are flavour independent, we have used $B_i^b \equiv B_i^q$ and $f_i^b \equiv f_i^q$ in G_i^b . The constants C_i^b are controlled by the beta function of the strong coupling constant through renormalization group invariance of the bare form factor:

$$C_1^b = 0, \quad C_2^b = -2\beta_0 g_1^{b,1}, \quad C_3^b = -2\beta_1 g_1^{b,1} - 2\beta_0 (g_2^{b,1} + 2\beta_0 g_1^{b,2}). \quad (6.61)$$

The coefficients $g_i^{b,k}$ can be extracted from the finite part of the form factor. Up to two loop level, we use [77, 96, 97] and at three loop level the recent computation by Gehrmann and Kara [155] enable us to compute the relevant $g_3^{b,1}$ in [157] where $g_3^{b,1}$ was already used to obtain threshold correction to inclusive Higgs production in bottom anti-bottom annihilation process:

$$g_1^{b,1} = C_F \left\{ -2 + \zeta_2 \right\}, \quad g_1^{b,2} = C_F \left\{ 2 - \frac{7}{3} \zeta_3 \right\}, \quad g_1^{b,3} = C_F \left\{ -2 + \frac{1}{4} \zeta_2 + \frac{47}{80} \zeta_2^2 \right\},$$

$$\begin{aligned}
g_2^{b,1} &= C_F n_f \left\{ \frac{616}{81} + \frac{10}{9} \zeta_2 - \frac{8}{3} \zeta_3 \right\} + C_F C_A \left\{ -\frac{2122}{81} - \frac{103}{9} \zeta_2 + \frac{88}{5} \zeta_2^2 + \frac{152}{3} \zeta_3 \right\} \\
&\quad + C_F^2 \left\{ 8 + 32 \zeta_2 - \frac{88}{5} \zeta_2^2 - 60 \zeta_3 \right\}, \\
g_2^{b,2} &= C_F n_f \left\{ \frac{7}{12} \zeta_2^2 - \frac{55}{27} \zeta_2 + \frac{130}{27} \zeta_3 - \frac{3100}{243} \right\} + C_A C_F \left\{ -\frac{365}{24} \zeta_2^2 + \frac{89}{3} \zeta_2 \zeta_3 + \frac{1079}{54} \zeta_2 \right. \\
&\quad \left. - \frac{2923}{27} \zeta_3 - 51 \zeta_5 + \frac{9142}{243} \right\} + C_F^2 \left\{ \frac{96}{5} \zeta_2^2 - 28 \zeta_2 \zeta_3 - 44 \zeta_2 + 116 \zeta_3 + 12 \zeta_5 - 24 \right\}, \\
g_3^{b,1} &= C_A^2 C_F \left\{ -\frac{6152}{63} \zeta_2^3 + \frac{2738}{9} \zeta_2^2 + \frac{976}{9} \zeta_2 \zeta_3 - \frac{342263}{486} \zeta_2 - \frac{1136}{3} \zeta_3^2 + \frac{19582}{9} \zeta_3 \right. \\
&\quad \left. + \frac{1228}{3} \zeta_5 + \frac{4095263}{8748} \right\} + C_A C_F^2 \left\{ -\frac{15448}{105} \zeta_2^3 - \frac{3634}{45} \zeta_2^2 - \frac{2584}{3} \zeta_2 \zeta_3 + \frac{13357}{9} \zeta_2 \right. \\
&\quad \left. + 296 \zeta_3^2 - \frac{11570}{9} \zeta_3 - \frac{1940}{3} \zeta_5 - \frac{613}{3} \right\} + C_A C_F n_f \left\{ -\frac{1064}{45} \zeta_2^2 + \frac{392}{9} \zeta_2 \zeta_3 + \frac{44551}{243} \zeta_2 \right. \\
&\quad \left. - \frac{41552}{81} \zeta_3 - 72 \zeta_5 - \frac{6119}{4374} \right\} + C_F^2 n_f \left\{ \frac{772}{45} \zeta_2^2 - \frac{152}{3} \zeta_2 \zeta_3 - \frac{3173}{18} \zeta_2 + \frac{15956}{27} \zeta_3 - \frac{368}{3} \zeta_5 \right. \\
&\quad \left. + \frac{32899}{324} \right\} + C_F n_f^2 \left\{ -\frac{40}{9} \zeta_2^2 - \frac{892}{81} \zeta_2 + \frac{320}{81} \zeta_3 - \frac{27352}{2187} \right\} + C_F^3 \left\{ \frac{21584}{105} \zeta_2^3 - \frac{1644}{5} \zeta_2^2 \right. \\
&\quad \left. + 624 \zeta_2 \zeta_3 - 275 \zeta_2 + 48 \zeta_3^2 - 2142 \zeta_3 + 1272 \zeta_5 + 603 \right\}. \tag{6.62}
\end{aligned}$$

Using the expressions for K^b and G^b given in Eq. 6.54 and Eq. 6.58, respectively, we obtain the renormalized form factor up to order $\mathcal{O}(a_s^3)$ as

$$\begin{aligned}
\ln |\hat{F}^b|^2(Q^2, \varepsilon) &= a_s(q^2) \left[\frac{1}{\varepsilon^2} \left(-4A_1^q \right) + \frac{1}{\varepsilon} \left(2f_1^q + 4B_1^q - 4\gamma_0^b \right) + \left(2g_1^{b,1} + 3\zeta_2 A_1^q \right) \right] \\
&\quad + a_s^2(q^2) \left[\frac{1}{\varepsilon^3} \left(-6\beta_0 A_1^q \right) + \frac{1}{\varepsilon^2} \left(-A_2^q + 2\beta_0 \left(f_1^q + 2B_1^q - 2\gamma_0^b \right) \right) + \frac{1}{\varepsilon} \left(f_2^q \right. \right. \\
&\quad \left. \left. + 2B_2^q - 2\gamma_1^b \right) + \left(g_2^{b,1} + 2\beta_0 g_1^{b,2} + 3\zeta_2 A_2^q + 3\zeta_2 \beta_0 \left(f_1^q + 2B_1^q - 2\gamma_0^b \right) \right) \right] \\
&\quad + a_s^3(q^2) \left[\frac{1}{\varepsilon^4} \left(-\frac{88}{9} \beta_0^2 A_1^q \right) + \frac{1}{\varepsilon^3} \left(-\frac{32}{9} \beta_1 A_1^q - \frac{20}{9} \beta_0 A_2^q + \frac{8}{3} \beta_0^2 \left(f_1^q + 2B_1^q \right) \right) \right]
\end{aligned}$$

$$\begin{aligned}
& -2\gamma_0^b) \Big) 0 + \frac{1}{\varepsilon^2} \left(-\frac{4}{9}A_3^q + \frac{4}{3}\beta_1 \left(f_1^q + 2B_1^q - 2\gamma_0^b \right) + \frac{4}{3}\beta_0 \left(f_2^q + 2B_2^q - 2\gamma_1^b \right) \right) \\
& + \frac{1}{\varepsilon} \left(\frac{2}{3}f_3^q + \frac{4}{3}B_3^q - \frac{4}{3}\gamma_2^b \right) + \left(\frac{2}{3}g_3^{b,1} + \frac{4}{3}\beta_1 g_1^{b,2} + \frac{4}{3}\beta_0 g_2^{b,2} + \frac{8}{3}\beta_0^2 g_1^{b,3} + 3\zeta_2 A_3^q \right. \\
& + 3\zeta_2 \beta_1 \left(f_1^q + 2B_1^q - 2\gamma_0^b \right) + 6\zeta_2 \beta_0 \left(f_2^q + 2B_2^q - 2\gamma_1^b \right) \\
& \left. - 12\zeta_2 \beta_0^2 g_1^{b,1} - 3\zeta_2^2 \beta_0^2 A_1^q \right) \Big]. \tag{6.63}
\end{aligned}$$

Note that the poles of $\ln |\hat{F}^b|^2$ are fully controlled by the universal anomalous dimensions A^q, γ^b, B^q and f^q while the constant terms require vertex dependent constants $g_i^{b,k}$.

In $\overline{\text{MS}}$ scheme, the mass factorization kernels $\Gamma_{bb}(\hat{a}_s, \mu^2, \mu_F^2, z_j, \varepsilon)$ remove the collinear singularities which arise due to massless partons. These kernels satisfy the following RG equation :

$$\mu_F^2 \frac{d}{d\mu_F^2} \Gamma_{bb}(z_j, \mu_F^2, \varepsilon) = \frac{1}{2} \sum_c P_{bc}(z_j, \mu_F^2) \otimes \Gamma_{cb}(z_j, \mu_F^2, \varepsilon), \tag{6.64}$$

where $P_{bc}(z_j, \mu_F^2)$ are AP splitting functions. We can expand the $P_{bc}(z_j, \mu_F^2)$ in powers of a_s as

$$P_{bc}(z_j, \mu_F^2) = \sum_{i=1}^{\infty} a_s^i(\mu_F^2) P_{bc}^{(i-1)}(z_j). \tag{6.65}$$

The off diagonal splitting functions are regular as $z_j \rightarrow 1$. The diagonal ones contain in addition distributions such as $\delta(1-z_j)$ and \mathcal{D}_0 multiplied by the universal anomalous dimensions B_i^q and A_i^q , respectively:

$$P_{bb}^{(i)}(z_j) = 2 \left(B_{i+1}^b \delta(1-z_j) + A_{i+1}^b \mathcal{D}_0 \right) + P_{reg,bb}^{(i)}(z_j). \tag{6.66}$$

As we are interested in results from the threshold region, we can ignore all the non-diagonal splitting functions and also the regular part $P_{reg,bb}^{(i)}$ arising from the diagonal terms. Hence, the solution to Eq. 6.64 takes the following form:

$$\ln \Gamma_{bb}(z_j, \mu_F^2) = a_s(\mu_F^2) \left[\delta(1-z_j) \left(\frac{1}{\varepsilon} (2B_1^q) \right) + \mathcal{D}_0 \left(\frac{1}{\varepsilon} (2A_1^q) \right) \right]$$

$$\begin{aligned}
& + a_s^2(\mu_F^2) \left[\delta(1-z_j) \left(\frac{1}{\varepsilon^2} (2\beta_0 B_1^q) + \frac{1}{\varepsilon} (B_2^q) \right) + \mathcal{D}_0 \left(\frac{1}{\varepsilon^2} (2\beta_0 A_1^q) + \frac{1}{\varepsilon} (A_2^q) \right) \right] \\
& + a_s^3(\mu_F^2) \left[\delta(1-z_j) \left(\frac{1}{\varepsilon^3} \left(\frac{8}{3} \beta_0^2 B_1^q \right) + \frac{1}{\varepsilon^2} \left(\frac{4}{3} \beta_1 B_1^q + \frac{4}{3} \beta_0 B_2^q \right) + \frac{1}{\varepsilon} \left(\frac{2}{3} B_3^q \right) \right) \right. \\
& \left. + \mathcal{D}_0 \left(\frac{1}{\varepsilon^3} \left(\frac{8}{3} \beta_0^2 A_1^q \right) + \frac{1}{\varepsilon^2} \left(\frac{4}{3} \beta_1 A_1^q + \frac{4}{3} \beta_0 A_2^q \right) + \frac{1}{\varepsilon} \left(\frac{2}{3} A_3^q \right) \right) \right]. \quad (6.67)
\end{aligned}$$

Finally, we need to determine the soft distribution function $\Phi_d^b(\hat{a}_s, q^2, \mu^2, z_1, z_2, \varepsilon)$ in $\Delta_{d,b}^{\text{SV}}$. Its most general form can be systematically constructed if Φ_d^b also satisfies a differential equation similar to the form factor. It is indeed the case because the q^2 dependence and pole structure of Φ_d^b have to be similar to those of $\ln|\hat{F}^b|^2$ in order to obtain finite distribution Ψ in the limit $\varepsilon \rightarrow 0$ [96, 97]. Hence, we propose that Φ_d^b satisfies

$$q^2 \frac{d}{dq^2} \Phi_d^b = \frac{1}{2} \left[\bar{K}_d^b(\hat{a}_s, \frac{\mu_R^2}{\mu^2}, z_1, z_2, \varepsilon) + \bar{G}_d^b(\hat{a}_s, \frac{q^2}{\mu_R^2}, \frac{\mu_R^2}{\mu^2}, z_1, z_2, \varepsilon) \right]. \quad (6.68)$$

It is natural to move all the singular terms in ε of Φ_d^b to \bar{K}_d^b and keep \bar{G}_d^b finite as $\varepsilon \rightarrow 0$ similar to K_d^b and G_d^b of the logarithm of the form factor, $\ln \hat{F}^b$. The RG invariance of $\Phi_d^b(\hat{a}_s, q^2, \mu^2, z_1, z_2, \varepsilon)$ leads to

$$\mu_R^2 \frac{d}{d\mu_R^2} \Phi_d^b(\hat{a}_s, q^2, \mu^2, z_1, z_2, \varepsilon) = 0 \quad (6.69)$$

and consequently

$$\mu_R^2 \frac{d}{d\mu_R^2} \bar{K}_d^b = -\mu_R^2 \frac{d}{d\mu_R^2} \bar{G}_d^b = -\delta(1-z_1)\delta(1-z_2)a_s(\mu_R^2)\bar{A}^q. \quad (6.70)$$

The right hand side of the above equation is proportion to $\delta(1-z_1)\delta(1-z_2)$ as the most singular terms resulting from \bar{K}_d^b should cancel with those from the form factor contribution which is proportional to only pure delta functions. To make the $\Delta_{d,b}^{\text{SV}}$ finite, the poles from $\Phi_d^b(\hat{a}_s, q^2, \mu^2, z_1, z_2, \varepsilon)$

have to cancel those coming from \hat{F}^b and Γ_{bb} . Hence the constants \bar{A}^q should satisfy

$$\bar{A}^q = -A^q. \quad (6.71)$$

The RGE 6.70 for \bar{G}_d^b can be solved using the above relation to get

$$\begin{aligned} \bar{G}_d^b \left(\hat{a}_s, \frac{q^2}{\mu_R^2}, \frac{\mu_R^2}{\mu^2}, z_1, z_2, \varepsilon \right) &= \bar{G}_d^b \left(a_s(\mu_R^2), \frac{q^2}{\mu_R^2}, z_1, z_2, \varepsilon \right) \\ &= \bar{G}_d^b(a_s(q^2), 1, z_1, z_2, \varepsilon) - \delta(1-z_1)\delta(1-z_2) \int_{\frac{q^2}{\mu_R^2}}^1 \frac{d\lambda^2}{\lambda^2} A^q(a_s(\lambda^2 \mu_R^2)). \end{aligned} \quad (6.72)$$

With these solutions, it is now straightforward to solve the above differential equations 6.68 for Φ_d^b to get

$$\begin{aligned} \Phi_d^b &= \Phi_d^b(\hat{a}_s, q^2(1-z_1)(1-z_2), \mu^2, \varepsilon) \\ &= \sum_{i=1}^{\infty} \hat{a}_s^i \left(\frac{q^2(1-z_1)(1-z_2)}{\mu^2} \right)^{i\frac{\varepsilon}{2}} S_\varepsilon^i \left(\frac{(i\varepsilon)^2}{4(1-z_1)(1-z_2)} \right) \hat{\Phi}_d^{b,(i)}(\varepsilon), \end{aligned} \quad (6.73)$$

where,

$$\hat{\Phi}_d^{b,(i)}(\varepsilon) = \frac{1}{i\varepsilon} \left[\bar{K}_d^{b,(i)}(\varepsilon) + \bar{G}_d^{b,(i)}(\varepsilon) \right]. \quad (6.74)$$

The form of z_j dependence part of the solution in the above solution is inspired by our one loop computation in the previous section and it can be justified from the factorization property of the QCD amplitudes and the corresponding partonic cross sections. The constants $\bar{K}_d^{b,(i)}(\varepsilon)$ are determined by expanding \bar{K}_d^b in powers of \hat{a}_s as follows

$$\bar{K}_d^b \left(\hat{a}_s, \frac{\mu_R^2}{\mu^2}, z_1, z_2, \varepsilon \right) = \delta(1-z_1)\delta(1-z_2) \sum_{i=1}^{\infty} \hat{a}_s^i \left(\frac{\mu_R^2}{\mu^2} \right)^{i\frac{\varepsilon}{2}} S_\varepsilon^i \bar{K}_d^{b,(i)}(\varepsilon) \quad (6.75)$$

and solving the RGE 6.70 for \bar{K}_d^b . The constants $\bar{K}_d^{b,(i)}(\varepsilon)$ are identical to $\bar{K}^{b,(i)}(\varepsilon)$ given in [96,97].

$\overline{G}_d^{b,(i)}(\varepsilon)$ are related to the finite functions $\overline{G}_d^b(a_s(q^2), 1, z_1, z_2, \varepsilon)$. In terms of renormalized coupling constant, we find

$$\sum_{i=1}^{\infty} \hat{a}_s^i \left(\frac{q^2(1-z_1)(1-z_2)}{\mu^2} \right)^{i\frac{\varepsilon}{2}} S_\varepsilon^i \overline{G}_d^{b,(i)}(\varepsilon) = \sum_{i=1}^{\infty} a_s^i (q^2(1-z_1)(1-z_2)) \overline{\mathcal{G}}_{d,i}^b(\varepsilon) \quad (6.76)$$

where the constants $\overline{\mathcal{G}}_{d,i}^b(\varepsilon)$ are flavour independent and they satisfy the following structure similar to $G_i^b(\varepsilon)$ of the form factor, i.e.,

$$\overline{\mathcal{G}}_{d,i}^b(\varepsilon) = -f_i^q + \mathcal{C}_{d,i}^b + \sum_{k=1}^{\infty} \varepsilon^k \overline{\mathcal{G}}_{d,i}^{b,k}, \quad (6.77)$$

where

$$\mathcal{C}_{d,1}^b = 0, \quad \mathcal{C}_{d,2}^b = -2\beta_0 \overline{\mathcal{G}}_{d,1}^{b,1}, \quad \mathcal{C}_{d,3}^b = -2\beta_1 \overline{\mathcal{G}}_{d,1}^{b,1} - 2\beta_0 (\overline{\mathcal{G}}_{d,2}^{b,1} + 2\beta_0 \overline{\mathcal{G}}_{d,1}^{b,2}). \quad (6.78)$$

Using $\overline{K}_d^{b,(i)}$ from Eq. 6.75 and $\overline{G}_d^{b,(i)}$ from Eq. 6.76 and using Eq. 6.26, we find that the soft distribution function up to third order in $a_s(q^2)$ takes the form

$$\begin{aligned} \Phi_d^b = a_s(q^2) & \left[\delta(1-z_1)\delta(1-z_2) \left(\frac{1}{\varepsilon^2} (2A_1^q) + \frac{1}{\varepsilon} (-f_1^q) + \overline{\mathcal{G}}_{d,1}^{q,1} \right) + \mathcal{D}_0 \delta(1-z_2) \left(\frac{1}{\varepsilon} (A_1^q) \right. \right. \\ & \left. \left. + \left(-\frac{1}{2}f_1^q\right) \right) + \mathcal{D}_0 \overline{\mathcal{D}}_0 \left(\frac{1}{2}A_1^q \right) + \mathcal{D}_1 \delta(1-z_2) \left(\frac{1}{2}A_1^q \right) + \overline{\mathcal{D}}_0 \delta(1-z_1) \left(\frac{1}{\varepsilon} (A_1^q) + \left(-\frac{1}{2}f_1^q\right) \right) \right. \\ & \left. + \overline{\mathcal{D}}_1 \delta(1-z_1) \left(\frac{1}{2}A_1^q \right) \right] + a_s^2(q^2) \left[\delta(1-z_1)\delta(1-z_2) \left(\frac{1}{\varepsilon^3} (3\beta_0 A_1^q) + \frac{1}{\varepsilon^2} \left(\frac{1}{2}A_2^q - \beta_0 f_1^q \right) \right. \right. \\ & \left. \left. + \frac{1}{\varepsilon} \left(-\frac{1}{2}f_2^q \right) + \left(\frac{1}{2}\overline{\mathcal{G}}_{d,2}^{q,1} + \beta_0 \overline{\mathcal{G}}_{d,1}^{q,2} \right) \right) + \mathcal{D}_0 \delta(1-z_2) \left(\frac{1}{\varepsilon^2} (\beta_0 A_1^q) + \frac{1}{\varepsilon} \left(\frac{1}{2}A_2^q \right) \right. \right. \\ & \left. \left. + \left(-\frac{1}{2}f_2^q - \beta_0 \overline{\mathcal{G}}_{d,1}^{q,1} \right) \right) + \mathcal{D}_0 \overline{\mathcal{D}}_0 \left(\frac{1}{2}A_2^q + \frac{1}{2}\beta_0 f_1^q \right) + \mathcal{D}_0 \overline{\mathcal{D}}_1 \left(-\frac{1}{2}\beta_0 A_1^q \right) \right. \\ & \left. + \mathcal{D}_1 \delta(1-z_2) \left(\frac{1}{2}A_2^q + \frac{1}{2}\beta_0 f_1^q \right) + \mathcal{D}_1 \overline{\mathcal{D}}_0 \left(-\frac{1}{2}\beta_0 A_1^q \right) + \mathcal{D}_2 \delta(1-z_2) \left(-\frac{1}{4}\beta_0 A_1^q \right) \right] \end{aligned}$$

$$\begin{aligned}
& + \overline{\mathcal{D}}_0 \delta(1-z_1) \left(\frac{1}{\varepsilon^2} (\beta_0 A_1^q) + \frac{1}{\varepsilon} \left(\frac{1}{2} A_2^q \right) + \left(-\frac{1}{2} f_2^q - \beta_0 \overline{\mathcal{G}}_{d,1}^{q,1} \right) \right) \\
& + \overline{\mathcal{D}}_1 \delta(1-z_1) \left(\frac{1}{2} A_2^q + \frac{1}{2} \beta_0 f_1^q \right) + \overline{\mathcal{D}}_2 \delta(1-z_1) \left(-\frac{1}{4} \beta_0 A_1^q \right) \Big] \\
& + a_s^3 (q^2) \left[\delta(1-z_1) \delta(1-z_2) \left(\frac{1}{\varepsilon^4} \left(\frac{44}{9} \beta_0^2 A_1^q \right) + \frac{1}{\varepsilon^3} \left(\frac{16}{9} \beta_1 A_1^q + \frac{10}{9} \beta_0 A_2^q - \frac{4}{3} \beta_0^2 f_1^q \right) \right. \right. \\
& + \left. \frac{1}{\varepsilon^2} \left(\frac{2}{9} A_3^q - \frac{2}{3} \beta_1 f_1^q - \frac{2}{3} \beta_0 f_2^q \right) - \frac{1}{\varepsilon} \left(\frac{1}{3} f_3^q \right) + \left(\frac{1}{3} \overline{\mathcal{G}}_{d,3}^{q,1} + \frac{2}{3} \beta_1 \overline{\mathcal{G}}_{d,1}^{q,2} + \frac{2}{3} \beta_0 \overline{\mathcal{G}}_{d,2}^{q,2} + \frac{4}{3} \beta_0^2 \overline{\mathcal{G}}_{d,1}^{q,3} \right) \right) \\
& + \mathcal{D}_0 \delta(1-z_2) \left(\frac{1}{\varepsilon^3} \left(\frac{4}{3} \beta_0^2 A_1^q \right) + \frac{1}{\varepsilon^2} \left(\frac{2}{3} \beta_1 A_1^q + \frac{2}{3} \beta_0 A_2^q \right) + \frac{1}{\varepsilon} \left(\frac{1}{3} A_3^q \right) + \left(-\frac{1}{2} f_3^q - \beta_1 \overline{\mathcal{G}}_{d,1}^{q,1} \right. \right. \\
& - \left. \left. \beta_0 \overline{\mathcal{G}}_{d,2}^{q,1} - 2\beta_0^2 \overline{\mathcal{G}}_{d,1}^{q,2} \right) \right) + \mathcal{D}_0 \overline{\mathcal{D}}_0 \left(\frac{1}{2} A_3^q + \frac{1}{2} \beta_1 f_1^q + \beta_0 f_2^q + 2\beta_0^2 \overline{\mathcal{G}}_{d,1}^{q,1} \right) + \mathcal{D}_0 \overline{\mathcal{D}}_1 \left(-\frac{1}{2} \beta_1 A_1^q \right. \\
& - \left. \beta_0 A_2^q - \beta_0^2 f_1^q \right) + \mathcal{D}_0 \overline{\mathcal{D}}_2 \left(\frac{1}{2} \beta_0^2 A_1^q \right) + \mathcal{D}_1 \delta(1-z_2) \left(\frac{1}{2} A_3^q + \frac{1}{2} \beta_1 f_1^q + \beta_0 f_2^q + 2\beta_0^2 \overline{\mathcal{G}}_{d,1}^{q,1} \right) \\
& + \mathcal{D}_1 \overline{\mathcal{D}}_0 \left(-\frac{1}{2} \beta_1 A_1^q - \beta_0 A_2^q - \beta_0^2 f_1^q \right) + \mathcal{D}_1 \overline{\mathcal{D}}_1 \left(\beta_0^2 A_1^q \right) \\
& + \mathcal{D}_2 \delta(1-z_2) \left(-\frac{1}{4} \beta_1 A_1^q - \frac{1}{2} \beta_0 A_2^q - \frac{1}{2} \beta_0^2 f_1^q \right) + \mathcal{D}_2 \overline{\mathcal{D}}_0 \left(\frac{1}{2} \beta_0^2 A_1^q \right) \\
& + \mathcal{D}_3 \delta(1-z_2) \left(\frac{1}{6} \beta_0^2 A_1^q \right) + \overline{\mathcal{D}}_0 \delta(1-z_1) \left(\frac{1}{\varepsilon^3} \left(\frac{4}{3} \beta_0^2 A_1^q \right) + \frac{1}{\varepsilon^2} \left(\frac{2}{3} \beta_1 A_1^q + \frac{2}{3} \beta_0 A_2^q \right) \right. \\
& + \left. \frac{1}{\varepsilon} \left(\frac{1}{3} A_3^q \right) + \left(-\frac{1}{2} f_3^q - \beta_1 \overline{\mathcal{G}}_{d,1}^{q,1} - \beta_0 \overline{\mathcal{G}}_{d,2}^{q,1} - 2\beta_0^2 \overline{\mathcal{G}}_{d,1}^{q,2} \right) \right) \\
& + \overline{\mathcal{D}}_1 \delta(1-z_1) \left(\frac{1}{2} A_3^q + \frac{1}{2} \beta_1 f_1^q + \beta_0 f_2^q + 2\beta_0^2 \overline{\mathcal{G}}_{d,1}^{q,1} \right) \\
& + \overline{\mathcal{D}}_2 \delta(1-z_1) \left(-\frac{1}{4} \beta_1 A_1^q - \frac{1}{2} \beta_0 A_2^q - \frac{1}{2} \beta_0^2 f_1^q \right) \\
& + \overline{\mathcal{D}}_3 \delta(1-z_1) \left(\frac{1}{6} \beta_0^2 A_1^q \right) \Big]. \tag{6.79}
\end{aligned}$$

In the above expression, we have used $\overline{\mathcal{G}}_{d,i}^{b,k} = \overline{\mathcal{G}}_{d,i}^{q,k}$, being flavour independent. The soft distribution function depends in addition to the universal anomalous dimensions A_i^q, B_i^q, γ_i^q and f_i^q , the constants $\overline{\mathcal{G}}_{d,i}^{q,k}$ which need to be determined. At $\mathcal{O}(a_s)$ level $\overline{\mathcal{G}}_{d,1}^{q,1}, \overline{\mathcal{G}}_{d,2}^{q,1}, \overline{\mathcal{G}}_{d,3}^{q,1}$, at $\mathcal{O}(a_s^2)$ $\overline{\mathcal{G}}_{d,1}^{q,2}, \overline{\mathcal{G}}_{d,2}^{q,2}$ and at

$\mathcal{O}(a_s^3) \overline{\mathcal{G}}_{d,1}^{q,3}$ are needed to obtain Φ_d^b . We achieve this using the following identity:

$$\int_0^1 dx_1^0 \int_0^1 dx_2^0 (x_1^0 x_2^0)^{N-1} \frac{d\sigma^b}{dy} = \int_0^1 d\tau \tau^{N-1} \sigma^b, \quad (6.80)$$

where σ^b is known to NNLO level [77] exactly and to N³LO level in the threshold limit [157]. In large N limit *i.e.* $N \rightarrow \infty$ the above Eq. 6.80 relates $\hat{\phi}_d^{q,(i)}(\varepsilon)$ to $\hat{\phi}^{q,(i)}(\varepsilon)$ that appears in inclusive threshold corrections to Drell-Yan process (see [96,97, 103, 157]) as follows

$$\hat{\phi}_d^{b,(i)}(\varepsilon) = \frac{\Gamma(1+i\varepsilon)}{\Gamma^2(1+i\frac{\varepsilon}{2})} \hat{\phi}^{b,(i)}(\varepsilon) \quad (6.81)$$

and

$$\hat{\phi}_d^{b,(i)}(\varepsilon) = \hat{\phi}^{q,(i)}(\varepsilon) \quad (6.82)$$

since $\hat{\phi}^{q,(i)}(\varepsilon)$ is flavour independent. Hence

$$\hat{\phi}_d^{b,(i)}(\varepsilon) = \hat{\phi}_d^{q,(i)}(\varepsilon) \quad (6.83)$$

and all the relevant constants $\overline{\mathcal{G}}_{d,i}^{q,k}$ required for threshold prediction up to $\mathcal{O}(a_s^3)$ can be obtained from $\overline{\mathcal{G}}_i^{q,k}$ which are analogous to these factors appeared in the computation of inclusive threshold cross-section to Drell-Yan process. The relevant $\overline{\mathcal{G}}_i^{q,k}$'s at $\mathcal{O}(a_s)$ and $\mathcal{O}(a_s^2)$ [96,97] are

$$\begin{aligned} \overline{\mathcal{G}}_1^{q,1} &= C_F(-3\zeta_2), \\ \overline{\mathcal{G}}_1^{q,2} &= C_F\left(\frac{7}{3}\zeta_3\right), \\ \overline{\mathcal{G}}_1^{q,3} &= C_F\left(-\frac{3}{16}\zeta_2^2\right), \\ \overline{\mathcal{G}}_2^{q,1} &= C_F n_f \left(-\frac{328}{81} + \frac{70}{9}\zeta_2 + \frac{32}{3}\zeta_3\right) + C_A C_F \left(\frac{2428}{81} - \frac{469}{9}\zeta_2 + 4\zeta_2^2 - \frac{176}{3}\zeta_3\right), \\ \overline{\mathcal{G}}_2^{q,2} &= C_A C_F \left(\frac{11}{40}\zeta_2^2 - \frac{203}{3}\zeta_2\zeta_3 + \frac{1414}{27}\zeta_2 + \frac{2077}{27}\zeta_3 + 43\zeta_5 - \frac{7288}{243}\right) \end{aligned}$$

$$+ C_{Fn_f} \left(-\frac{1}{20} \zeta_2^2 - \frac{196}{27} \zeta_2 - \frac{310}{27} \zeta_3 + \frac{976}{243} \right)$$

and at $\mathcal{O}(a_s^3)$ [103]

$$\begin{aligned} \overline{\mathcal{G}}_3^{q,1} = & C_F \left\{ C_A^2 \left(\frac{152}{63} \zeta_2^3 + \frac{1964}{9} \zeta_2^2 + \frac{11000}{9} \zeta_2 \zeta_3 - \frac{765127}{486} \zeta_2 + \frac{536}{3} \zeta_3^2 - \frac{59648}{27} \zeta_3 \right. \right. \\ & - \frac{1430}{3} \zeta_5 + \frac{7135981}{8748} \left. \right) + C_{An_f} \left(-\frac{532}{9} \zeta_2^2 - \frac{1208}{9} \zeta_2 \zeta_3 + \frac{105059}{243} \zeta_2 + \frac{45956}{81} \zeta_3 \right. \\ & + \frac{148}{3} \zeta_5 - \frac{716509}{4374} \left. \right) + C_{Fn_f} \left(\frac{152}{15} \zeta_2^2 - 88 \zeta_2 \zeta_3 + \frac{605}{6} \zeta_2 + \frac{2536}{27} \zeta_3 + \frac{112}{3} \zeta_5 \right. \\ & \left. \left. - \frac{42727}{324} \right) + n_f^2 \left(\frac{32}{9} \zeta_2^2 - \frac{1996}{81} \zeta_2 - \frac{2720}{81} \zeta_3 + \frac{11584}{2187} \right) \right\}. \end{aligned} \quad (6.84)$$

These lead to the following expressions of $\overline{\mathcal{G}}_{d,i}^{q,k}$'s at $\mathcal{O}(a_s)$, $\mathcal{O}(a_s^2)$ [115] and $\mathcal{O}(a_s^3)$ [116] :

$$\begin{aligned} \overline{\mathcal{G}}_{d,1}^{q,1} &= -C_F \zeta_2, & \overline{\mathcal{G}}_{d,2}^{q,1} &= C_F \left\{ \frac{1}{3} \zeta_3 \right\}, & \overline{\mathcal{G}}_{d,3}^{q,1} &= C_F \left\{ \frac{1}{80} \zeta_2^2 \right\}, \\ \overline{\mathcal{G}}_{d,1}^{q,2} &= C_A C_F \left\{ -4 \zeta_2^2 - \frac{67}{3} \zeta_2 - \frac{44}{3} \zeta_3 + \frac{2428}{81} \right\} + C_{Fn_f} \left\{ \frac{8}{3} \zeta_3 + \frac{10}{3} \zeta_2 - \frac{328}{81} \right\}, \\ \overline{\mathcal{G}}_{d,2}^{q,2} &= C_A C_F \left\{ -\frac{319}{120} \zeta_2^2 - \frac{71}{3} \zeta_2 \zeta_3 + \frac{202}{9} \zeta_2 + \frac{469}{27} \zeta_3 + 43 \zeta_5 - \frac{7288}{243} \right\} \\ &+ C_{Fn_f} \left\{ \frac{29}{60} \zeta_2^2 - \frac{28}{9} \zeta_2 - \frac{70}{27} \zeta_3 + \frac{976}{243} \right\}, \\ \overline{\mathcal{G}}_{d,1}^{q,3} &= C_A^2 C_F \left\{ \frac{17392}{315} \zeta_2^3 + \frac{1538}{45} \zeta_2^2 + \frac{4136}{9} \zeta_2 \zeta_3 - \frac{379417}{486} \zeta_2 + \frac{536}{3} \zeta_3^2 - 936 \zeta_3 \right. \\ &- \frac{1430}{3} \zeta_5 + \frac{7135981}{8748} \left. \right\} + C_A C_{Fn_f} \left\{ -\frac{1372}{45} \zeta_2^2 - \frac{392}{9} \zeta_2 \zeta_3 + \frac{51053}{243} \zeta_2 \right. \\ &+ \frac{12356}{81} \zeta_3 + \frac{148}{3} \zeta_5 - \frac{716509}{4374} \left. \right\} + C_{Fn_f}^2 \left\{ \frac{152}{45} \zeta_2^2 - \frac{316}{27} \zeta_2 - \frac{320}{81} \zeta_3 + \frac{11584}{2187} \right\} \\ &+ C_F^2 n_f \left\{ \frac{152}{15} \zeta_2^2 - 40 \zeta_2 \zeta_3 + \frac{275}{6} \zeta_2 + \frac{1672}{27} \zeta_3 + \frac{112}{3} \zeta_5 - \frac{42727}{324} \right\}. \end{aligned} \quad (6.85)$$

With all these information available at hand, it is now straightforward to obtain threshold cor-

rections to rapidity distribution of Higgs boson in the bottom quark annihilation processes. We substitute Eq. 6.50, 6.63, 6.67, 6.79 in Eq. 6.40 to obtain $\Psi_d^b(\varepsilon)$. Since all the UV and IR singularities cancel among various terms, we can set $\varepsilon = 0$ in the the distribution $\Psi_d^b(\varepsilon)$ to obtain $\Delta_{d,b}^{SV}$. Expanding the finite distribution $\Psi_d^b(\varepsilon = 0)$ in Eq. 6.38 in terms of convolutions Eq. 6.39 and performing all those convolutions using the formula given in Eq. 52 of [97], we obtain $\Delta_b^{SV,(i)}$ defined by

$$\Delta_{d,b}^{SV}(z_1, z_2, q^2, \mu_R^2, \mu_F^2) = \sum_{i=0}^{\infty} a_s^i(q^2) \Delta_{d,b}^{SV,(i)}(z_1, z_2, q^2, \mu_R^2, \mu_F^2) \quad (6.86)$$

We present below our results for $\Delta_{d,b}^{SV,(i)}$ up to N³LO level in terms of of the constants $A_j^q, B_j^q, f_j^q, \gamma_j^b, \beta_j, g_j^{b,k}$ and $\overline{\mathcal{G}}_{d,j}^{q,k}$:

$$\begin{aligned} \Delta_{d,b}^{SV,(1)} &= \delta(1-z_1)\delta(1-z_2) \left[\overline{\mathcal{G}}_{d,1}^{q,1} + g_1^{b,1} + \frac{3}{2}\zeta_2 A_1^q \right] + \mathcal{D}_0 \delta(1-z_2) \left[-f_1^q \right] \\ &\quad + \mathcal{D}_0 \overline{\mathcal{D}}_0 \left[\frac{1}{2} A_1^q \right] + \mathcal{D}_1 \delta(1-z_2) \left[A_1^q \right] + \left\{ z_1 \leftrightarrow z_2 \right\} \\ \Delta_{d,b}^{SV,(2)} &= \delta(1-z_1)\delta(1-z_2) \left[\frac{1}{2} \overline{\mathcal{G}}_{d,2}^{q,1} + \overline{\mathcal{G}}_{d,1}^{q,1,2} + \frac{1}{2} g_2^{b,1} + 2g_1^{b,1} \overline{\mathcal{G}}_{d,1}^{q,1} + g_1^{b,1,2} + \beta_0 \left(\overline{\mathcal{G}}_{d,1}^{q,2} + g_1^{b,2} \right) \right. \\ &\quad - \zeta_3 A_1^q f_1^q + \zeta_2 \left(-\frac{1}{2} (f_1^q)^2 + \frac{3}{2} A_2^q + 3\overline{\mathcal{G}}_{d,1}^{q,1} A_1^q + 3g_1^{b,1} A_1^q \right) + \zeta_2 \beta_0 \left(\frac{3}{2} f_1^q + 3B_1^q - 3\gamma_0^b \right) \\ &\quad \left. + \frac{49}{20} \zeta_2^2 (A_1^q)^2 \right] + \mathcal{D}_0 \delta(1-z_2) \left[-f_2^q - 2\overline{\mathcal{G}}_{d,1}^{q,1} f_1^q - 2g_1^{b,1} f_1^q - 2\beta_0 \overline{\mathcal{G}}_{d,1}^{q,1} + 2\zeta_3 (A_1^q)^2 \right. \\ &\quad \left. - \zeta_2 A_1^q f_1^q \right] + \mathcal{D}_0 \overline{\mathcal{D}}_0 \left[\frac{1}{2} (f_1^q)^2 + \frac{1}{2} A_2^q + \overline{\mathcal{G}}_{d,1}^{q,1} A_1^q + g_1^{b,1} A_1^q + \frac{1}{2} \beta_0 f_1^q + \frac{1}{2} \zeta_2 (A_1^q)^2 \right] \\ &\quad + \mathcal{D}_1 \delta(1-z_2) \left[(f_1^q)^2 + A_2^q + 2\overline{\mathcal{G}}_{d,1}^{q,1} A_1^q + 2g_1^{b,1} A_1^q + \beta_0 f_1^q + \zeta_2 (A_1^q)^2 \right] \\ &\quad + \mathcal{D}_1 \overline{\mathcal{D}}_0 \left[-3A_1^q f_1^q - \beta_0 A_1^q \right] + \mathcal{D}_1 \overline{\mathcal{D}}_1 \left[\frac{3}{2} (A_1^q)^2 \right] + \mathcal{D}_2 \delta(1-z_2) \left[-\frac{3}{2} A_1^q f_1^q - \frac{1}{2} \beta_0 A_1^q \right] \\ &\quad + \mathcal{D}_2 \overline{\mathcal{D}}_0 \left[\frac{3}{2} (A_1^q)^2 \right] + \mathcal{D}_3 \delta(1-z_2) \left[\frac{1}{2} (A_1^q)^2 \right] + \left\{ z_1 \leftrightarrow z_2 \right\} \end{aligned} \quad (6.87)$$

$$\begin{aligned}
\Delta_{d,b}^{\text{SV},(3)} = & \delta(1-z_1)\delta(1-z_2) \left[\frac{1}{3}\overline{\mathcal{G}}_{d,3}^{q,1} + \overline{\mathcal{G}}_{d,1}^{q,1}\overline{\mathcal{G}}_{d,2}^{q,1} + \frac{2}{3}\overline{\mathcal{G}}_{d,1}^{q,1^3} + \frac{1}{3}g_3^{b,1} + g_2^{b,1}\overline{\mathcal{G}}_{d,1}^{q,1} + g_1^{b,1}\overline{\mathcal{G}}_{d,2}^{q,1} \right. \\
& + 2g_1^{b,1}\overline{\mathcal{G}}_{d,1}^{q,1^2} + g_1^{b,1}g_2^{b,1} + 2g_1^{b,1^2}\overline{\mathcal{G}}_{d,1}^{q,1} + \frac{2}{3}g_1^{b,1^3} + \frac{2}{3}\beta_1\left(\overline{\mathcal{G}}_{d,1}^{q,2} + g_1^{b,2}\right) + 2\beta_0\left(\frac{1}{3}\overline{\mathcal{G}}_{d,2}^{q,2} + \overline{\mathcal{G}}_{d,1}^{q,1}\overline{\mathcal{G}}_{d,1}^{q,2} \right. \\
& + \frac{1}{3}g_2^{b,2} + g_1^{b,2}\overline{\mathcal{G}}_{d,1}^{q,1} + g_1^{b,1}\overline{\mathcal{G}}_{d,1}^{q,2} + g_1^{b,1}g_1^{b,2}\left. \right) + \frac{4}{3}\beta_0^2\left(\overline{\mathcal{G}}_{d,1}^{q,3} + g_1^{b,3}\right) - 3\zeta_5(A_1^q)^2 f_1^q - 2\zeta_5\beta_0(A_1^q)^2 \\
& - \zeta_3\left(\frac{1}{3}(f_1^q)^3 + A_2^q f_1^q + A_1^q f_2^q + 2\overline{\mathcal{G}}_{d,1}^{q,1}A_1^q f_1^q + 2g_1^{b,1}A_1^q f_1^q + \beta_0(f_1^q)^2 + 2\beta_0\overline{\mathcal{G}}_{d,1}^{q,1}A_1^q\right) \\
& + \frac{5}{3}\zeta_3^2(A_1^q)^3 + \zeta_2\left(-f_1^q f_2^q + \frac{3}{2}A_3^q + \frac{3}{2}\overline{\mathcal{G}}_{d,2}^{q,1}A_1^q - \overline{\mathcal{G}}_{d,1}^{q,1}(f_1^q)^2 + 3\overline{\mathcal{G}}_{d,1}^{q,1}A_2^q + 3\overline{\mathcal{G}}_{d,1}^{q,1^2}A_1^q \right. \\
& + \frac{3}{2}g_2^{b,1}A_1^q - g_1^{b,1}(f_1^q)^2 + 3g_1^{b,1}A_2^q + 6g_1^{b,1}\overline{\mathcal{G}}_{d,1}^{q,1}A_1^q + 3g_1^{b,1^2}A_1^q\left. \right) + \frac{3}{2}\zeta_2\beta_1\left(f_1^q + 2B_1^q - 2\gamma_0^b\right) \\
& + 3\zeta_2\beta_0\left(f_2^q + 2B_2^q + \overline{\mathcal{G}}_{d,1}^{q,2}A_1^q + \frac{1}{3}\overline{\mathcal{G}}_{d,1}^{q,1}f_1^q + 2\overline{\mathcal{G}}_{d,1}^{q,1}B_1^q + g_1^{b,2}A_1^q + g_1^{b,1}f_1^q + 2g_1^{b,1}B_1^q - 2\gamma_1^b \right. \\
& - 2\gamma_0^b\overline{\mathcal{G}}_{d,1}^{q,1} - 2\gamma_0^b g_1^{b,1}\left. \right) - 6\zeta_2\beta_0^2 g_1^{b,1} + \zeta_2\zeta_3(A_1^q)^2 f_1^q + 2\zeta_2\zeta_3\beta_0(A_1^q)^2 + \frac{49}{10}\zeta_2^2\left(-\frac{11}{49}A_1^q(f_1^q)^2 \right. \\
& + A_1^q A_2^q + \overline{\mathcal{G}}_{d,1}^{q,1}(A_1^q)^2 + g_1^{b,1}(A_1^q)^2\left. \right) + \frac{9}{2}\zeta_2^2\beta_0\left(A_1^q f_1^q + 2A_1^q B_1^q - 2\gamma_0^b A_1^q - \frac{1}{3}A_1^q\right) \\
& + \frac{1181}{420}\zeta_2^3(A_1^q)^3\left. \right] + \mathcal{D}_0\delta(1-z_2) \left[-f_3^q - \overline{\mathcal{G}}_{d,2}^{q,1}f_1^q - 2\overline{\mathcal{G}}_{d,1}^{q,1}f_2^q - 2\overline{\mathcal{G}}_{d,1}^{q,1^2}f_1^q - g_2^{b,1}f_1^q - 2g_1^{b,1}f_2^q \right. \\
& - 4g_1^{b,1}\overline{\mathcal{G}}_{d,1}^{q,1}f_1^q - 2g_1^{b,1^2}f_1^q - 2\beta_1\overline{\mathcal{G}}_{d,1}^{q,1} - 2\beta_0\left(\overline{\mathcal{G}}_{d,2}^{q,1} + \overline{\mathcal{G}}_{d,1}^{q,2}f_1^q + 2\overline{\mathcal{G}}_{d,1}^{q,1^2} + g_1^{b,2}f_1^q + 2g_1^{b,1}\overline{\mathcal{G}}_{d,1}^{q,1}\right) \\
& - 4\beta_0^2\overline{\mathcal{G}}_{d,1}^{q,2} + 6\zeta_5(A_1^q)^3 + 4\zeta_3\left(A_1^q(f_1^q)^2 + A_1^q A_2^q + \overline{\mathcal{G}}_{d,1}^{q,1}(A_1^q)^2 + g_1^{b,1}(A_1^q)^2 + \frac{3}{2}\beta_0 A_1^q f_1^q\right) \\
& + \zeta_2\left((f_1^q)^3 - A_2^q f_1^q - A_1^q f_2^q - 2\overline{\mathcal{G}}_{d,1}^{q,1}A_1^q f_1^q - 2g_1^{b,1}A_1^q f_1^q\right) - \zeta_2\beta_0\left((f_1^q)^2 + 6B_1^q f_1^q + 2\overline{\mathcal{G}}_{d,1}^{q,1}A_1^q \right. \\
& - 6\gamma_0^b f_1^q\left. \right) - 2\zeta_2\zeta_3(A_1^q)^3 - \frac{1}{2}\zeta_2^2(A_1^q)^2 f_1^q\left. \right] + \mathcal{D}_0\overline{\mathcal{D}}_0 \left[f_1^q f_2^q + \frac{1}{2}A_3^q + \frac{1}{2}\overline{\mathcal{G}}_{d,2}^{q,1}A_1^q + \overline{\mathcal{G}}_{d,1}^{q,1}(f_1^q)^2 \right. \\
& + \overline{\mathcal{G}}_{d,1}^{q,1}A_2^q + \overline{\mathcal{G}}_{d,1}^{q,1^2}A_1^q + \frac{1}{2}g_2^{b,1}A_1^q + g_1^{b,1}(f_1^q)^2 + g_1^{b,1}A_2^q + 2g_1^{b,1}\overline{\mathcal{G}}_{d,1}^{q,1}A_1^q + g_1^{b,1^2}A_1^q + \frac{1}{2}\beta_1 f_1^q \\
& + \beta_0\left(f_2^q + \overline{\mathcal{G}}_{d,1}^{q,2}A_1^q + 3\overline{\mathcal{G}}_{d,1}^{q,1}f_1^q + g_1^{b,2}A_1^q + g_1^{b,1}f_1^q\right) + 2\beta_0^2\overline{\mathcal{G}}_{d,1}^{q,1} - 5\zeta_3(A_1^q)^2 f_1^q - 3\zeta_3\beta_0(A_1^q)^2 \\
& + \zeta_2\left(A_1^q A_2^q - A_1^q(f_1^q)^2 + \overline{\mathcal{G}}_{d,1}^{q,1}(A_1^q)^2 + g_1^{b,1}(A_1^q)^2\right) + 3\zeta_2\beta_0\left(A_1^q B_1^q - \gamma_0^b A_1^q\right) + \frac{1}{4}\zeta_2^2(A_1^q)^3\left. \right] \\
& + \mathcal{D}_1\delta(1-z_2) \left[2f_1^q f_2^q + A_3^q + \overline{\mathcal{G}}_{d,2}^{q,1}A_1^q + 2\overline{\mathcal{G}}_{d,1}^{q,1}(f_1^q)^2 + 2\overline{\mathcal{G}}_{d,1}^{q,1}A_2^q + 2\overline{\mathcal{G}}_{d,1}^{q,1^2}A_1^q + g_2^{b,1}A_1^q \right. \\
& + 2g_1^{b,1}(f_1^q)^2 + 2g_1^{b,1}A_2^q + 4g_1^{b,1}\overline{\mathcal{G}}_{d,1}^{q,1}A_1^q + 2g_1^{b,1^2}A_1^q + \beta_1 f_1^q + 2\beta_0\left(f_2^q + \overline{\mathcal{G}}_{d,1}^{q,2}A_1^q + 3\overline{\mathcal{G}}_{d,1}^{q,1}f_1^q \right.
\end{aligned}$$

$$\begin{aligned}
& + g_1^{b,2} A_1^q + g_1^{b,1} f_1^q) + 4\beta_0^2 \overline{\mathcal{G}}_{d,1}^{q,1} - 10\zeta_3 (A_1^q)^2 f_1^q - 6\zeta_3 \beta_0 (A_1^q)^2 + 2\zeta_2 \left(-A_1^q (f_1^q)^2 + A_1^q A_2^q \right. \\
& + \overline{\mathcal{G}}_{d,1}^{q,1} (A_1^q)^2 + g_1^{b,1} (A_1^q)^2) + 6\zeta_2 \beta_0 \left(A_1^q B_1^q - \gamma_0^b A_1^q \right) + \frac{1}{2} \zeta_2^2 (A_1^q)^3 \left. \right] + \mathcal{D}_1 \overline{\mathcal{D}}_0 \left[- (f_1^q)^3 \right. \\
& - 3A_2^q f_1^q - 3A_1^q f_2^q - 6\overline{\mathcal{G}}_{d,1}^{q,1} A_1^q f_1^q - 6g_1^{b,1} A_1^q f_1^q - \beta_1 A_1^q - \beta_0 \left(3(f_1^q)^2 + 2A_2^q + 8\overline{\mathcal{G}}_{d,1}^{q,1} A_1^q \right. \\
& + 2g_1^{b,1} A_1^q) - 2\beta_0^2 f_1^q + 10\zeta_3 (A_1^q)^3 + 3\zeta_2 (A_1^q)^2 f_1^q + 3\zeta_2 \beta_0 (A_1^q)^2 \left. \right] + \mathcal{D}_1 \overline{\mathcal{D}}_1 \left[3A_1^q (f_1^q)^2 \right. \\
& + 3A_1^q A_2^q + 3\overline{\mathcal{G}}_{d,1}^{q,1} (A_1^q)^2 + 3g_1^{b,1} (A_1^q)^2 + 5\beta_0 A_1^q f_1^q + \beta_0^2 A_1^q - \frac{3}{2} \zeta_2 (A_1^q)^3 \left. \right] \\
& + \mathcal{D}_2 \delta(1-z_2) \left[-\frac{1}{2} (f_1^q)^3 - \frac{3}{2} A_2^q f_1^q - \frac{3}{2} A_1^q f_2^q - 3\overline{\mathcal{G}}_{d,1}^{q,1} A_1^q f_1^q - 3g_1^{b,1} A_1^q f_1^q - \frac{1}{2} \beta_1 A_1^q \right. \\
& - \beta_0 \left(\frac{3}{2} (f_1^q)^2 + A_2^q + 4\overline{\mathcal{G}}_{d,1}^{q,1} A_1^q + g_1^{b,1} A_1^q \right) - \beta_0^2 f_1^q + 5\zeta_3 (A_1^q)^3 + \frac{3}{2} \zeta_2 (A_1^q)^2 f_1^q \\
& + \frac{3}{2} \zeta_2 \beta_0 (A_1^q)^2 \left. \right] + \mathcal{D}_2 \overline{\mathcal{D}}_0 \left[3A_1^q (f_1^q)^2 + 3A_1^q A_2^q + 3\overline{\mathcal{G}}_{d,1}^{q,1} (A_1^q)^2 + 3g_1^{b,1} (A_1^q)^2 + 5\beta_0 A_1^q f_1^q \right. \\
& + \beta_0^2 A_1^q - \frac{3}{2} \zeta_2 (A_1^q)^3 \left. \right] + \mathcal{D}_2 \overline{\mathcal{D}}_1 \left[-\frac{15}{2} (A_1^q)^2 f_1^q - 5\beta_0 (A_1^q)^2 \right] + \mathcal{D}_2 \overline{\mathcal{D}}_2 \left[\frac{15}{8} (A_1^q)^3 \right] \\
& + \mathcal{D}_3 \delta(1-z_2) \left[A_1^q (f_1^q)^2 + A_1^q A_2^q + \overline{\mathcal{G}}_{d,1}^{q,1} (A_1^q)^2 + g_1^{b,1} (A_1^q)^2 + \frac{5}{3} \beta_0 A_1^q f_1^q + \frac{1}{3} \beta_0^2 A_1^q \right. \\
& - \frac{1}{2} \zeta_2 (A_1^q)^3 \left. \right] + \mathcal{D}_3 \overline{\mathcal{D}}_0 \left[-\frac{5}{2} (A_1^q)^2 f_1^q - \frac{5}{3} \beta_0 (A_1^q)^2 \right] + \mathcal{D}_3 \overline{\mathcal{D}}_1 \left[\frac{5}{2} (A_1^q)^3 \right] \\
& + \mathcal{D}_4 \delta(1-z_2) \left[-\frac{5}{8} (A_1^q)^2 f_1^q - \frac{5}{12} \beta_0 (A_1^q)^2 \right] + \mathcal{D}_4 \overline{\mathcal{D}}_0 \left[\frac{5}{8} (A_1^q)^3 \right] \\
& + \mathcal{D}_5 \delta(1-z_2) \left[\frac{1}{8} (A_1^q)^3 \right] + \left\{ z_1 \leftrightarrow z_2 \right\}. \tag{6.88}
\end{aligned}$$

At the stage, we can demonstrate that integration over the rapidity correctly reproduces inclusive threshold contribution to the Higgs production in bottom anti-bottom annihilation reported in [157]

:

$$\int dy \frac{d}{dy} \sigma_b(\tau, y, q^2) = \sigma_b(\tau, q^2). \tag{6.89}$$

The integration over the rapidity y leads to the following relation between $\Delta_{d,b}^{\text{SV}}(z_1, z_2)$ obtained in this paper and $\Delta_b^{\text{SV}}(z)$ in [157]:

$$\Delta_b^{\text{SV}}(z) = \int dz_1 \int dz_2 \delta(z - z_1 z_2) \Delta_{d,b}^{\text{SV}}(z_1, z_2). \quad (6.90)$$

We have explicitly checked that the results presented here for $\Delta_{d,b}^{\text{SV}}$ and those for Δ_b^{SV} in the [157] up to N³LO level satisfy the above relation confirming the consistency of the formalism used. For completeness, we present the results for $\Delta_{d,b}^{\text{SV},(i)}$ up to N³LO after substituting all the constants that are required to this order:

$$\begin{aligned} \Delta_{d,b}^{\text{SV},(1)} &= \delta(1-z_1)\delta(1-z_2)C_F(-2+6\zeta_2) + \mathcal{D}_0\bar{\mathcal{D}}_0(2C_F) + \mathcal{D}_1\delta(1-z_2)(4C_F) + \left\{z_1 \leftrightarrow z_2\right\}, \\ \Delta_{d,b}^{\text{SV},(2)} &= \delta(1-z_1)\delta(1-z_2) \left[C_F C_A \left(\frac{83}{9} + \frac{32}{3}\zeta_3 + \frac{250}{9}\zeta_2 - \frac{26}{5}\zeta_2^2 \right) + C_F^2 \left(8 - 30\zeta_3 - 8\zeta_2 \right. \right. \\ &\quad \left. \left. + \frac{152}{5}\zeta_2^2 \right) + n_f C_F \left(\frac{4}{9} + \frac{4}{3}\zeta_3 - \frac{40}{9}\zeta_2 \right) \right] + \mathcal{D}_0\delta(1-z_2) \left[C_F C_A \left(-\frac{808}{27} + 28\zeta_3 + \frac{44}{3}\zeta_2 \right) \right. \\ &\quad \left. + C_F^2 \left(32\zeta_3 \right) + n_f C_F \left(\frac{112}{27} - \frac{8}{3}\zeta_2 \right) \right] + \mathcal{D}_0\bar{\mathcal{D}}_0 \left[C_F C_A \left(\frac{134}{9} - 4\zeta_2 \right) + C_F^2 \left(-8 + 8\zeta_2 \right) \right. \\ &\quad \left. + n_f C_F \left(-\frac{20}{9} \right) \right] + \mathcal{D}_1\delta(1-z_2) \left[C_F C_A \left(\frac{268}{9} - 8\zeta_2 \right) + C_F^2 \left(-16 + 16\zeta_2 \right) \right. \\ &\quad \left. + n_f C_F \left(-\frac{40}{9} \right) \right] + \mathcal{D}_1\bar{\mathcal{D}}_0 \left[C_F C_A \left(-\frac{44}{3} \right) + n_f C_F \left(\frac{8}{3} \right) \right] + \mathcal{D}_1\bar{\mathcal{D}}_1 \left[C_F^2 \left(24 \right) \right] \\ &\quad + \mathcal{D}_2\delta(1-z_2) \left[C_F C_A \left(-\frac{22}{3} \right) + n_f C_F \left(\frac{4}{3} \right) \right] + \mathcal{D}_2\bar{\mathcal{D}}_0 \left[C_F^2 \left(24 \right) \right] \\ &\quad + \mathcal{D}_3\delta(1-z_2) \left[C_F^2 \left(8 \right) \right] + \left\{z_1 \leftrightarrow z_2\right\} \end{aligned}$$

and

$$\Delta_{d,b}^{\text{SV},(3)} = \delta(1-z_1)\delta(1-z_2) \left[C_F C_A^2 \left(\frac{34495}{81} - 42\zeta_5 + \frac{14254}{81}\zeta_3 - \frac{200}{3}\zeta_3^2 + \frac{4487}{81}\zeta_2 - 324\zeta_2\zeta_3 \right) \right]$$

$$\begin{aligned}
& -\frac{2446}{135}\zeta_2^2 + \frac{12176}{315}\zeta_2^3) + C_F^2 C_A \left(-\frac{491}{3} - \frac{2732}{9}\zeta_5 - \frac{922}{3}\zeta_3 + \frac{632}{3}\zeta_3^2 + \frac{10441}{27}\zeta_2 \right. \\
& + \frac{4288}{9}\zeta_2\zeta_3 + \frac{21302}{135}\zeta_2^2 - \frac{39136}{315}\zeta_2^3) + C_F^3 \left(\frac{539}{3} + 424\zeta_5 - 594\zeta_3 + \frac{368}{3}\zeta_3^2 - \frac{179}{3}\zeta_2 \right. \\
& - 152\zeta_2\zeta_3 - \frac{196}{5}\zeta_2^2 + \frac{45008}{315}\zeta_2^3) + n_f C_F C_A \left(-\frac{5770}{81} - 4\zeta_5 - \frac{5660}{81}\zeta_3 - \frac{806}{27}\zeta_2 \right. \\
& + \frac{136}{3}\zeta_2\zeta_3 - \frac{380}{27}\zeta_2^2) + n_f C_F^2 \left(-\frac{35}{9} - \frac{112}{9}\zeta_5 + 180\zeta_3 - \frac{1507}{27}\zeta_2 - \frac{736}{9}\zeta_2\zeta_3 - \frac{1604}{135}\zeta_2^2 \right) \\
& + n_f^2 C_F \left(\frac{8}{27} - \frac{80}{81}\zeta_3 + \frac{184}{81}\zeta_2 + \frac{296}{135}\zeta_2^2 \right) \Big] + \mathcal{D}_0 \delta(1-z_2) \left[C_F C_A^2 \left(-\frac{297029}{729} - 192\zeta_5 \right. \right. \\
& + \frac{14264}{27}\zeta_3 + \frac{27752}{81}\zeta_2 - \frac{176}{3}\zeta_2\zeta_3 - \frac{616}{15}\zeta_2^2) + C_F^2 C_A \left(\frac{3232}{27} + \frac{3280}{9}\zeta_3 - \frac{4816}{27}\zeta_2 - 16\zeta_2\zeta_3 \right. \\
& + \frac{176}{3}\zeta_2^2) + C_F^3 \left(384\zeta_5 - 128\zeta_3 - 128\zeta_2\zeta_3 \right) + n_f C_F C_A \left(\frac{62626}{729} - \frac{536}{9}\zeta_3 - \frac{7760}{81}\zeta_2 \right. \\
& + \frac{208}{15}\zeta_2^2) + n_f C_F^2 \left(\frac{421}{9} - \frac{944}{9}\zeta_3 + \frac{520}{27}\zeta_2 - \frac{256}{15}\zeta_2^2) + n_f^2 C_F \left(-\frac{1856}{729} - \frac{32}{27}\zeta_3 \right. \\
& + \left. \left. \frac{160}{27}\zeta_2 \right) \right] + \mathcal{D}_0 \overline{\mathcal{D}}_0 \left[C_F C_A^2 \left(\frac{15503}{81} - 88\zeta_3 - \frac{340}{3}\zeta_2 + \frac{88}{5}\zeta_2^2 \right) + C_F^2 C_A \left(-\frac{68}{3} - \frac{400}{3}\zeta_3 \right. \right. \\
& + \left. \left. \frac{608}{9}\zeta_2 - \frac{24}{5}\zeta_2^2 \right) + C_F^3 \left(32 - 120\zeta_3 + 32\zeta_2 - \frac{96}{5}\zeta_2^2 \right) + n_f C_F C_A \left(-\frac{4102}{81} + \frac{256}{9}\zeta_2 \right) \right. \\
& + n_f C_F^2 \left(-\frac{23}{3} + \frac{160}{3}\zeta_3 - \frac{80}{9}\zeta_2 \right) + n_f^2 C_F \left(\frac{200}{81} - \frac{16}{9}\zeta_2 \right) \Big] + \mathcal{D}_1 \delta(1-z_2) \left[C_F C_A^2 \left(\frac{31006}{81} \right. \right. \\
& - 176\zeta_3 - \frac{680}{3}\zeta_2 + \frac{176}{5}\zeta_2^2) + C_F^2 C_A \left(-\frac{136}{3} - \frac{800}{3}\zeta_3 + \frac{1216}{9}\zeta_2 - \frac{48}{5}\zeta_2^2) + C_F^3 \left(64 \right. \\
& - 240\zeta_3 + 64\zeta_2 - \frac{192}{5}\zeta_2^2) + n_f C_F C_A \left(-\frac{8204}{81} + \frac{512}{9}\zeta_2 \right) + n_f C_F^2 \left(-\frac{46}{3} + \frac{320}{3}\zeta_3 \right. \\
& - \left. \left. \frac{160}{9}\zeta_2 \right) + n_f^2 C_F \left(\frac{400}{81} - \frac{32}{9}\zeta_2 \right) \right] + \mathcal{D}_1 \overline{\mathcal{D}}_0 \left[C_F C_A^2 \left(-\frac{7120}{27} + \frac{176}{3}\zeta_2 \right) \right. \\
& + C_F^2 C_A \left(-\frac{2704}{9} + 336\zeta_3 + 352\zeta_2 \right) + C_F^3 \left(640\zeta_3 \right) + n_f C_F C_A \left(\frac{2312}{27} - \frac{32}{3}\zeta_2 \right) \\
& + n_f C_F^2 \left(\frac{424}{9} - 64\zeta_2 \right) + n_f^2 C_F \left(-\frac{160}{27} \right) \Big] + \mathcal{D}_1 \overline{\mathcal{D}}_1 \left[C_F C_A^2 \left(\frac{484}{9} \right) + C_F^2 C_A \left(\frac{1072}{3} \right. \right. \\
& - 96\zeta_2) + C_F^3 \left(-96 - 96\zeta_2 \right) + n_f C_F C_A \left(-\frac{176}{9} \right) + n_f C_F^2 \left(-\frac{160}{3} \right) + n_f^2 C_F \left(\frac{16}{9} \right) \Big] \\
& + \mathcal{D}_2 \delta(1-z_2) \left[C_F C_A^2 \left(-\frac{3560}{27} + \frac{88}{3}\zeta_2 \right) + C_F^2 C_A \left(-\frac{1352}{9} + 168\zeta_3 + 176\zeta_2 \right) \right. \\
& + \left. \left. C_F^3 \left(320\zeta_3 \right) + n_f C_F C_A \left(\frac{1156}{27} - \frac{16}{3}\zeta_2 \right) + n_f C_F^2 \left(\frac{212}{9} - 32\zeta_2 \right) + n_f^2 C_F \left(-\frac{80}{27} \right) \right]
\end{aligned}$$

$$\begin{aligned}
& + \mathcal{D}_2 \bar{\mathcal{D}}_0 \left[C_F C_A^2 \left(\frac{484}{9} \right) + C_F^2 C_A \left(\frac{1072}{3} - 96 \zeta_2 \right) + C_F^3 \left(-96 - 96 \zeta_2 \right) \right. \\
& + n_f C_F C_A \left(-\frac{176}{9} \right) + n_f C_F^2 \left(-\frac{160}{3} \right) + n_f^2 C_F \left(\frac{16}{9} \right) \left. \right] + \mathcal{D}_2 \bar{\mathcal{D}}_1 \left[C_F^2 C_A \left(-\frac{880}{3} \right) \right. \\
& + n_f C_F^2 \left(\frac{160}{3} \right) \left. \right] + \mathcal{D}_2 \bar{\mathcal{D}}_2 \left[C_F^3 \left(120 \right) \right] + \mathcal{D}_3 \delta(1-z_2) \left[C_F C_A^2 \left(\frac{484}{27} \right) + C_F^2 C_A \left(\frac{1072}{9} \right. \right. \\
& \left. \left. - 32 \zeta_2 \right) + C_F^3 \left(-32 - 32 \zeta_2 \right) + n_f C_F C_A \left(-\frac{176}{27} \right) + n_f C_F^2 \left(-\frac{160}{9} \right) + n_f^2 C_F \left(\frac{16}{27} \right) \right] \\
& + \mathcal{D}_3 \bar{\mathcal{D}}_0 \left[C_F^2 C_A \left(-\frac{880}{9} \right) + n_f C_F^2 \left(\frac{160}{9} \right) \right] + \mathcal{D}_3 \bar{\mathcal{D}}_1 \left[C_F^3 \left(160 \right) \right] \\
& + \mathcal{D}_4 \delta(1-z_2) \left[C_F^2 C_A \left(-\frac{220}{9} \right) + n_f C_F^2 \left(\frac{40}{9} \right) \right] + \mathcal{D}_4 \bar{\mathcal{D}}_0 \left[C_F^3 \left(40 \right) \right] \\
& + \mathcal{D}_5 \delta(1-z_2) \left[C_F^3 \left(8 \right) \right] + \left\{ z_1 \leftrightarrow z_2 \right\}. \tag{6.91}
\end{aligned}$$

Substituting $\Delta_{d,b}^{\text{SV},(1)}$, $\Delta_{d,b}^{\text{SV},(2)}$ and $\Delta_{d,b}^{\text{SV},(3)}$ in the Eq. 6.13, we obtain $W_b^{\text{SV},(i)}$ or equivalently $\frac{d}{dy} \sigma^{b,\text{SV},(i)}$ (Eq. 6.4) at the hadronic level order by order up to $\mathcal{O}(a_s^3)$.

6.2.3 Numerical Results

In this section, we present the numerical impact of the rapidity distribution of the Higgs boson, produced via bottom anti-bottom annihilation subprocess at the LHC. The rapidity distribution can be expanded in powers of the strong coupling constant a_s as

$$\frac{d\sigma^b}{dY} = \frac{d\sigma^{b,(0)}}{dY} + \sum_{i=1}^{\infty} a_s^i \frac{d\sigma^{b,(i)}}{dY}. \tag{6.92}$$

Beyond LO, the distribution is split into hard and SV parts as

$$\frac{d\sigma^{b,(i)}}{dY} = \frac{d\sigma^{\text{hard},b,(i)}}{dY} + \frac{d\sigma^{\text{SV},b,(i)}}{dY}. \tag{6.93}$$

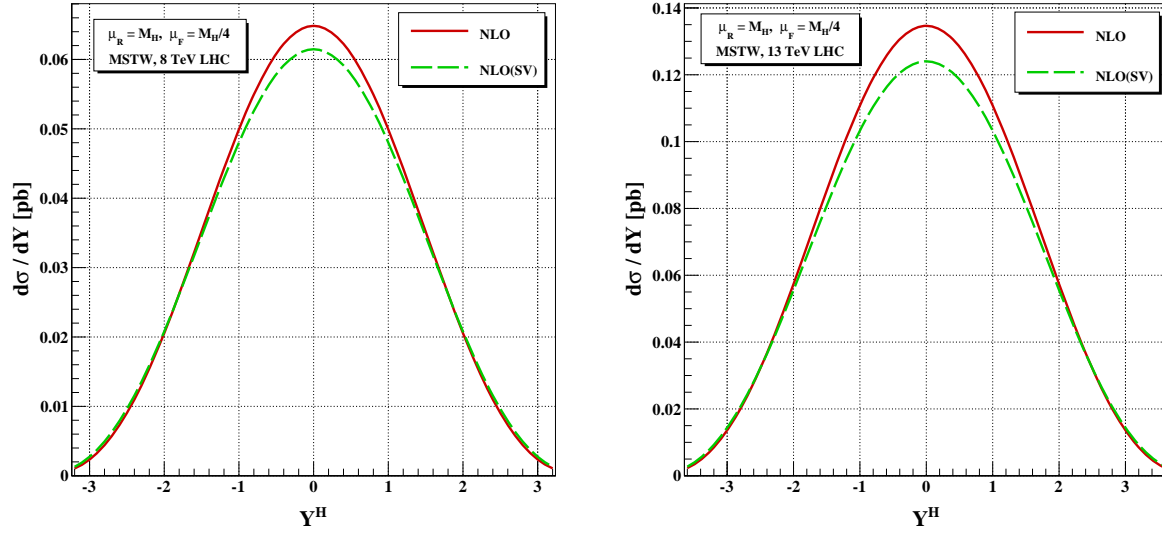


Figure 6.1: The comparison between NLO and NLO_{SV} with the renormalization scale $\mu_R = m_H$ and factorization scale $\mu_F = m_H/4$ at 8 TeV(left panel) and 13 TeV (right panel) LHC.

In the following, for our numerical study we will use the exact results up to NLO level but at NNLO, we use exact NLO and only threshold contribution at $\mathcal{O}(a_s^2)$ as we do not have access to the hard part at $\mathcal{O}(a_s^2)$ computed in [112]¹. We call it NNLO(SV). Similarly at N³LO level, we will use NNLO(SV) and threshold contribution at $\mathcal{O}(a_s^3)$, denoted by N³LO(SV) hereafter. We present results for the center of mass energies 8 and 13 TeV at the LHC. The standard model parameters which enter into our computation are the Z boson mass $m_Z = 91.1876$ GeV, top quark mass $m_t = 173.4$ GeV and mass of the Higgs boson $m_H = 125$ GeV. The strong coupling constant is evolved using the 4-loop RG equations with $\alpha_s^{\text{N}^3\text{LO}}(m_Z) = 0.117$. Following the Ref. [174], the solution to RGE 6.47 for $\lambda(\mu_R^2)$ is given by,

$$\lambda(\mu_R^2) = \lambda(\mu_0^2) \frac{M(a_s(\mu_R^2))}{M(a_s(\mu_0^2))} \quad (6.94)$$

¹The authors informed us that the code is not yet ready for public distribution.

Y	0.0	0.4	0.8	1.2	1.6	2.0	2.4	2.8	3.2
10^2 LO	4.137	4.027	3.705	3.196	2.549	1.828	1.126	5.427	1.686
10^2 NLO	6.485	6.225	5.495	4.429	3.217	2.054	1.097	4.419	1.065
10^2 NNLO(SV)	6.921	6.650	5.879	4.731	3.407	2.135	1.113	4.417	1.118
10^2 N ³ LO(SV)	6.984	6.707	5.922	4.757	3.415	2.130	1.105	4.340	1.084

Table 6.1: Contributions at LO, NLO, NNLO(SV) and N³LO(SV) with the renormalization scale $\mu_R = m_H$ and factorization scale $\mu_F = m_H/4$ at 8 TeV LHC.

with

$$M(a_s) = \alpha_s^{A_0} \sum_{i=0}^{\infty} \alpha_s^i M_i. \quad (6.95)$$

The K_i are given by

$$\begin{aligned} M_0 &= 1, & M_1 &= A_1, \\ M_2 &= \frac{1}{2}(A_1^2 + A_2), & M_3 &= \frac{1}{6}(A_1^3 + 3A_1A_2 + 2A_3), \end{aligned} \quad (6.96)$$

with

$$\begin{aligned} A_0 &= c_0, & A_1 &= c_1 - b_1c_0, & A_2 &= c_2 - b_1c_1 + c_0(b_1^2 - b_2), \\ A_3 &= c_3 - b_1c_2 + c_1(b_1^2 - b_2) + c_0(b_1b_2 - b_1(b_1^2 - b_2) - b_3), \end{aligned} \quad (6.97)$$

and

$$c_i = \frac{\gamma_i^b}{\beta_0}, \quad b_i = \frac{\gamma_i^b}{\beta_0}, \quad (6.98)$$

where μ_0 is some reference scale at which λ is known. We have numerically evaluated $\lambda(\mu_R^2)$ to relevant order namely LO, NLO, NNLO and N³LO by truncating the terms in the RHS of

Y	0.0	0.4	0.8	1.2	1.6	2.0	2.4	2.8	3.2
10^2 LO	8.465	8.293	7.787	6.981	5.925	4.686	3.371	2.115	1.068
10^2 NLO	13.466	13.063	11.903	10.133	7.985	5.737	3.671	2.001	0.849
10^2 NNLO(SV)	14.284	13.875	12.689	10.844	8.549	6.099	3.833	2.035	0.848
10^2 N ³ LO(SV)	14.475	14.057	12.843	10.959	8.620	6.131	3.837	2.025	0.838

Table 6.2: Contributions at LO, NLO, NNLO(SV) and N³LO(SV) with the renormalization scale $\mu_R = m_H$ and factorization scale $\mu_F = m_H/4$ at 13 TeV LHC.

Eq. 6.47. We have used $\lambda(\mu_0^2) = \sqrt{2}m_b(\mu_0)/v$ and $m_b(\mu_0) = 3.63$ GeV with the choice $\mu_0 = 10$ GeV. We use the MSTW2008 [129] parton density sets with errors estimated at 68% confidence level with five active flavours. Parton densities and α_s are evaluated at each corresponding perturbative order. Specifically, we use $(n + 1)$ -loop α_s at NⁿLO, with $n = 0, 1, 2, 3$. However, we use MSTW2008NNLO PDFs at N³LO, the N³LO kernels not being available at the moment. We set the renormalization scale $\mu_R = m_H$ and factorization scale $\mu_F = m_H/4$ [74] as their central values.

Several checks have been performed on our numerical code. We have found complete agreement with the literature on the inclusive Higgs production rate [77, 157] after performing an additional numerical integration on our distribution over the rapidity Y . The check was also performed at the analytical level. However, we were not able to reproduce the plot given in [112], after using the same set of values of the input parameters. We begin our discussion with the results at NLO level. In Sect. 6.2.1, we presented the contributions coming from the exact results, containing the regular as well as pure threshold ones to the rapidity distribution at $\mathcal{O}(a_s)$. In Fig. 6.1, we plot both the NLO(SV) and exact NLO rapidity distributions to exhibit the dominance of threshold over the entire rapidity range after setting the values of the renormalization and factorization scales to their central values. From now on, we adopt a consistent representation to display the figures corresponding to our results. In every figure, the left panel shows the result for 8 TeV whereas the right panel corresponds to 13 TeV at the LHC. We observe that the exact NLO contribution is well approximated by the NLO(SV), thanks to the intrinsic property of the matrix element, where the phase-space points corresponding to the born kinematics contribute towards the largest radiative

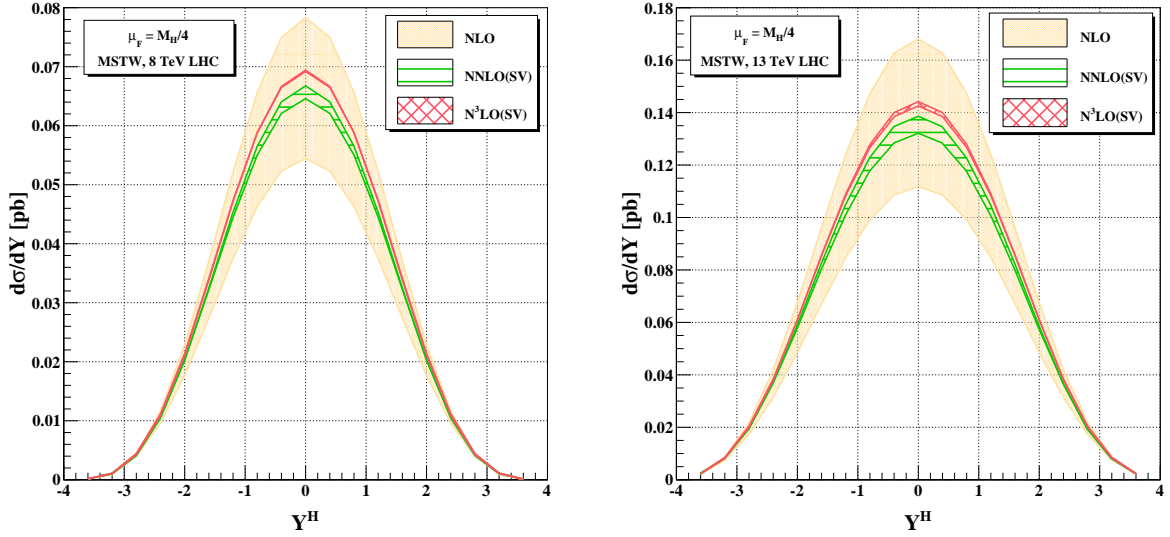


Figure 6.2: The rapidity distribution of the Higgs boson at NLO, NNLO(SV) and N^3 LO(SV) at 8 TeV(left panel) and 13 TeV (right panel) LHC. The band indicates the uncertainty due to renormalization scale.

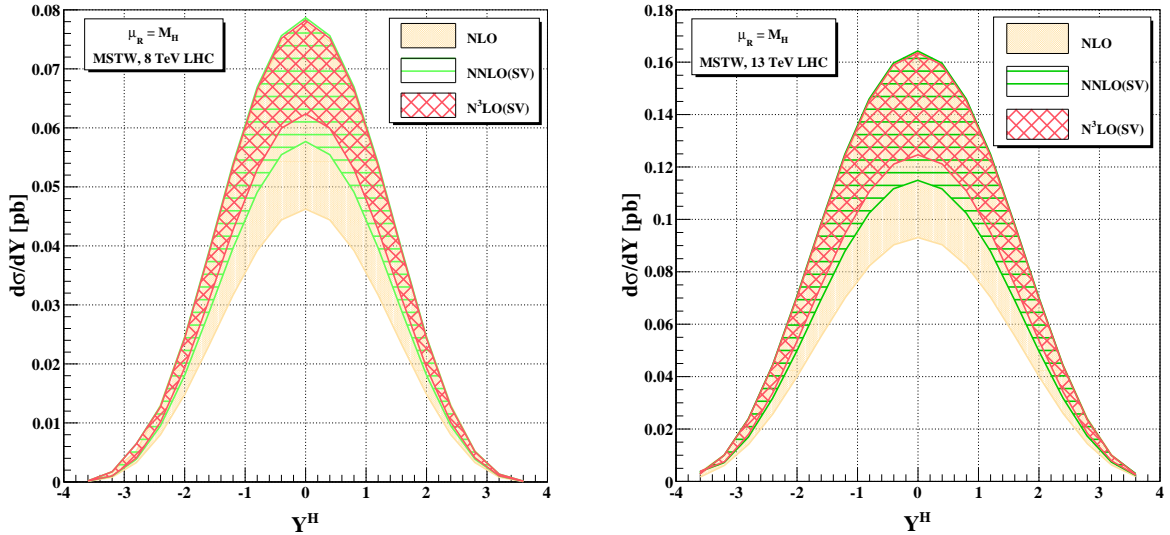


Figure 6.3: The rapidity distribution of the Higgs boson at NLO, NNLO(SV) and N^3 LO(SV) at 8 TeV(left panel) and 13 TeV (right panel) LHC. The band indicates the uncertainty due to factorization scale.

corrections for the low τ ($m_H^2/s \approx 10^{-4}$) values [175]. So, we expect that the trend of approximating the exact results by threshold corrections at that order to remain same after the inclusion of

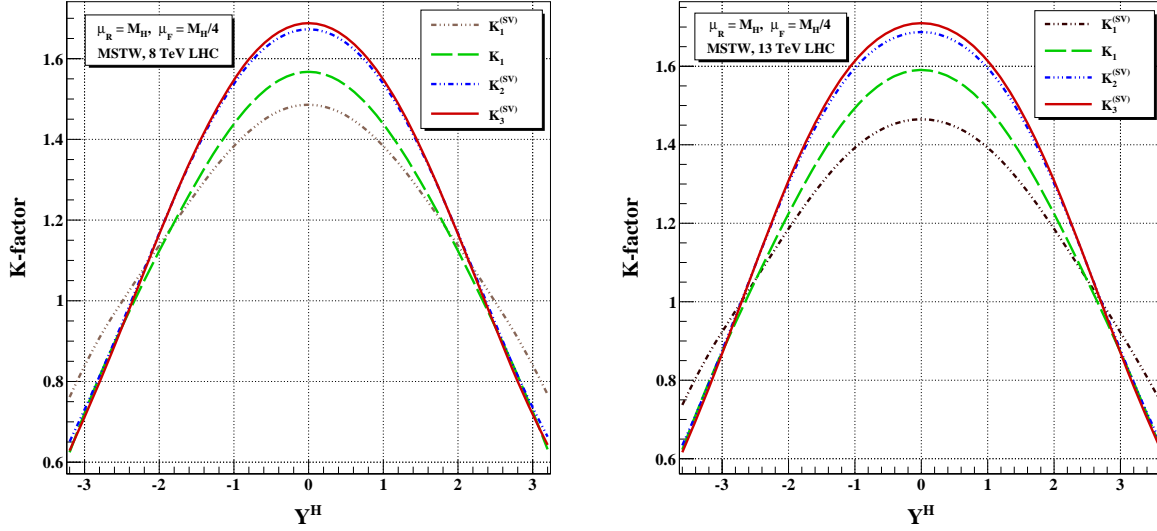


Figure 6.4: The distribution of $K_1^{(SV)}$, K_1 , $K_2^{(SV)}$ and $K_3^{(SV)}$ at different perturbative order at 8 TeV(left panel) and 13 TeV (right panel) LHC.

higher order terms also.

With this in mind, we present the results at LO, NLO, NNLO(SV), N³LO(SV) for different values of the rapidity Y after setting the central values for renormalization and factorization scales for 8 TeV in Table 6.1 and for 13 TeV in Table 6.2 at LHC. The hadronic cross-section, obtained by the convolution of the partonic cross section with the parton densities, suffers from the theoretical uncertainties, arising from the missing higher order corrections, through the renormalization (μ_R) and factorization (μ_F) scales. These can be estimated through the variation of the differential hadronic cross section with μ_R and μ_F , thereby exhibiting the size of the higher order effects.

In Fig. 6.2, we plot two curves for each order for the predictions at NLO, NNLO(SV), N³LO(SV) corresponding to two different choices of the renormalization scale, $\mu_R = 0.1m_H$ and $\mu_R = 10m_H$, keeping the factorization scale fixed at $\mu_F = m_H/4$, whereas in Fig. 6.3, we plot the predictions at each order corresponding to two different choices of the factorization scale, $\mu_F = m_H/8$ and $\mu_F = m_H/2$, keeping the renormalization scale fixed at $\mu_R = m_H$. We observe a consistent improvement in the accuracy of the predictions with the inclusion of the higher order terms, the width of the bands being an clear indicator of the theoretical uncertainties. Moreover, we can see that the

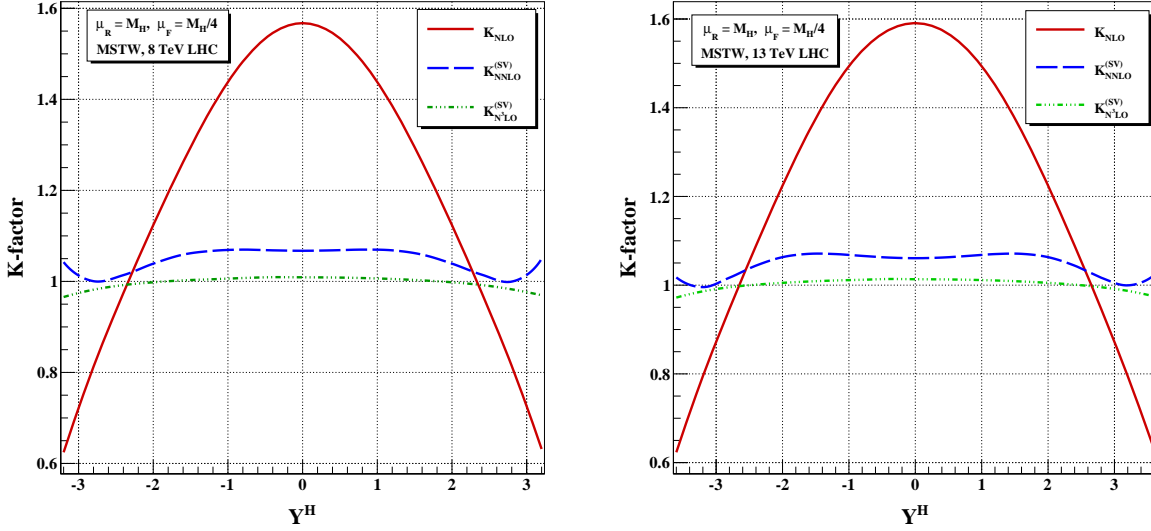


Figure 6.5: The distribution of K_{NLO} , $K_{NNLO}^{(SV)}$ and $K_{N^3LO}^{(SV)}$ at different perturbative order at 8 TeV (left panel) and 13 TeV (right panel) LHC.

dependence on the renormalization scale for this process is very mild. Another way to assess the reliability of the prediction is to study the rate of convergence of the perturbation series, represented by the K-factor.

In the Fig. 6.4, we plot the K-factors defined as $K_1 = \frac{d\sigma^{NLO}}{d\sigma^{LO}}$ and $K_i^{(SV)} = \frac{d\sigma^{N^iLO(SV)}}{d\sigma^{LO}}$, $i = 2, 3$ as a function of Y . For 8 TeV LHC, we see that the K_1 varies from 1.57 to 0.63 over the entire rapidity range, while the value of K_1 for the inclusive rate is 1.37. Similarly, for $K_2^{(SV)}$, the variation is from 1.67 to 0.66, while for the inclusive rate it is 1.35. It shows, particularly, that the shape at higher orders can not be rescaled from lower orders as the differential K-factor varies significantly over the full rapidity range. In the Fig. 6.5 we plot K factors defined by $K_{NLO}^{(SV)} = d\sigma^{NLO(SV)}/d\sigma^{LO}$, $K_{NNLO}^{(SV)} = d\sigma^{NNLO(SV)}/d\sigma^{NLO}$ and $K_{N^3LO}^{(SV)} = d\sigma^{N^3LO(SV)}/d\sigma^{NNLO(SV)}$. The values of the K-factors with the inclusion of higher order terms decrease, thereby implying a considerable amount of improvement in the rate of convergence.

6.3 Conclusions

To summarize, we present threshold enhanced $N^3\text{LO}$ QCD correction to rapidity distribution of the Higgs boson produced through bottom quark annihilation at the LHC. We show in detail the infrared structure of the QCD amplitudes at NLO level as well as the cancellation of the various soft and collinear singularities through the summation of all possible degenerate states and the renormalization of the PDFs in order to demonstrate a general framework to obtain threshold corrections to rapidity distributions to all orders in perturbation theory. We have used factorization properties, along with Sudakov resummation of soft gluons and renormalization group invariance to achieve this. The recent result on three loop form factor by Gehrmann and Kara [155] and the universal soft distribution obtained in [103] provide the last missing information to obtain threshold correction to $N^3\text{LO}$ for the rapidity distribution of the Higgs boson in bottom quark annihilation. We find the dominance of the threshold contribution over the entire rapidity range at NLO. We extend this approximation beyond NLO to make predictions for center of mass energies 8 and 13 TeV. We observe that the inclusion of $N^3\text{LO}$ contributions reduces the scale dependency further, as expected, through the variation of the renormalization and factorization scales around their central values and that K-factors show stability at higher orders.

Chapter 7

Summary

In the coming years, the LHC will be running at an increased collision energy approximately at 13 TeV and with a larger luminosity, shedding light on the still unexplored regime of energy in SM and also probing the BSMs at multi TeV range. In this scenario it will be necessary to produce the results for the processes of interest at LHC after the inclusion of higher order terms in QCD to reduce the theoretical uncertainty as well as performing a complete phenomenological analysis to get any hint of new physics buried in the data. In this thesis, we have obtained precise results for different processes of interest at the LHC. In particular, we have computed fixed order NLO corrections and then extended these results through the matching with the PS. On the other hand, we have calculated threshold corrections beyond NNLO, which serves as the initial step towards the computation of the full N³LO correction for the processes of interests.

We have studied three photon production in the SM, $\ell^+\ell^-$, ZZ , W^+W^- production in SM and ADD model at NLO+PS accuracy. The three photon production acts as a background for the techni-pion production in association with a photon, where the techni-pion decays into a photon. From the di-final states in the ADD model, one can in principle probe the potential reach of the LHC in finding out the extra dimensions. As, these processes are certainly going to be studied with the data from the upcoming runs at LHC, we have produced the results at NLO+PS accuracy within the AMC@NLO framework, thus producing a set of realistic events directly comparable with the

experiment. For the three photon production, We have calculated this process at NLO, confirming the earlier result reported in the literature and then made interface with the MADFKS in the AMC@NLO framework to produce the necessary results. We have also checked the effect of the frizione isolation parameters on the prediction for the three photon production and observed that the total inclusive cross-section depends heavily on these parameters. In case of the di-final states in ADD model we have used the already available analytical results for the NLO correction and implemented them in the AMC@NLO framework to match with the PS. Various kinemtical distributions has been studied for all of these processes and the effect of the PS has been discussed. Moreover, we have also studied the potential reach for 14 TeV LHC at 10 fb^{-1} to probe these extra dimensions at this accuracy. The scale uncertainty has been observed to decrease consistently with the inclusion of the PS. In the process of obtaining these results, we have also established interfaces between different analytical and numerical tools, thereby creating a framework suitable for study of other processes of interest at this accuracy.

On the other hand, we have produced results for threshold corrections at third order in QCD, which constitutes a certain part of the complete correction at this order. We have studied the total inclusive cross-section for the associated production of the Higgs with vector boson and the rapidity distribution of the Higgs boson produced through bottom quark annihilation. In case of VH production, we have exploited the fact that at LO this is an electroweak process and the QCD corrections enter only in the initial state, making it a DY look alike process. We have used the available results for DY production with the inclusion of $N^3\text{LO}$ QCD threshold corrections and implemented it in the framework of `vh@nnlo` code to obtain the threshold corrected results at third order in QCD for the VH production. For the study of the rapidity distribution of the Higgs boson produced through bottom quark annihilation we have outlined a complete framework to calculate these threshold corrections in a consistent, systematic and accurate way for a final state colorless particle. The framework, which is based on the factorization properties of the QCD amplitudes along with Sudakov resummation and the renormalization group invariance has been extensively described at the NLO level. Then it has been extended to calculate the corrections beyond NNLO. For this purpose, the recent

results on threshold N^3LO correction in QCD for the Drell-Yan production and on three loop QCD correction to Higgs form factor with bottom anti-bottom quark has been used to achieve this task. It has been observed that the inclusion of the N^3LO corrections reduce the scale uncertainty further for both the processes.

Bibliography

- [1] **ATLAS Collaboration** Collaboration, G. Aad *et al.*, *Observation of a new particle in the search for the Standard Model Higgs boson with the ATLAS detector at the LHC*, *Phys.Lett.* **B716** (2012) 1–29, arXiv:1207.7214 [hep-ex].
- [2] **CMS Collaboration** Collaboration, S. Chatrchyan *et al.*, *Observation of a new boson at a mass of 125 GeV with the CMS experiment at the LHC*, *Phys.Lett.* **B716** (2012) 30–61, arXiv:1207.7235 [hep-ex].
- [3] M. Gell-Mann, *A Schematic Model of Baryons and Mesons*, *Phys.Lett.* **8** (1964) 214–215.
- [4] H. Fritzsch, M. Gell-Mann, and H. Leutwyler, *Advantages of the Color Octet Gluon Picture*, *Phys.Lett.* **B47** (1973) 365–368.
- [5] S. Glashow, *Partial Symmetries of Weak Interactions*, *Nucl.Phys.* **22** (1961) 579–588.
- [6] S. Weinberg, *A Model of Leptons*, *Phys.Rev.Lett.* **19** (1967) 1264–1266.
- [7] P. W. Higgs, *Broken symmetries, massless particles and gauge fields*, *Phys.Lett.* **12** (1964) 132–133.
- [8] P. W. Higgs, *Broken Symmetries and the Masses of Gauge Bosons*, *Phys.Rev.Lett.* **13** (1964) 508–509.
- [9] F. Englert and R. Brout, *Broken Symmetry and the Mass of Gauge Vector Mesons*, *Phys.Rev.Lett.* **13** (1964) 321–323.

- [10] G. Guralnik, C. Hagen, and T. Kibble, *Global Conservation Laws and Massless Particles*, *Phys.Rev.Lett.* **13** (1964) 585–587.
- [11] N. Arkani-Hamed, S. Dimopoulos, and G. Dvali, *The Hierarchy problem and new dimensions at a millimeter*, *Phys.Lett.* **B429** (1998) 263–272, arXiv:hep-ph/9803315 [hep-ph].
- [12] I. Antoniadis, N. Arkani-Hamed, S. Dimopoulos, and G. Dvali, *New dimensions at a millimeter to a Fermi and superstrings at a TeV*, *Phys.Lett.* **B436** (1998) 257–263, arXiv:hep-ph/9804398 [hep-ph].
- [13] N. Arkani-Hamed, S. Dimopoulos, and G. Dvali, *Phenomenology, astrophysics and cosmology of theories with submillimeter dimensions and TeV scale quantum gravity*, *Phys.Rev.* **D59** (1999) 086004, arXiv:hep-ph/9807344 [hep-ph].
- [14] D. Kapner, T. Cook, E. Adelberger, J. Gundlach, B. R. Heckel, *et al.*, *Tests of the gravitational inverse-square law below the dark-energy length scale*, *Phys.Rev.Lett.* **98** (2007) 021101, arXiv:hep-ph/0611184 [hep-ph].
- [15] T. Han, J. D. Lykken, and R.-J. Zhang, *On Kaluza-Klein states from large extra dimensions*, *Phys.Rev.* **D59** (1999) 105006, arXiv:hep-ph/9811350 [hep-ph].
- [16] G. F. Giudice, R. Rattazzi, and J. D. Wells, *Quantum gravity and extra dimensions at high-energy colliders*, *Nucl.Phys.* **B544** (1999) 3–38, arXiv:hep-ph/9811291 [hep-ph].
- [17] J. M. Campbell, J. Huston, and W. Stirling, *Hard Interactions of Quarks and Gluons: A Primer for LHC Physics*, *Rept.Prog.Phys.* **70** (2007) 89, arXiv:hep-ph/0611148 [hep-ph].
- [18] **SM and NLO Multileg Working Group** Collaboration, T. Binoth *et al.*, *The SM and NLO Multileg Working Group: Summary report*, arXiv:1003.1241 [hep-ph].

- [19] **SM and NLO MULTILEG Working Group, SM MC Working Group** Collaboration, J. Alcaraz Maestre *et al.*, *The SM and NLO Multileg and SM MC Working Groups: Summary Report*, arXiv:1203.6803 [hep-ph].
- [20] T. Muta, *Foundations of quantum chromodynamics: An introduction to perturbative methods in gauge theories*, .
- [21] T. Kinoshita, *Mass singularities of Feynman amplitudes*, *J.Math.Phys.* **3** (1962) 650–677.
- [22] L. Brown and R. Feynman, *Radiative corrections to Compton scattering*, *Phys.Rev.* **85** (1952) 231–244.
- [23] G. 't Hooft and M. Veltman, *Scalar One Loop Integrals*, *Nucl.Phys.* **B153** (1979) 365–401.
- [24] G. Passarino and M. Veltman, *One Loop Corrections for $e^+ e^-$ Annihilation Into $\mu^+ \mu^-$ in the Weinberg Model*, *Nucl.Phys.* **B160** (1979) 151.
- [25] A. I. Davydychev, *A Simple formula for reducing Feynman diagrams to scalar integrals*, *Phys.Lett.* **B263** (1991) 107–111.
- [26] O. Tarasov, *Connection between Feynman integrals having different values of the space-time dimension*, *Phys.Rev.* **D54** (1996) 6479–6490, arXiv:hep-th/9606018 [hep-th].
- [27] J. Fleischer, F. Jegerlehner, and O. Tarasov, *Algebraic reduction of one loop Feynman graph amplitudes*, *Nucl.Phys.* **B566** (2000) 423–440, arXiv:hep-ph/9907327 [hep-ph].
- [28] W. van Neerven and J. Vermaseren, *LARGE LOOP INTEGRALS*, *Phys.Lett.* **B137** (1984) 241.
- [29] G. van Oldenborgh and J. Vermaseren, *New Algorithms for One Loop Integrals*, *Z.Phys.* **C46** (1990) 425–438.

- [30] J. M. Campbell, E. N. Glover, and D. Miller, *One loop tensor integrals in dimensional regularization*, *Nucl.Phys.* **B498** (1997) 397–442, arXiv:hep-ph/9612413 [hep-ph].
- [31] T. Binoth, J. Guillet, and G. Heinrich, *Reduction formalism for dimensionally regulated one loop N point integrals*, *Nucl.Phys.* **B572** (2000) 361–386, arXiv:hep-ph/9911342 [hep-ph].
- [32] F. Campanario, *Towards $pp \rightarrow VVjj$ at NLO QCD: Bosonic contributions to triple vector boson production plus jet*, *JHEP* **1110** (2011) 070, arXiv:1105.0920 [hep-ph].
- [33] F. Campanario, Q. Li, M. Rauch, and M. Spira, *ZZ +jet production via gluon fusion at the LHC*, *JHEP* **1306** (2013) 069, arXiv:1211.5429 [hep-ph].
- [34] F. Campanario, H. Czy, J. Gluza, M. Gunia, T. Riemann, *et al.*, *Complete QED NLO contributions to the reaction $e^+e^- \rightarrow \mu^+\mu^-\gamma$ and their implementation in the event generator PHOKHARA*, *JHEP* **1402** (2014) 114, arXiv:1312.3610 [hep-ph].
- [35] W. Giele and E. N. Glover, *A Computational formalism for one loop integrals*, *JHEP* **0404** (2004) 029, arXiv:hep-ph/0402152 [hep-ph].
- [36] A. Denner and S. Dittmaier, *Reduction schemes for one-loop tensor integrals*, *Nucl.Phys.* **B734** (2006) 62–115, arXiv:hep-ph/0509141 [hep-ph].
- [37] T. Binoth, J. P. Guillet, G. Heinrich, E. Pilon, and C. Schubert, *An Algebraic/numerical formalism for one-loop multi-leg amplitudes*, *JHEP* **0510** (2005) 015, arXiv:hep-ph/0504267 [hep-ph].
- [38] T. Diakonidis, J. Fleischer, J. Gluza, K. Kajda, T. Riemann, *et al.*, *A Complete reduction of one-loop tensor 5 and 6-point integrals*, *Phys.Rev.* **D80** (2009) 036003, arXiv:0812.2134 [hep-ph].
- [39] J. Fleischer and T. Riemann, *A Complete algebraic reduction of one-loop tensor Feynman integrals*, *Phys.Rev.* **D83** (2011) 073004, arXiv:1009.4436 [hep-ph].

- [40] V. Yundin, *Massive loop corrections for collider physics*, .
<http://edoc.hu-berlin.de/docviews/abstract.php?id=39163>.
- [41] V. Yundin, *The link for the download*, . <https://github.com/Vayu/PJFry/>.
- [42] R. K. Ellis and G. Zanderighi, *Scalar one-loop integrals for QCD*, *JHEP* **0802** (2008) 002, arXiv:0712.1851 [hep-ph].
- [43] A. van Hameren, *OneLoop: For the evaluation of one-loop scalar functions*,
Comput.Phys.Commun. **182** (2011) 2427–2438, arXiv:1007.4716 [hep-ph].
- [44] S. Catani and M. Seymour, *A General algorithm for calculating jet cross-sections in NLO QCD*, *Nucl.Phys.* **B485** (1997) 291–419, arXiv:hep-ph/9605323 [hep-ph].
- [45] S. Frixione, Z. Kunszt, and A. Signer, *Three jet cross-sections to next-to-leading order*,
Nucl.Phys. **B467** (1996) 399–442, arXiv:hep-ph/9512328 [hep-ph].
- [46] R. Frederix, S. Frixione, F. Maltoni, and T. Stelzer, *Automation of next-to-leading order computations in QCD: The FKS subtraction*, *JHEP* **0910** (2009) 003, arXiv:0908.4272 [hep-ph].
- [47] J. Alwall, R. Frederix, S. Frixione, V. Hirschi, F. Maltoni, *et al.*, *The automated computation of tree-level and next-to-leading order differential cross sections, and their matching to parton shower simulations*, *JHEP* **1407** (2014) 079, arXiv:1405.0301 [hep-ph].
- [48] G. Marchesini, B. Webber, G. Abbiendi, I. Knowles, M. Seymour, *et al.*, *HERWIG: A Monte Carlo event generator for simulating hadron emission reactions with interfering gluons. Version 5.1 - April 1991*, *Comput.Phys.Commun.* **67** (1992) 465–508.
- [49] G. Corcella, I. Knowles, G. Marchesini, S. Moretti, K. Odagiri, *et al.*, *HERWIG 6: An Event generator for hadron emission reactions with interfering gluons (including supersymmetric processes)*, *JHEP* **0101** (2001) 010, arXiv:hep-ph/0011363 [hep-ph].

- [50] G. Corcella, I. Knowles, G. Marchesini, S. Moretti, K. Odagiri, *et al.*, *HERWIG 6.5 release note*, arXiv:hep-ph/0210213 [hep-ph].
- [51] T. Sjostrand, S. Mrenna, and P. Z. Skands, *PYTHIA 6.4 Physics and Manual*, *JHEP* **0605** (2006) 026, arXiv:hep-ph/0603175 [hep-ph].
- [52] R. Frederix, S. Frixione, V. Hirschi, F. Maltoni, R. Pittau, *et al.*, *Scalar and pseudoscalar Higgs production in association with a top-antitop pair*, *Phys.Lett.* **B701** (2011) 427–433, arXiv:1104.5613 [hep-ph].
- [53] R. Frederix, S. Frixione, V. Hirschi, F. Maltoni, R. Pittau, *et al.*, *W and Z/ γ^* boson production in association with a bottom-antibottom pair*, *JHEP* **1109** (2011) 061, arXiv:1106.6019 [hep-ph].
- [54] T. Stelzer and W. Long, *Automatic generation of tree level helicity amplitudes*, *Comput.Phys.Commun.* **81** (1994) 357–371, arXiv:hep-ph/9401258 [hep-ph].
- [55] J. Alwall, P. Demin, S. de Visscher, R. Frederix, M. Herquet, *et al.*, *MadGraph/MadEvent v4: The New Web Generation*, *JHEP* **0709** (2007) 028, arXiv:0706.2334 [hep-ph].
- [56] S. Frixione, *A General approach to jet cross-sections in QCD*, *Nucl.Phys.* **B507** (1997) 295–314, arXiv:hep-ph/9706545 [hep-ph].
- [57] D. Appell, G. F. Sterman, and P. B. Mackenzie, *Soft Gluons and the Normalization of the Drell-Yan Cross-section*, *Nucl.Phys.* **B309** (1988) 259.
- [58] S. Catani, *Higher order QCD corrections in hadron collisions: Soft gluon resummation and exponentiation*, *Nucl.Phys.Proc.Suppl.* **54A** (1997) 107–113, arXiv:hep-ph/9610413 [hep-ph].
- [59] H. Georgi, S. Glashow, M. Machacek, and D. V. Nanopoulos, *Higgs Bosons from Two Gluon Annihilation in Proton Proton Collisions*, *Phys.Rev.Lett.* **40** (1978) 692.

- [60] A. Djouadi, M. Spira, and P. Zerwas, *Production of Higgs bosons in proton colliders: QCD corrections*, *Phys.Lett.* **B264** (1991) 440–446.
- [61] S. Dawson, *Radiative corrections to Higgs boson production*, *Nucl.Phys.* **B359** (1991) 283–300.
- [62] M. Spira, A. Djouadi, D. Graudenz, and P. Zerwas, *Higgs boson production at the LHC*, *Nucl.Phys.* **B453** (1995) 17–82, arXiv:hep-ph/9504378 [hep-ph].
- [63] S. Catani, D. de Florian, and M. Grazzini, *Higgs production in hadron collisions: Soft and virtual QCD corrections at NNLO*, *JHEP* **0105** (2001) 025, arXiv:hep-ph/0102227 [hep-ph].
- [64] R. V. Harlander and W. B. Kilgore, *Soft and virtual corrections to proton proton $\rightarrow H + x$ at NNLO*, *Phys.Rev.* **D64** (2001) 013015, arXiv:hep-ph/0102241 [hep-ph].
- [65] R. V. Harlander and W. B. Kilgore, *Next-to-next-to-leading order Higgs production at hadron colliders*, *Phys.Rev.Lett.* **88** (2002) 201801, arXiv:hep-ph/0201206 [hep-ph].
- [66] C. Anastasiou and K. Melnikov, *Higgs boson production at hadron colliders in NNLO QCD*, *Nucl.Phys.* **B646** (2002) 220–256, arXiv:hep-ph/0207004 [hep-ph].
- [67] V. Ravindran, J. Smith, and W. L. van Neerven, *NNLO corrections to the total cross-section for Higgs boson production in hadron hadron collisions*, *Nucl.Phys.* **B665** (2003) 325–366, arXiv:hep-ph/0302135 [hep-ph].
- [68] T. Han, G. Valencia, and S. Willenbrock, *Structure function approach to vector boson scattering in $p p$ collisions*, *Phys.Rev.Lett.* **69** (1992) 3274–3277, arXiv:hep-ph/9206246 [hep-ph].
- [69] P. Bolzoni, F. Maltoni, S.-O. Moch, and M. Zaro, *Higgs production via vector-boson fusion at NNLO in QCD*, *Phys.Rev.Lett.* **105** (2010) 011801, arXiv:1003.4451 [hep-ph].

- [70] T. Han and S. Willenbrock, *QCD correction to the $p p \rightarrow W H$ and $Z H$ total cross-sections*, *Phys.Lett.* **B273** (1991) 167–172.
- [71] O. Brein, A. Djouadi, and R. Harlander, *NNLO QCD corrections to the Higgs-strahlung processes at hadron colliders*, *Phys.Lett.* **B579** (2004) 149–156, arXiv:hep-ph/0307206 [hep-ph].
- [72] D. A. Dicus and S. Willenbrock, *Higgs Boson Production from Heavy Quark Fusion*, *Phys.Rev.* **D39** (1989) 751.
- [73] D. Dicus, T. Stelzer, Z. Sullivan, and S. Willenbrock, *Higgs boson production in association with bottom quarks at next-to-leading order*, *Phys.Rev.* **D59** (1999) 094016, arXiv:hep-ph/9811492 [hep-ph].
- [74] F. Maltoni, Z. Sullivan, and S. Willenbrock, *Higgs-boson production via bottom-quark fusion*, *Phys.Rev.* **D67** (2003) 093005, arXiv:hep-ph/0301033 [hep-ph].
- [75] F. I. Olness and W.-K. Tung, *When Is a Heavy Quark Not a Parton? Charged Higgs Production and Heavy Quark Mass Effects in the QCD Based Parton Model*, *Nucl.Phys.* **B308** (1988) 813.
- [76] J. Gunion, H. Haber, F. Paige, W.-K. Tung, and S. Willenbrock, *Neutral and Charged Higgs Detection: Heavy Quark Fusion, Top Quark Mass Dependence and Rare Decays*, *Nucl.Phys.* **B294** (1987) 621.
- [77] R. V. Harlander and W. B. Kilgore, *Higgs boson production in bottom quark fusion at next-to-next-to leading order*, *Phys.Rev.* **D68** (2003) 013001, arXiv:hep-ph/0304035 [hep-ph].
- [78] S. Catani, D. de Florian, M. Grazzini, and P. Nason, *Soft gluon resummation for Higgs boson production at hadron colliders*, *JHEP* **0307** (2003) 028, arXiv:hep-ph/0306211 [hep-ph].

- [79] U. Aglietti, R. Bonciani, G. Degrossi, and A. Vicini, *Two loop light fermion contribution to Higgs production and decays*, *Phys.Lett.* **B595** (2004) 432–441, arXiv:hep-ph/0404071 [hep-ph].
- [80] S. Actis, G. Passarino, C. Sturm, and S. Uccirati, *NLO Electroweak Corrections to Higgs Boson Production at Hadron Colliders*, *Phys.Lett.* **B670** (2008) 12–17, arXiv:0809.1301 [hep-ph].
- [81] G. Altarelli, R. K. Ellis, and G. Martinelli, *Leptoproduction and Drell-Yan Processes Beyond the Leading Approximation in Chromodynamics*, *Nucl.Phys.* **B143** (1978) 521.
- [82] T. Matsuura and W. van Neerven, *Second Order Logarithmic Corrections to the Drell-Yan Cross-section*, *Z.Phys.* **C38** (1988) 623.
- [83] T. Matsuura, S. van der Marck, and W. van Neerven, *The Calculation of the Second Order Soft and Virtual Contributions to the Drell-Yan Cross-Section*, *Nucl.Phys.* **B319** (1989) 570.
- [84] R. Hamberg, W. van Neerven, and T. Matsuura, *A Complete calculation of the order $\alpha - s^2$ correction to the Drell-Yan K factor*, *Nucl.Phys.* **B359** (1991) 343–405.
- [85] S. Moch, J. Vermaseren, and A. Vogt, *The Quark form-factor at higher orders*, *JHEP* **0508** (2005) 049, arXiv:hep-ph/0507039 [hep-ph].
- [86] S. Moch, J. Vermaseren, and A. Vogt, *Three-loop results for quark and gluon form-factors*, *Phys.Lett.* **B625** (2005) 245–252, arXiv:hep-ph/0508055 [hep-ph].
- [87] T. Gehrmann, T. Huber, and D. Maitre, *Two-loop quark and gluon form-factors in dimensional regularisation*, *Phys.Lett.* **B622** (2005) 295–302, arXiv:hep-ph/0507061 [hep-ph].
- [88] P. Baikov, K. Chetyrkin, A. Smirnov, V. Smirnov, and M. Steinhauser, *Quark and gluon form factors to three loops*, *Phys.Rev.Lett.* **102** (2009) 212002, arXiv:0902.3519 [hep-ph].

- [89] T. Gehrmann, E. Glover, T. Huber, N. Ikizlerli, and C. Studerus, *Calculation of the quark and gluon form factors to three loops in QCD*, *JHEP* **1006** (2010) 094, arXiv:1004.3653 [hep-ph].
- [90] S. Moch, J. Vermaseren, and A. Vogt, *The Three loop splitting functions in QCD: The Nonsinglet case*, *Nucl.Phys.* **B688** (2004) 101–134, arXiv:hep-ph/0403192 [hep-ph].
- [91] K. Chetyrkin, B. A. Kniehl, and M. Steinhauser, *Decoupling relations to $O(\alpha_s^3)$ and their connection to low-energy theorems*, *Nucl.Phys.* **B510** (1998) 61–87, arXiv:hep-ph/9708255 [hep-ph].
- [92] D. de Florian and J. Mazzitelli, *A next-to-next-to-leading order calculation of soft-virtual cross sections*, *JHEP* **1212** (2012) 088, arXiv:1209.0673 [hep-ph].
- [93] S. Moch and A. Vogt, *Higher-order soft corrections to lepton pair and Higgs boson production*, *Phys.Lett.* **B631** (2005) 48–57, arXiv:hep-ph/0508265 [hep-ph].
- [94] E. Laenen and L. Magnea, *Threshold resummation for electroweak annihilation from DIS data*, *Phys.Lett.* **B632** (2006) 270–276, arXiv:hep-ph/0508284 [hep-ph].
- [95] A. Idilbi, X.-d. Ji, J.-P. Ma, and F. Yuan, *Threshold resummation for Higgs production in effective field theory*, *Phys.Rev.* **D73** (2006) 077501, arXiv:hep-ph/0509294 [hep-ph].
- [96] V. Ravindran, *On Sudakov and soft resummations in QCD*, *Nucl.Phys.* **B746** (2006) 58–76, arXiv:hep-ph/0512249 [hep-ph].
- [97] V. Ravindran, *Higher-order threshold effects to inclusive processes in QCD*, *Nucl.Phys.* **B752** (2006) 173–196, arXiv:hep-ph/0603041 [hep-ph].
- [98] W. B. Kilgore, *One-Loop Single-Real-Emission Contributions to $pp \rightarrow H + X$ at Next-to-Next-to-Next-to-Leading Order*, *Phys.Rev.* **D89** (2014) 073008, arXiv:1312.1296 [hep-ph].

- [99] C. Anastasiou, C. Duhr, F. Dulat, F. Herzog, and B. Mistlberger, *Real-virtual contributions to the inclusive Higgs cross-section at N^3LO* , *JHEP* **1312** (2013) 088, arXiv:1311.1425 [hep-ph].
- [100] C. Duhr, T. Gehrmann, and M. Jaquier, *Two-loop splitting amplitudes and the single-real contribution to inclusive Higgs production at N^3LO* , arXiv:1411.3587 [hep-ph].
- [101] F. Dulat and B. Mistlberger, *Real-Virtual-Virtual contributions to the inclusive Higgs cross section at N^3LO* , arXiv:1411.3586 [hep-ph].
- [102] C. Anastasiou, C. Duhr, F. Dulat, E. Furlan, T. Gehrmann, *et al.*, *Higgs boson gluonfusion production at threshold in N^3LO QCD*, *Phys.Lett.* **B737** (2014) 325–328, arXiv:1403.4616 [hep-ph].
- [103] T. Ahmed, M. Mahakhud, N. Rana, and V. Ravindran, *Drell-Yan production at threshold in N^3LO QCD*, *Phys.Rev.Lett.* **113** (2014) 112002, arXiv:1404.0366 [hep-ph].
- [104] Y. Li, A. von Manteuffel, R. M. Schabinger, and H. X. Zhu, *N^3LO Higgs and Drell-Yan production at threshold: the one-loop two-emission contribution*, *Phys.Rev.* **D90** (2014) 053006, arXiv:1404.5839 [hep-ph].
- [105] S. Catani, L. Cieri, D. de Florian, G. Ferrera, and M. Grazzini, *Threshold resummation at N^3LL accuracy and soft-virtual cross sections at N^3LO* , *Nucl.Phys.* **B888** (2014) 75–91, arXiv:1405.4827 [hep-ph].
- [106] N. Lo Presti, A. Almasy, and A. Vogt, *Leading large- x logarithms of the quarkgluon contributions to inclusive Higgs-boson and lepton-pair production*, *Phys.Lett.* **B737** (2014) 120–123, arXiv:1407.1553 [hep-ph].
- [107] D. de Florian, J. Mazzitelli, S. Moch, and A. Vogt, *Approximate N^3LO Higgs-boson production cross section using physical-kernel constraints*, *JHEP* **1410** (2014) 176, arXiv:1408.6277 [hep-ph].

- [108] C. Anastasiou, C. Duhr, F. Dulat, E. Furlan, T. Gehrmann, *et al.*, *Higgs boson gluon-fusion production beyond threshold in N³LO QCD*, arXiv:1411.3584 [hep-ph].
- [109] C. Anastasiou, L. J. Dixon, K. Melnikov, and F. Petriello, *Dilepton rapidity distribution in the Drell-Yan process at NNLO in QCD*, *Phys.Rev.Lett.* **91** (2003) 182002, arXiv:hep-ph/0306192 [hep-ph].
- [110] C. Anastasiou, K. Melnikov, and F. Petriello, *Higgs boson production at hadron colliders: Differential cross sections through next-to-next-to-leading order*, *Phys.Rev.Lett.* **93** (2004) 262002, arXiv:hep-ph/0409088 [hep-ph].
- [111] C. Anastasiou, K. Melnikov, and F. Petriello, *Fully differential Higgs boson production and the di-photon signal through next-to-next-to-leading order*, *Nucl.Phys.* **B724** (2005) 197–246, arXiv:hep-ph/0501130 [hep-ph].
- [112] S. Bhler, F. Herzog, A. Lazopoulos, and R. Miller, *The fully differential hadronic production of a Higgs boson via bottom quark fusion at NNLO*, *JHEP* **1207** (2012) 115, arXiv:1204.4415 [hep-ph].
- [113] G. Ferrera, M. Grazzini, and F. Tramontano, *Associated WH production at hadron colliders: a fully exclusive QCD calculation at NNLO*, *Phys.Rev.Lett.* **107** (2011) 152003, arXiv:1107.1164 [hep-ph].
- [114] G. Ferrera, M. Grazzini, and F. Tramontano, *Higher-order QCD effects for associated WH production and decay at the LHC*, *JHEP* **1404** (2014) 039, arXiv:1312.1669 [hep-ph].
- [115] V. Ravindran, J. Smith, and W. van Neerven, *QCD threshold corrections to di-lepton and Higgs rapidity distributions beyond N² LO*, *Nucl.Phys.* **B767** (2007) 100–129, arXiv:hep-ph/0608308 [hep-ph].

- [116] T. Ahmed, M. Mandal, N. Rana, and V. Ravindran, *Rapidity Distributions in Drell-Yan and Higgs Productions at Threshold to Third Order in QCD*, *Phys.Rev.Lett.* **113** (2014) 212003, arXiv:1404.6504 [hep-ph].
- [117] A. Zerwekh, C. Dib, and R. Rosenfeld, *Triple photon production at the Tevatron in technicolor models*, *Phys.Lett.* **B549** (2002) 154–158, arXiv:hep-ph/0207270 [hep-ph].
- [118] M. Golden and S. R. Sharpe, *Three Weak Gauge Boson Production at the SSC*, *Nucl.Phys.* **B261** (1985) 217.
- [119] V. D. Barger and T. Han, *Triple Gauge Boson Production at e^+e^- and pp Supercolliders*, *Phys.Lett.* **B212** (1988) 117.
- [120] G. Bozzi, F. Campanario, M. Rauch, and D. Zeppenfeld, *$Z\gamma\gamma$ production with leptonic decays and triple photon production at next-to-leading order QCD*, *Phys.Rev.* **D84** (2011) 074028, arXiv:1107.3149 [hep-ph].
- [121] P. Nogueira, *Automatic Feynman graph generation*, *J.Comput.Phys.* **105** (1993) 279–289.
- [122] M. Tentyukov and J. Vermaseren, *The Multithreaded version of FORM*, *Comput.Phys.Commun.* **181** (2010) 1419–1427, arXiv:hep-ph/0702279 [hep-ph].
- [123] M. Kumar, P. Mathews, V. Ravindran, and A. Tripathi, *Direct photon pair production at the LHC to order α_s in TeV scale gravity models*, *Nucl.Phys.* **B818** (2009) 28–51, arXiv:0902.4894 [hep-ph].
- [124] M. Kumar, P. Mathews, V. Ravindran, and A. Tripathi, *Diphoton signals in theories with large extra dimensions to NLO QCD at hadron colliders*, *Phys.Lett.* **B672** (2009) 45–50, arXiv:0811.1670 [hep-ph].

- [125] R. Frederix, M. K. Mandal, P. Mathews, V. Ravindran, S. Seth, *et al.*, *Diphoton production in the ADD model to NLO+parton shower accuracy at the LHC*, *JHEP* **1212** (2012) 102, arXiv:1209.6527 [hep-ph].
- [126] S. Frixione, *Isolated photons in perturbative QCD*, *Phys.Lett.* **B429** (1998) 369–374, arXiv:hep-ph/9801442 [hep-ph].
- [127] J. M. Campbell and C. Williams, *Triphoton production at hadron colliders*, *Phys.Rev.* **D89** no. 11, (2014) 113001, arXiv:1403.2641 [hep-ph].
- [128] V. Del Duca, F. Maltoni, Z. Nagy, and Z. Trocsanyi, *QCD radiative corrections to prompt diphoton production in association with a jet at hadron colliders*, *JHEP* **0304** (2003) 059, arXiv:hep-ph/0303012 [hep-ph].
- [129] A. Martin, W. Stirling, R. Thorne, and G. Watt, *Parton distributions for the LHC*, *Eur.Phys.J.* **C63** (2009) 189–285, arXiv:0901.0002 [hep-ph].
- [130] R. Frederix, S. Frixione, V. Hirschi, F. Maltoni, R. Pittau, *et al.*, *Four-lepton production at hadron colliders: aMC@NLO predictions with theoretical uncertainties*, *JHEP* **1202** (2012) 099, arXiv:1110.4738 [hep-ph].
- [131] P. Torrielli and S. Frixione, *Matching NLO QCD computations with PYTHIA using MC@NLO*, *JHEP* **1004** (2010) 110, arXiv:1002.4293 [hep-ph].
- [132] CMS Collaboration, S. Chatrchyan *et al.*, *Search for signatures of extra dimensions in the diphoton mass spectrum at the Large Hadron Collider*, *Phys.Rev.Lett.* **108** (2012) 111801, arXiv:1112.0688 [hep-ex].
- [133] ATLAS Collaboration, G. Aad *et al.*, *Search for Extra Dimensions using diphoton events in 7 TeV proton-proton collisions with the ATLAS detector*, *Phys.Lett.* **B710** (2012) 538–556, arXiv:1112.2194 [hep-ex].

- [134] P. Mathews, V. Ravindran, K. Sridhar, and W. van Neerven, *Next-to-leading order QCD corrections to the Drell-Yan cross section in models of TeV-scale gravity*, *Nucl.Phys.* **B713** (2005) 333–377, arXiv:hep-ph/0411018 [hep-ph].
- [135] P. Mathews and V. Ravindran, *Angular distribution of Drell-Yan process at hadron colliders to NLO-QCD in models of TeV scale gravity*, *Nucl.Phys.* **B753** (2006) 1–15, arXiv:hep-ph/0507250 [hep-ph].
- [136] M. Kumar, P. Mathews, and V. Ravindran, *PDF and scale uncertainties of various DY distributions in ADD and RS models at hadron colliders*, *Eur.Phys.J.* **C49** (2007) 599–611, arXiv:hep-ph/0604135 [hep-ph].
- [137] N. Agarwal, V. Ravindran, V. Tiwari, and A. Tripathi, *Z boson pair production at the LHC to $O(\alpha(s))$ in TeV scale gravity models*, *Nucl.Phys.* **B830** (2010) 248–270, arXiv:0909.2651 [hep-ph].
- [138] N. Agarwal, V. Ravindran, V. K. Tiwari, and A. Tripathi, *Next-to-leading order QCD corrections to the Z boson pair production at the LHC in Randall Sundrum model*, *Phys.Lett.* **B686** (2010) 244–248, arXiv:0910.1551 [hep-ph].
- [139] N. Agarwal, V. Ravindran, V. K. Tiwari, and A. Tripathi, *Next-to-leading order QCD corrections to W^+W^- production at the LHC in Randall Sundrum model*, *Phys.Lett.* **B690** (2010) 390–395, arXiv:1003.5445 [hep-ph].
- [140] N. Agarwal, V. Ravindran, V. K. Tiwari, and A. Tripathi, *W^+W^- production in Large extra dimension model at next-to-leading order in QCD at the LHC*, *Phys.Rev.* **D82** (2010) 036001, arXiv:1003.5450 [hep-ph].
- [141] P. Artoisenet, R. Frederix, O. Mattelaer, and R. Rietkerk, *Automatic spin-entangled decays of heavy resonances in Monte Carlo simulations*, *JHEP* **1303** (2013) 015, arXiv:1212.3460 [hep-ph].

- [142] H. Baer, B. Bailey, and J. Owens, *O (α -s) Monte Carlo approach to $W + \text{Higgs}$ associated production at hadron supercolliders*, *Phys.Rev.* **D47** (1993) 2730–2734.
- [143] J. Ohnemus and W. J. Stirling, *Order α -s corrections to the differential cross-section for the WH intermediate mass Higgs signal*, *Phys.Rev.* **D47** (1993) 2722–2729.
- [144] S. Mrenna and C. Yuan, *Effects of QCD resummation on $W + h$ and t anti- b production at the Tevatron*, *Phys.Lett.* **B416** (1998) 200–207, arXiv:hep-ph/9703224 [hep-ph].
- [145] O. Brein, R. Harlander, M. Wiesemann, and T. Zirke, *Top-Quark Mediated Effects in Hadronic Higgs-Strahlung*, *Eur.Phys.J.* **C72** (2012) 1868, arXiv:1111.0761 [hep-ph].
- [146] B. A. Kniehl, *Associated Production of Higgs and Z Bosons From Gluon Fusion in Hadron Collisions*, *Phys.Rev.* **D42** (1990) 2253–2258.
- [147] G. Ferrera, M. Grazzini, and F. Tramontano, *Associated ZH production at hadron colliders: the fully differential NNLO QCD calculation*, arXiv:1407.4747 [hep-ph].
- [148] G. Ferrera, M. Grazzini, and F. Tramontano, *Associated WH production at hadron colliders: a fully exclusive QCD calculation at NNLO*, *Phys.Rev.Lett.* **107** (2011) 152003, arXiv:1107.1164 [hep-ph].
- [149] S. Dawson, T. Han, W. Lai, A. Leibovich, and I. Lewis, *Resummation Effects in Vector-Boson and Higgs Associated Production*, *Phys.Rev.* **D86** (2012) 074007, arXiv:1207.4207 [hep-ph].
- [150] L. Altenkamp, S. Dittmaier, R. V. Harlander, H. Rzehak, and T. J. Zirke, *Gluon-induced Higgs-strahlung at next-to-leading order QCD*, *JHEP* **1302** (2013) 078, arXiv:1211.5015 [hep-ph].
- [151] R. V. Harlander, A. Kulesza, V. Theeuwes, and T. Zirke, *Soft gluon resummation for gluon-induced Higgs Strahlung*, *JHEP* **1411** (2014) 082, arXiv:1410.0217 [hep-ph].

- [152] O. Brein, R. V. Harlander, and T. J. Zirke, *vh@nnlo - Higgs Strahlung at hadron colliders*, *Comput.Phys.Commun.* **184** (2013) 998–1003, arXiv:1210.5347 [hep-ph].
- [153] M. Ciccolini, S. Dittmaier, and M. Kramer, *Electroweak radiative corrections to associated WH and ZH production at hadron colliders*, *Phys.Rev.* **D68** (2003) 073003, arXiv:hep-ph/0306234 [hep-ph].
- [154] O. Brein, M. Ciccolini, S. Dittmaier, A. Djouadi, R. Harlander, *et al.*, *Precision calculations for associated WH and ZH production at hadron colliders*, arXiv:hep-ph/0402003 [hep-ph].
- [155] T. Gehrmann and D. Kara, *The $Hb\bar{b}$ form factor to three loops in QCD*, *JHEP* **09** (2014) 174, arXiv:1407.8114 [hep-ph].
- [156] N. Kidonakis, *Collinear and soft gluon corrections to Higgs production at NNNLO*, *Phys.Rev.* **D77** (2008) 053008, arXiv:0711.0142 [hep-ph].
- [157] T. Ahmed, N. Rana, and V. Ravindran, *Higgs boson production through $b\bar{b}$ annihilation at threshold in N^3LO QCD*, *JHEP* **1410** (2014) 139, arXiv:1408.0787 [hep-ph].
- [158] D. Choudhury, S. Majhi, and V. Ravindran, *NLO corrections to lepton pair production beyond the standard model at hadron colliders*, *JHEP* **0601** (2006) 027, arXiv:hep-ph/0509057 [hep-ph].
- [159] O. Tarasov, A. Vladimirov, and A. Y. Zharkov, *The Gell-Mann-Low Function of QCD in the Three Loop Approximation*, *Phys.Lett.* **B93** (1980) 429–432.
- [160] O. Tarasov, *ANOMALOUS DIMENSIONS OF QUARK MASSES IN THREE LOOP APPROXIMATION*, .
- [161] T. van Ritbergen, J. Vermaseren, and S. Larin, *The Four loop beta function in quantum chromodynamics*, *Phys.Lett.* **B400** (1997) 379–384, arXiv:hep-ph/9701390 [hep-ph].

- [162] M. Czakon, *The Four-loop QCD beta-function and anomalous dimensions*, *Nucl.Phys.* **B710** (2005) 485–498, arXiv:hep-ph/0411261 [hep-ph].
- [163] V. Sudakov, *Vertex parts at very high-energies in quantum electrodynamics*, *Sov.Phys.JETP* **3** (1956) 65–71.
- [164] A. H. Mueller, *On the Asymptotic Behavior of the Sudakov Form-factor*, *Phys.Rev.* **D20** (1979) 2037.
- [165] J. C. Collins, *Algorithm to Compute Corrections to the Sudakov Form-factor*, *Phys.Rev.* **D22** (1980) 1478.
- [166] A. Sen, *Asymptotic Behavior of the Sudakov Form-Factor in QCD*, *Phys.Rev.* **D24** (1981) 3281.
- [167] A. Vogt, S. Moch, and J. Vermaseren, *The Three-loop splitting functions in QCD: The Singlet case*, *Nucl.Phys.* **B691** (2004) 129–181, arXiv:hep-ph/0404111 [hep-ph].
- [168] S. Catani and L. Trentadue, *Resummation of the QCD Perturbative Series for Hard Processes*, *Nucl.Phys.* **B327** (1989) 323.
- [169] S. Catani and L. Trentadue, *Comment on QCD exponentiation at large x* , *Nucl.Phys.* **B353** (1991) 183–186.
- [170] A. Vogt, *Next-to-next-to-leading logarithmic threshold resummation for deep inelastic scattering and the Drell-Yan process*, *Phys.Lett.* **B497** (2001) 228–234, arXiv:hep-ph/0010146 [hep-ph].
- [171] V. Ravindran, J. Smith, and W. van Neerven, *Two-loop corrections to Higgs boson production*, *Nucl.Phys.* **B704** (2005) 332–348, arXiv:hep-ph/0408315 [hep-ph].
- [172] T. Becher and M. Neubert, *Infrared singularities of scattering amplitudes in perturbative QCD*, *Phys.Rev.Lett.* **102** no. 19, (2009) 162001, arXiv:0901.0722 [hep-ph].

- [173] E. Gardi and L. Magnea, *Factorization constraints for soft anomalous dimensions in QCD scattering amplitudes*, *JHEP* **0903** (2009) 079, arXiv:0901.1091 [hep-ph].
- [174] J. Vermaseren, S. Larin, and T. van Ritbergen, *The four loop quark mass anomalous dimension and the invariant quark mass*, *Phys.Lett.* **B405** (1997) 327–333, arXiv:hep-ph/9703284 [hep-ph].
- [175] T. Becher, M. Neubert, and G. Xu, *Dynamical Threshold Enhancement and Resummation in Drell-Yan Production*, *JHEP* **0807** (2008) 030, arXiv:0710.0680 [hep-ph].